Republic of Iraq

Ministry of Higher Education and Scientific Research

University of Babylon

College of Information Technology

Department of Software

Glaucoma level Detection Based on Retinal Features

A Thesis

Submitted to the Council of the College of Information Technology for Postgraduate Studies of the University of Babylon in Partial Fulfillment of the Requirements for the Degree of Master in Information Technology – Software

By

Wesam Adnan Kareem Omran

Supervised By

Asst. Prof. Dr. Enas Hamood Muhaisun Abdalaha

2022 A.D. *1444 A.H.*

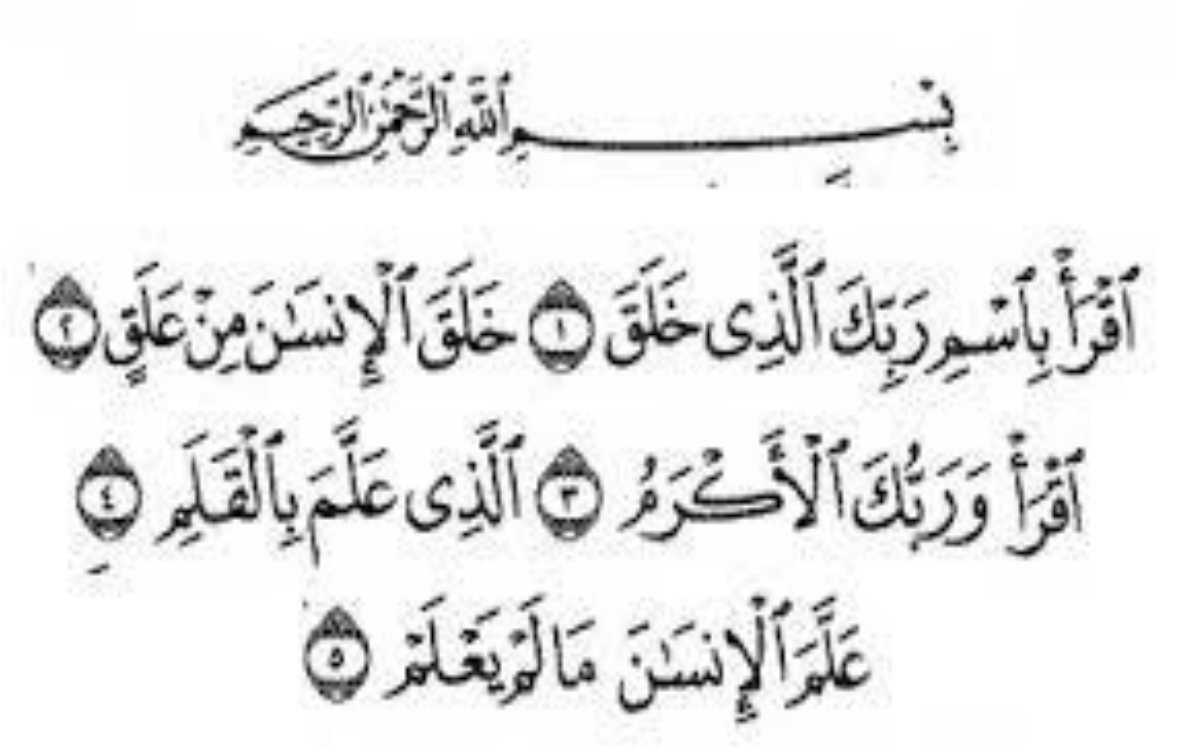

صدقـ الله العلي العظيم

سورة العلق (5)

Dedication

To

For God's sake, my Creator and my Master,

My great teacher and messenger, Mohammed (May Allah bless and grant him), who taught us the purpose of life,

My homeland Palestine, the warmest womb;

The great martyrs and prisoners, the symbol of sacrifice;

My second magnificent home;

My great parents, who never stop giving of themselves in countless ways,

My beloved brothers and sisters;

All my family, the symbol of love and giving,

My friends who encourage and support me,

All the people in my life who touch my heart

I dedicate this humble effort.

Supervisor Certification

I certify that the thesis entitled (**Glaucoma Level Detection Based on Retinal Features**)was prepared under my supervision at the department of Software/ College of Information Technology/ University of Babylon as partial fulfillment of the requirements of the degree of Master of Philosophy in Information Technology-Software.

Signature:

Supervisor Name**: Asst. Prof. Dr. Enas Hamood Al-Saadi**

Date: / /2022

The Head of the Department Certification

In view of the available recommendations, I forward the thesis entitled "**Glaucoma Level Detection Based on Retinal Features** for debate by the examination committee.

Signature:

Asst. Prof. Dr. Ahmed Saleem Abbas

Head of Software Department

Date: / /2022

Acknowledgements

Praise be to God, whose will and guidance enabled me to complete my higher education.

I would like to thank God Almighty, our Prophet Muhammad (peace be upon him) and all his pure family.

I would also like to acknowledge the University of Babylon - College of Information Technology - Department of Software Science for their support in carrying out this thesis.

In addition, my sincerest appreciation and love goes to all the members of my family who encouraged me to pursue this study and give me pure love and affection.

Finally, I would like to thank the people who have given me help and advice.

Certification of the Examination Committee

We, the undersigned, certify that (**Wesam Adnan Kareem**) candidate for the degree of Master in Information Technology - Software, has presented his thesis of the following title "**Glaucoma level Detection Based on Retinal Features**" as it appears on the title page and front cover of the thesis that the said thesis is acceptable in form and content and displays a satisfactory knowledge of the field of study as demonstrated by the candidate through an oral examination held on:

Signature:
Name: **Dr. Tawfiq Al-Asadi**
Title: Professor
Date: / / 2022
(Chairman)

Signature:
Name: **Dr. Mokhtar Mohammed Hasan**
Title: Assistant Professor
Date: / / 2022
(Member)

Signature:
Name: **Dr. Safa Saad Al-Murib**
Title: Lecturer
Date: / / 2022
(Member)

Signature:
Name: **Dr. Enas Hamood Al-Saadi**
Title: Assistant Professor
Date: / / 2022
(Member and Supervisor)

Approved by the Dean of the College of Information Technology, University of Babylon.

Signature:
Name: **Dr.Hussein Atiya Lafta**
Title: Professor
Date: / / 2022
(Dean of Collage of Information Technology)

Abstract:

Glaucoma is one of the diseases that affect the eye, specifically the retina, which often leads to damage to the optic nerve tissue. This disease occurs because of an increase in intraocular pressure. Examining clinical images of the retina with computer examination methods is crucial, logically and clinically accurate, and it produces good results and accuracy after incorporating the main inputs based on the work on the applicable context of the World Health Origination Indicators for this disease and organizing them mathematically and programmatically.

The current study has two main goals: the first one is to develop a system for predicting or detecting whether a person has glaucoma or not. The purpose of the second step of study is to assess whether this disease is in the early, moderate, or severe stages of progression. All of them were completed with the help of efficient algorithms.

The most prominent signs of glaucoma is the increase in the size of the Optic Cup and the Optic Disk, as well as the inflation that occurs in the blood vessels, and the narrowing of the Neuro Retinal Rim (NRR) area that lies between the Optic Cup and the Optic Disk , an effective method based on pixel colors has been proposed for the color values of the part to be extracted with the rest of the parts inside it , can compare them to the rest of the sizes of the healthy portions of the eyes that are free of any other disease . Despite the existence and overlap of blood vessels with the optic disc, the algorithm used to identify and extract the optic disc can work accurately to separate the optic disc from the anatomical structure of the image of the retinal fundus, the algorithm uses two steps: the first is based on the density threshold, and the second is based on the morphological methodology of

detection about all units of the image element, effectively excluding any kind of fake (Noise).

Two artificial intelligence methods are utilized in this study: the artificial neural network (ANN) and the support vector machine (SVM) for early detection of glaucoma based on eight features retrieved and classified into positive and negative categories as a result. The (SVM) results were superior to the ANN outcomes. When categorizing images, the mix of features used by SVM makes it difficult to distinguish normal from pathological fundus images, so you need employ a non-linear kernel to get close to the best result. Finally, work was done to apply the idea and decision tree algorithm to determine the degree of disease based on the eight features retrieved from the retina and to determine the three levels detect (early, moderate, severe) with (99.4%) accuracy .The accuracy of classification results for (ANN) and (SVM) are (95.3) and (98.8) respectively, thus the results are very good and promising.

Table of Contents

List of Tables

List of Figures

List of Abbreviations

Abbreviation	Meaning
AUC	Area Under Curve
ACG	Angle-Closure Glaucoma
ANN	Artificial Neural Network
ACC	Accuracy
BR	Bayesian Regularization
BV	Blood Vessels
BVR	Blood Vessels Ratio
BW	Black White Image
CAD	Computer-Aided Diagnostic
CDR	Cup to Disc Ratio
CLAHE	Contrast Limited Adaptive Histogram Equalization
CNN	Convolution Neural Network
FN	False Negative
FP	False Positive
GLCM	Gray Level Co-occurrence Matrix
HE	Histogram Equalization
HE	Histogram Equalization
HSV	Hue Saturation Value
IOP	Intraocular Pressure
ISNT	Inferior, Superior Nasal Temporal

Abbreviation	*Meaning*
NRR	Neuro retinal Rim
OAG	Open-angle glaucoma
OC	Optic Cup
OCT	Optical Coherence Tomography
OD	Optic Disc
ONH	Optic Nerve Head
ORIGA	Online Retinal Fundus Image Database for GlaucomaAnalysis and Research
PPA	Parapapillary Atrophy
RBF	Radial Basis Function
RDR	Rim to Disc Ratio
RGB	Red Green and Blue
RNFL	Retinal Nerve Fiber Layer
ROI	Region of Interest
SD	Standard Deviation
SE	Structuring Element
SVM	Support Vector Machine
TN	True Negative
TP	True Positive
WHO	World Health Organization

Chapter One: Introduction

1.1 General Introduction

Glaucoma is the second most frequent eye condition that results in neurological illness. Inappropriate intraocular pressure within the human eye was the primary known cause of this disease. In its early stages, glaucoma does not manifest any symptoms, but if left untreated, it can result in total blindness. Glaucoma can be diagnosed early enough to prevent permanent vision loss. Potential treatment involves manual eye examination, which is labor-intensive (A.Latif.et al.2019).

Glaucoma is called the silent sight thief because it is, and population-based surveys indicate that only 10 to 50 percent of glaucoma patients are aware of the condition (Gómez-Valverde et al., 2019).

Glaucoma is increasing alarmingly, according to statistics (WHO), 60.5 million people were infected in 2010 (Garnavi, 2020).With aging and demographic expansion, the estimated number of people who will suffer from glaucoma globally is expected to rise to 80 million in 2020 and about 111.8 million in 2040 (MacCormick et al., 2019).

The morphological technique was used because it is very similar to the human strategy for understanding the image. Diagnosing glaucoma using a retinal image is one of the critical techniques in the medical field, which includes healthy and unhealthy retina for ophthalmologists. As a result, improved and mechanistic approaches are needed to accurately diagnose the disease in a shorter period of time (Thakur and Juneja, 2018). The main advantage of the retinal fundus is that in most therapeutic settings such as hospitals or clinics, images of the retinal fundus can be obtained easily. Next, information extraction from digital image analysis is used to detect eye diseases of glaucoma (Kanse and Yadav, 2019).

1.2 Related Works

In previously and still, there have been many researches and studies that have been carried out in this regard in the detection of glaucoma.

1- (Sarkar, Sarkar and Nag, 2018) worked on Clustering technique and ellipse-fitting to automated detection of glaucoma, the first step was extraction the green channel from the color fundus image, then the region of interest (ROI) is determined to prevent incorrect clustering. The next step is implementing K-means clustering to for three clusters, the third clustercan be identified and eliminate due to the optic cup is always inside the optic disc, the rest clusters are only two; optic disc and optic cup, a rectangle is then drawn over each cluster in order to enclose it. Finally, ellipse fitting is performed by carving ellipse to each of the two rectangles. The CDR is calculated by dividing the area of the ellipse enclosing the optic cup by the area of the ellipse enclosing the optic disc, the threshold used to measure theCDR is 0.3-0.6 by default, if the CDR is larger than the threshold, and the patient is suffered from glaucoma. the dataset used is consists of 455 collected colorfundus images which includes 200 glaucomatous and 255 normal images, the accuracy of this method achieved 61%.

2- (Guo et al, 2018) Yanbao App, a completely new mobile app has been introduced in this business. The smartphone application demonstrated a high level of accuracy for both public databases and actual clinical data. Eight aspects of the work relevant to glaucoma classification and corresponding descriptors were used, including CDR, cup area, and thickness ratio. Precision is primarily due to the application's own algorithm. The application has a high degree of accuracy in detection and classification. Artificial minority over-sampling (SMOTE) approach and category

weighting method are used to balance the amount of features in normal and abnormal categories, which makes the application suitable for practical glaucoma screening. A 10-fold cross validation is used to evaluate the glaucoma classification model and use the ORIGA, DRISHTI-GS1 and DRISHTI-GS databases. The working accuracy was 76.42%.

3- (Dutta *et al.*, 2018) utilized Area Cup to Disc Ratio (ACDR) to glaucoma detection. Optic disc was segmented using a statistical model in which the pixels of the disc are identified according to their intensity values.Rows that have abrupt changes to its histogram are selected as passing through the optic disc boundary due to the pixels of the optic disc have a higher density, then the mean of maximum pixels of these rows is calculatedas a threshold of rows, likewise, the column threshold is calculated and the disc threshold is the mean of both rows and columns threshold. This calculation operation was repeated for three channels, red, green and blue. The red channel is mainly used for the optic disc extraction because the redlayer of an image is empirically determined to be dominant over green and blue components. The next step is the suppression of blood vessels using morphological operations. The final step of segmentation operation is optic cup extract which is performed by calculating maxim in pixel in the optic disc and the rest pixels, then subtract the value of each pixel from the maximum pixel the threshold of the optic cup is calculated by subtracting the mean of the different pixels from the maximum pixel. The local dataset contains 63 images with glaucoma and 38 normal images, the classifier of the proposed method for diagnosing the disease has not been mentioned by researchers, and the accuracy reached 83.168%.

4- (Kavya and Padmaja, 2018) detected glaucoma by texture features extraction, their method summarized by contrast enhancement of the RGB

input images using adaptive histogram equalization and employment k-means clustering and Circular Hough Transformation to segment the optic disc, and Markov Random Field (MRF) and GLCM like Contrast, Correlation, Energy and Homogeneity are applied to extract texture features. SVM is used to classify images into healthy or glaucoma. The proposed mothed tested 50 images collected from Drishti dataset which includes 101 images. The accuracy of optic disc segmentation by Hough Transform and k-means was 94% and 84% respectively, while the accuracy of glaucoma detection was 86%.

5- (Pathan, Kumar and Pai, 2018) proposed an automated glaucoma detection method using RIM-One3 dataset which composed of 124 retinal fundus images. Initially, blood vessels in painting is performed by extract red, green and blue channels from the retinal image and applied median filtering and Laplacian filtering on each channel, the results of each channel are concatenated to obtain an image with in-painting blood vessels. Feature extraction involves texture features and color features are extracted from blood vessels in-painted images. Grey Level Co-occurrence Matrix (GLCM) is used for extracting texture features. Color features include variance, mean, skewness, entropy, standard deviation. Support Vector Machine (SVM) and Artificial Neural Network (ANN) are used for classification which achieved an accuracy of 92% and 94.7% respectively.

6- (X. Zhao *et al.*, 2019) introduced an algorithm to calculate Cup to DiskRatio which comprised of three stages, in the first stage, the top-hat andbottom-hat transformations are applied together on the retinal image toenhance the optic disc region, then extract blood vessels using ContrastLimited Adaptive Histogram Equalization (CLAHE) and top-hat andbottom-hat transformation, finally, enhanced optic disc region with theblood vessels

is combined to obtain the region of interest (ROI). The opticdisc and cup are segmented in the second stage using an improved U-shapedconvolutional neural network named Deep Fundus Segmented In the third stage, theCDR is calculated by dividing the region of the optic cup by dividing theregion of the optic disc. The datasets used are ORIGA, DRISHTI-GS1 and28local fundus images, the dice coefficient CDR of ORIGA dataset was 0.054.

7- (Talaat *et al.*, 2019) offers a proposed algorithm to glaucoma diagnosis based on the texture and statistical features for the region of opticnerve head. The optic disc is cropped manually from the retinal images, thenthe resizes operation is applied to the cropped images by 256×256, nextgeneration of the CIELAB and HSV is done from the original RGB images.In order to remove any noise which may contain in the acquisition process of image, the median filtering is performed with a kernel 3×3 kernel to all channels. Both CLAHE and HE are done to contrast enhancing. To extract feature, statistical features are utilized to calculate illumination ofthe optic disc which are (super pixels, mean, skewness) and contrast (interquartile range (IQR), kurtosis, variance), textural features are applied using RLM and GLCM in the directions (0^O, 45^O, 90^O, 135^O), and the average of overall characteristics of regions is computed. To get the most relevant features set, information gain is carried out. The classifier used is SVM with Radial Basis Function (RBF) and linear for classification, Best result was 92.5% of accuracy, 95.0% of sensitivity and 90.0% of specificity when textural features calculated from (HE) of CIELAB channel. The dataset used is a public dataset offered by "REFUGE challenge" which involves 40 healthy and 40 glaucomatous retinal images.

8- (Kanchana and Naga Kiran, 2019) designed a method for glaucoma detection. They use the Cup to Disc Ratio (CDR) and the Rim to Disc Ratio as their two

glaucoma markers (RDR). By using morphological procedures and the Otsu Threshold on the green channel of the retinal fundus picture, the optic disc and cup are segmented. The optic disc region is subtracted from the neuro-retinal rim (NRR), which is then subjected to the ISNT rule in order to determine the value of RDR. The dataset used is DIARETDB1, which contains 60 image, and Support Vector Machine (SVM) is employed as a classifier. The accuracy of this method was 94%.

9- (Carrillo *et al.*, 2019) proposed a method to diagnose glaucoma by measuring the ratio between the optic cup area and the optic disc area through (CDR) indicator which is a measure of the thickness of the "RetinalNerve Fiber Layer" (RNFL). The channel used to get the segmented optic disc is the red channel by fixingan initial threshold to determine the optic disc location. For estimating the average number of pixels needed to be considered an optic disc, a parameter "*P*" is computed depending on the retina diameter, the parameter "*P*" will beas a reference to find segmentation threshold. The image histogram which starts from 0 to 255, if the number of pixels between two sequential grayscale tones is larger (*P*), then it calculates the pixel ratio between the two grayscale tones and chooses the largest tone as the threshold if that ratio exceeds 10%. The blue channel is utilized to segment the optic cup. The optic disc region is divided into four segments: “Inferior, Superior, Nasal and temporal" according to ISNT rule. To detect the blood vessels boundaries within the optic cup, the first the 3 segments are employed to this purpose, while the temporal region is used to identified the cup external boundary. The dataset obtained from a "Center of Prevention and Attention of Glaucoma in Bucaramanga, Colombia" which involves 26 images and the percentage of success for glaucoma detection was 88.5%.

10- (H.Samawi, & A.Yousif, *et al.*, 2020)This study presented an automated

method for the development of OD segmentation by combining morphological techniques and intensity thresholding to obtain accurate detection of OD. Accuracy OD segmentation is a very important factor, this method gives smoothness and accuracy from the required OD limits and speeds up the detection of OD and segmentation even if it is cut off by blood vessels. The proposed method was applied to DRISTHI, MESSIDOR, DRIONS, DIARETDB0, DIARETDB1 different datasets, and the results were excellent and promising. Many medical and statistical advantages were relied upon to identify whether the eye was affected or not, such as cup-to-disc ratio, optic disc space, and blood vessels. The classification ANN algorithm was adopted. And the average accuracy for all data sets used was 97.12%.

11- (Rutuja Shinde, 2021) developed a desktop program as a component of an automated CAD system to identify glaucoma utilizing fundus images of the retina and input photos into the system using a (LeNet) deep learning approach, where ROI extraction was demonstrated using the brightest spot algorithm. To increase the precision of ROI recognition, the image was made grayscale and underwent Gaussian haze preprocessing. As additional choice criteria for glaucoma identification, three features—CDR, NRR ISNT, and ISNT angiogenesis ratio were taken into consideration. A majority vote was secured for classification from SVM, ANN and ADABOOST algorithms. The image was distributed throughout the four quadrants of the ISNT using a two-dimensional mask that was similar to the input image. The ISNT ratio is subsequently computed using the picture area in each quadrant. A p-value of 0.05 or lower in this algorithm denotes the significance of the features and classifiers employed for glaucoma identification. And the Datasets used for training and testing is a RIM-ONE(169 image),DRISHTI-

GS(101image),DRIONS-DB(110image), NIO(118 image), JSIEC(124 image), DRIVE(44image)and APTOS dataset 130 images are glaucomatous while 120 images are normal. The accuracy of this method achieved 98.5%.

Table 1.1 Summary of the literature review

	Researcher	Year	Method	Indicator	Dataset	Accuracy
1.	Sarkar and Nag	2018	Image Processing	CDR	A local dataset (455)image	61%
2.	Guo et al.	2018	Image Processing with SVM	Cup Area Thickness ratio CDR	OREGA DRISHTI-(GS,GS1)	76.42%
3.	Dutta *et al.*, 2018	2018	Image Processing	CDR	A local dataset(101)image	83.16%
4.	Kavya and Padmaja	2018	Image Processing with SVM	Textures Features	50 image of (101) from Drishti dataset	86
5.	Pathan Kumar and pai	2018	Image Processing with SVM,ANN	Textures Features	RIM-ONE3(124) image	92% svm 94.7 %ANN
6.	X.Zhao et al.	2019	Image Processing with CNN	CDR	OREGA, Drishti, GS1 ,and (208)local image	CDR error of OREGA Was 0.054
7.	Talaat et al.	2019	Image Processing	Textures Features	REFUGE(80)image	92.5%
8.	Kanchana and Naga	2019	Image Processing with SVM	CDR,RDR,ISNT rule	DLSRETDB1(60)	94%
9.	Carrillo et al.	2019	Image Processing	CDR	(26)image	88.5%
10	H.Samawi and A.Yousif	2020	Image Processing with ANN	CDR,RDR,BVR	DRISHTI,MESSIDOR ,DRIONS	97.21%

11	Rutuja Shinde,	2021	Image Processing with SVM,ANN	CDR,NRR,ISNT	RIM-ONE 169 image,DRISHT1-GS(101)image	98.5% 98.5%

1.3 Statement of the Problem

previously learned about the danger of disease day after day, so it is possible to use the proposed system in conjunction with ophthalmologists in hospitals to diagnose the disease in the first stage of it in order to treat it before it becomes complicated and leads to blindness of the patient and also to reduce the time of diagnosis by doctors. It is necessary to work on detecting glaucoma and it's firstly stages in order to detect early effective treatment that protects against vision loss. The current method of manually evaluating and detecting glaucoma is expensive and requires a trained ophthalmologist.

1.4 Aims of the Study

This study aims at:

A. Building a prediction system to identify the person who needs examination to detect and diagnose the level of glaucoma (early, moderate, and severe).

B. Proposing algorithm developed for Inferior, Superior, Temporal, and Nasal Quadrant Mask Creation for Neuro Retinal Rim and Blood Vessels, in order to get better feature extraction and reduce execution time.

C. Proposing algorithm developed for scattering features random, in order to train Artificial Intelligence algorithms more efficiently and effectively to prepare them for upcoming complex cases.

D. Proposed algorithm for identifying and segmenting of optical disc and optical cup.

E. Increasing the number of extracted features due to reaching the score for more accuracy and focusing on some of these features more than the rest.

F. Use machine-learning concepts to classify the retina image in order to diagnose glaucoma and machine-learning based neural network models and evaluate its performance.

1.5 Main Contributions of Thesis

A. The development of a single system that can diagnose glaucoma cases and their levels according to the approved characteristics such as the optic disc, blood vessels and other parts of the eye that may be affected by the aforementioned disease.

B. Achieving the results of the system compared to the results of previous researchers.

C. A fully automated localization method for the optic disc can give robust and accurate results.

1.6 Thesis Outline

The thesis consists of five chapters and their description is briefly given below.

Chapter One: (Introduction)

This chapter provided an overview of the disease and previous research, as well as some difficulties, objective, and problem statement.

Chapter Two: (Theoretical Background)

The positional architecture of the eye is briefly discussed in the scientific introduction to this chapter. Now let's talk about the basic segmentation process and the difficulties it faces. Methods for feature extraction and concepts related to machine learning are also covered. A few specifics about the condition's levels and evolution. Finally, the four performance metrics reach a conclusion.

Chapter Three: (The Proposed System)

This chapter presents the proposed glaucoma diagnostic system and explains the stages of the designed system, some classification algorithms that are used in classifying the disease and also the grading algorithm for the aforementioned disease.

Chapter Four: (Results and Discussions)

The different results of all the examined pathways are displayed and examined in order to understand the importance and effectiveness of each of

them. Furthermore, a comparison is made between them. Finally, the most promising result are promoted.

Chapter Five: (Conclusions and Suggestions for Future Works)

A conclusion of the work and the related results are discussed. Besides, further works to improve this work are suggested.

Chapter Two: Theoretical Background

2.1 Introduction

Glaucoma is described as a neuropathy that affect the retina is an eye condition that can lead to blindness or vision loss. Glaucoma causes fluid to accumulate in the eye, which increases pressure on the eye's back. Due to the optic nerve being damaged by this pressure, visual loss results. Front vision is frequently compromised first, then the side vision (Thakkar *et al.*, 2017).

In a healthy eye, the retina converts the light rays falling onto it into impulses and sent to the brain through the optic nerve, at this moment only they are distinguished as an image, in glaucoma eye, the nerve fibers are damaged and the blind spot is unable to discover, and the case may develop to leads to damage of optic nerve (Rot *et al.*, 2020).

The increased intraocular pressure that causes glaucoma is the result of an imbalance in fluid flow when the eye produces a lot of fluid or the system ofdrainage is blocked .As Show in Figure(2.1) (Manikandan *et al.*, 2019).

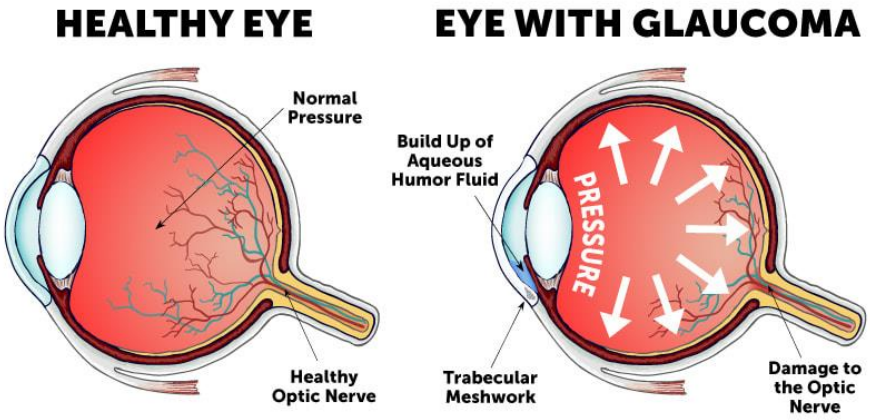

Figure 2.1 Normal and abnormal eye

The structural changing of the optic nerve head leads to disorder in peripheral vision and the patient feels as if looking through a tunnel Figure (2.2**)** depicts the progressive loss of vision due to glaucoma, as the advance of glaucoma, a patient's field of vision slowly narrows down, severeglaucoma without appropriate treatment cause of main vision loss, and blindness if remaining untreated (Kumar *et al.*, 2019).

Figure 2.2 Progressive loss of vision

(JKS Parihar et al. 2017)

2.2 Analysis of Retinal Fundus Images

The inside, posterior surface of the eye is depicted in the fundus image. The vascular system has both large, dark blood vessels and small blood vessels, and it is made up of the retina, macula, optic disc, and fovea. As show in Figure (2.3) displays a color image. (Sambandam. 2018).

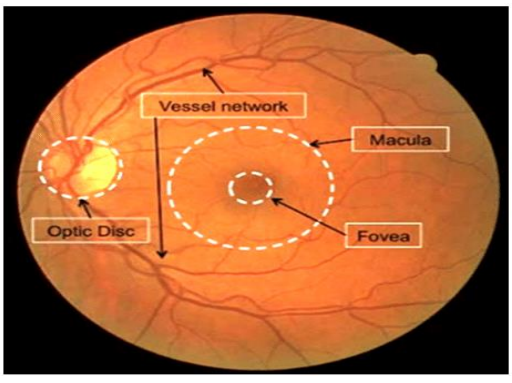

Figure 2.3 Digital photograph of the retina image

(Nugroho, Hanung Adi et al.2018)

2.2.1 Macula

Retinal macula is the light-sensitive tissue layer located at the back of the eye, and it is the central point of the retina which central vision responsible. In the center of the macula as show in Figure (2.4), there is a small depression called the fovea.(Al-Bander *etal*.2018).

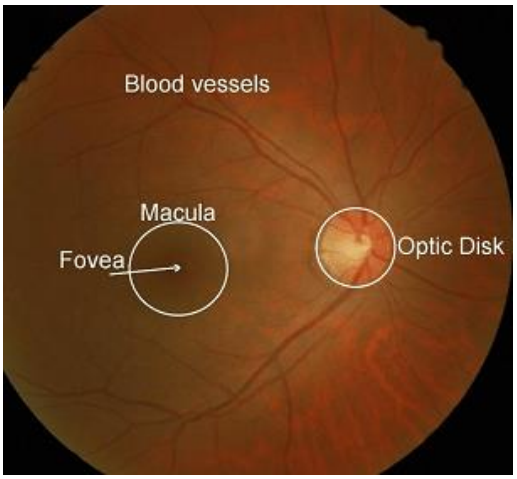

Figure 2.4 Localization of the macula and fovea

(Veras, Rodrigo & Medeiros et al.2013)

2.2.2 Optic Disc

OD segmentation plays a key role, that's gained a lot of attention from researchers and clinicians. OD detection often represents a main step in detecting other anatomical structures (Fan *et al.*, 2018).as show in Figure (2.5).

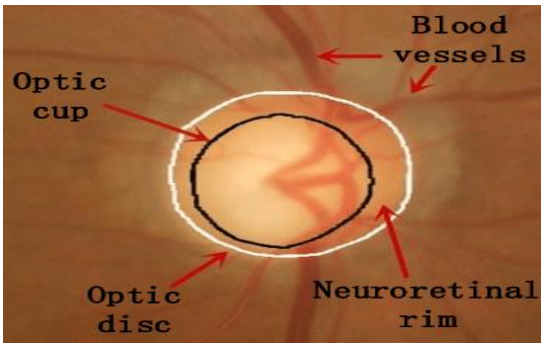

Figure 2.5 Optic disc components

(Gao, Yuan et al. 2019)

2.2.3 Vascular Network

It is so important to detect vessel networks which comprise of arteries and veins, The blood vessels are considered to be less reflective, for that reason, they appear darker. Process of extract vessel network is having tiny blood vessels,complex vessels network, and lopsided illumination when it can be difficult to acquire images from retinal images. (Hassan *et al.*, 2017).

2.3 Abnormalities Associated with Glaucoma Eye

Lately, the automatic identification and detection of anatomic retinal structures from digital fundus images have been attracting growing attention in the community medical image processing, this may help the development of (CAD) tools for better eye disease manage (Al-Bander et al., 2018).

2.3.1 The Variance of the Optic Disc

When glaucoma occurs more fibers of the optic nerve disappear, size of the optic cup becomes larger. Change in the cup size is analyzed by taking cup-disc ratio (CDR). The ratio can be defined in the area of both optic cup and optic disc. The indicator (CDR), as in Figure (2.6) is used to comparea normal eye with glaucoma (Fernandez-Granero *et al.*, 2017).

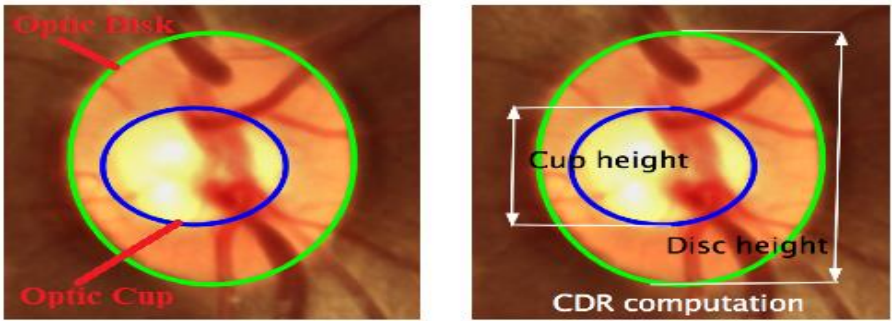

Figure 2.6 Cup to Disc Ratio (CDR)

(Kumar, J.R.H et al. 2019)

The following equation(2.12) is calculated (CDR).

$$\text{CDR} = \frac{OC\ Area}{\text{OD Area}} \qquad (2.1)$$

when the CDR value of the images feature is higher than 0.3, it is considered as glaucoma effected eye, otherwise, it is considered uninfected (Sujithra et al.2018).In Figure (2.7a) the region with white circle is the optic disc.And the optic cup is located optic disk, the eye is normal because the value of (CDR) is less than 0.3, whereas image in Figure (2.7b) is affectedby glaucoma due to the (CDR) value is large than 0.3.

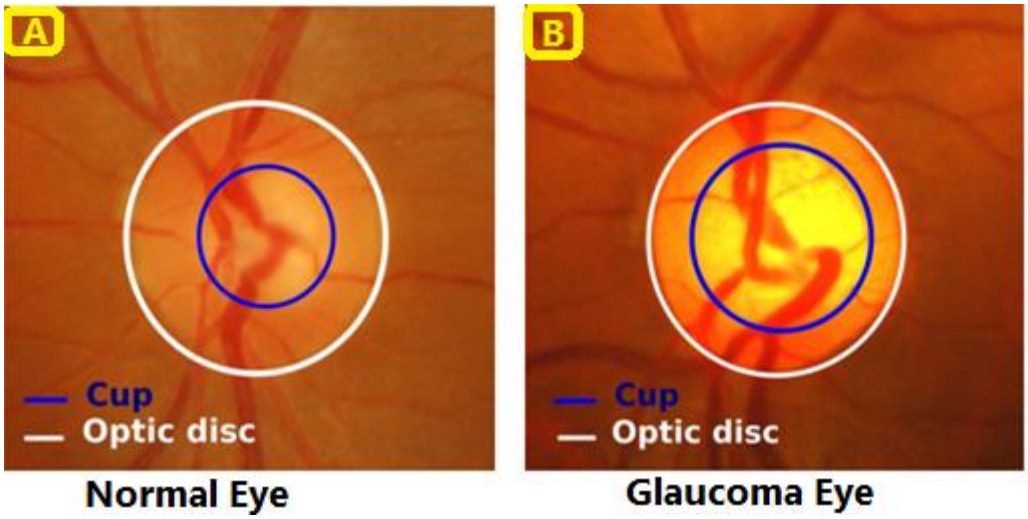

Figure 2.7 Fundus image for eyes

(Das, P., Nirmala, S.R. et al. 2016)

2.3.2 Loss of Neuro Retinal Rim (NRR)

The region between the optic disc and optic cup is called neuro retinal rim. **(**Poon LY *et al.*, 2017).

2.3.2.1 Inferior, Superior, Nasal, Temporal (ISNT) Rule

It contains neuro retinal rim elements. Figure (2.8) shows the characteristic patters of neuro retinal rim in normal images. Its length is not constant in all regions, it follows ISNT rule in normal eye. This rule says that the length of neuro retinal rim is more in inferior region then superior region, followed by nasal and at last temporal region. In glaucoma patients neuro retinal rim will notfollow ISNT rule.(Chethan K.et al.,2017)

Loss in fiber-optic nerves conduces to a changing in the composition structural ofthe OD, namely, the enlargement of cup region and neuro retinal rim thinning called cupping (Sedai *et al.*, 2017). Figure (2.8 a) shows that the healthy eye satisfies the ISNT rule, whereasthe affected eye breaks this rule as shown in Figure(2.8 b).

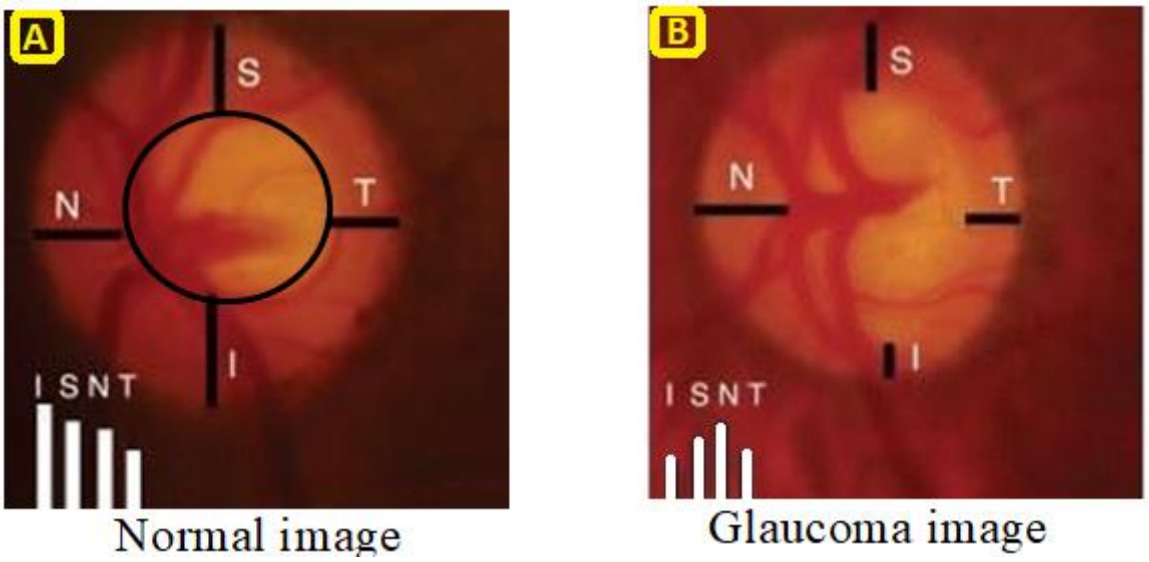

Figure 2.8 Characteristic of Retinal Image

(**Juan J. Gómez-Valverde et al. in 2019**)

Along with CDR neuro-retinal rim also plays an important role in glaucoma identification. So, rim to disc ratio need to be calculated.Retinal fundus image will treat as glaucomatous if the (RDR) value was equal or less than 0.5, otherwise, it considered to be normal. People may misdiagnose if cup to disc ratio alone is considered (Kumar, J.R.H. *et al.*, 2019).

Temporal quadrant is the leftmost for the right eye and nasal quadrant for the left eye and vice versa as shown in the following Figure (2.9) (Haruta, Kodama and Yamakawa, 2017).

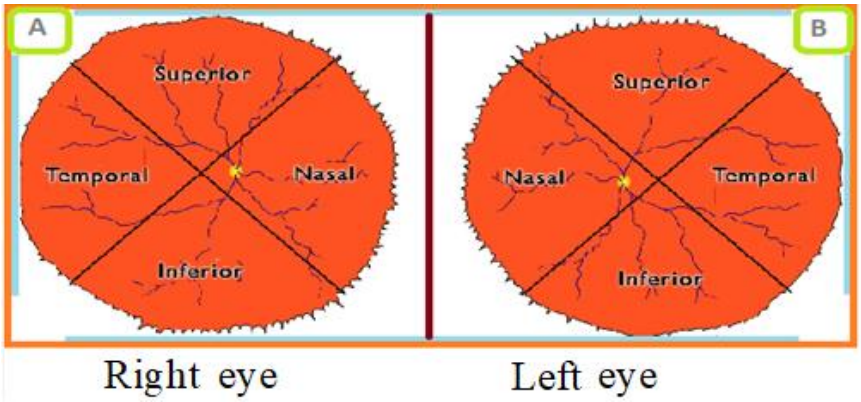

Figure 2.9 ISNT for eyes.

(Kumar, Jayant & Kohli, et al. 2021)

ISNT ration computes by below Equation (2.2).

$$ISNT\ Ratio = \frac{\text{NRR in inferior regin} + \text{NRR in Superior region}}{\text{NRR in Temproal regin} + \text{NRR in Nasal region}} \qquad 2.2$$

In the normal eye the value of ISNT ratio is less than ISNT ratio in glaucoma eye.

2.3.2.2 Rim to Disc Ratio

CDR It is considered one of the medical feature that play an effective role in detecting glaucoma. The Rim to Disk Ratio (RDR) need to be computed (RDR) is calculated for the inferior and superior quadrant as the ratio of the rim area to the disk area as show in equation (2.3).

$$RDR = \frac{(\text{Superior} + \text{Inferior})}{\text{Optic Disk Area}} \qquad 2.3$$

Now, in more from related works the value of feature for RDR was equal or less than 0.5 referee the eye is glaucoma. (Seelamantula. et al. 2019).

2.3.3 Variance of the Blood Vessels in the Optic Disc

When the cupping occurs, the blood vessels in the optic disc will be

high density in the left or right side compared to the healthy eye, this status appears clearly in moderate and severe cases, as shown in the Figure (2.10), in order to know the variance, Blood Vessels Ratio (BVR) is computed which equal summation the blood vessels in inferior and superior regions dividing by summation the blood vessels into temporal and nasal regions, as show in equation (2.4). (Shyam and Kumar, 2017).

$$BVR = \frac{\text{BV in inferior regin} + \text{BV in Superior region}}{\text{BV in Temproal regin} + \text{BV in Nasal region}} \qquad 2.4$$

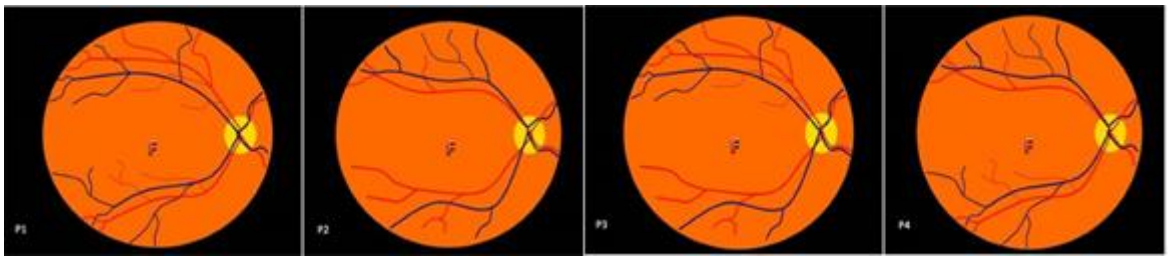

Figure 2.10 Stages of the blood vessels direction

(Oztas, Z., Akkin, 2017)

2.4 Dataset

The dataset used is ORIGA^{light} ("Online Retinal Fundus Image Database for Glaucoma Analysis and Research").

ORIGA dataset contains 650 retinal images with resolution 3072 * 2048 pixels, accompanied by annotations from Singapore Eye Research Institute's experienced professionals.168 glaucomatous images and 482 healthy photos are among a large number of important visual indicators for glaucoma diagnosis.

2.5 Image Cropping and Scaling

Cropping is one of the most fundamental image editing techniques, and it is used to eliminate unwanted objects or unimportant noise from a photograph's peripheral. Cropping is the elimination of unwanted portions from the outskirts of a photographic or graphical image, and to get rid of dark areas. (Wikiwand, 2011). As in the formula (2.5)

$$Crop\ Images = imcrop(InputImage, [L1 * m, L2 * n][W1 * m, W2 * n]) \quad 2.5$$

The “L, W” height and width for size crop of fundus image.

Resizing a digital image is known as image scaling. An image becomes smaller as it is scaled down, and larger when it is scaled up. Raster and vector graphics can both be scaled, but the outcomes are different. As in the formula (2.6).

$$ResizeImage = imresize(InputImage, TargetImage[m.n]) \quad 2.6$$

the “m”,”n” are the number of rows and columns.

2.6 Contrast Adjustment

The basic meaning of adjusting contrast is a procedure after adjustments, such as an increase or decrease in the value of a color pixel (contrast of an image) without regard to the properties of its neighbors. In the point process there is no change in image size or geometry (Zohra, B. F. and Mohamed, B. 2009). .As in the formula (2.7 and 2.8).

$$AdjustedImg. = imadjust(InputImage, [Rl, Gl, Bl, Rh. Gh, Bh,]) \quad 2.7$$

$$\text{Adjusted}Img. = (InputImage, [RGBlow\ input, RGB\ high\ input]) \quad 2.8$$

2.7 Morphological Operation

Morphological operations apply a structuring element to an input image, creating an output image of the same size. In a morphological operation, the value of each pixel in the output image is based on a comparison of the corresponding pixel in the input image with its neighbors.

Morphology is a mathematical operation that processes the main adjacent images of graphics and changes or shapes that are not available from the morphological operations program in the form of a structuring element, which indicates the creation of an image of the same size. In a morphological process, in the form of a mathematical model (Haggerty et al., 2014).

There are two basic morphological operations: dilation and erosion, closing and opening are two derived operations in terms of dilation and erosion. Here a brief introduction to the morphological operations.

Structuring Element: It is a matrix or a small-sized template that is used to traverse an image. The structuring element is positioned at all possible locations in the image, and it is compared with the connected pixels. It can be of any shape.

Fit: When all the pixels in the structuring element cover the pixels of the object, we call it Fit.

Hit: When at least one of the pixels in the structuring element cover the pixels of the object, we call it Hit.

Miss: When no pixel in the structuring element cover the pixels of the

object, we call it miss. As show in Figure (2.11).

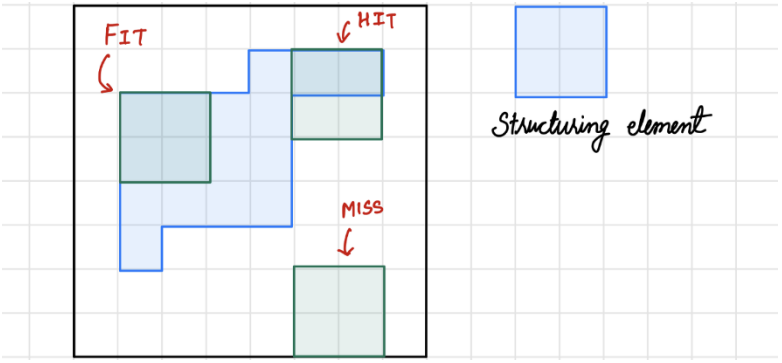

Figure 2.11 Morphology terminologies explained

Sometimes, the structuring element is called "kernel", but this word is reserved for specific objects used in operations of convolutions. The structuring element comprises of a pattern determined as the coordinates of several discrete points relative to some origin. The different structuring elements of varying sizes are shown in Figure (2.12). The origin in each case is identified with a ring around that point. The origin must not be at the center of the structuring element but is often. The most commonly seen form of structuring elements fitting into a 3 * 3 grid and its origin in the center.

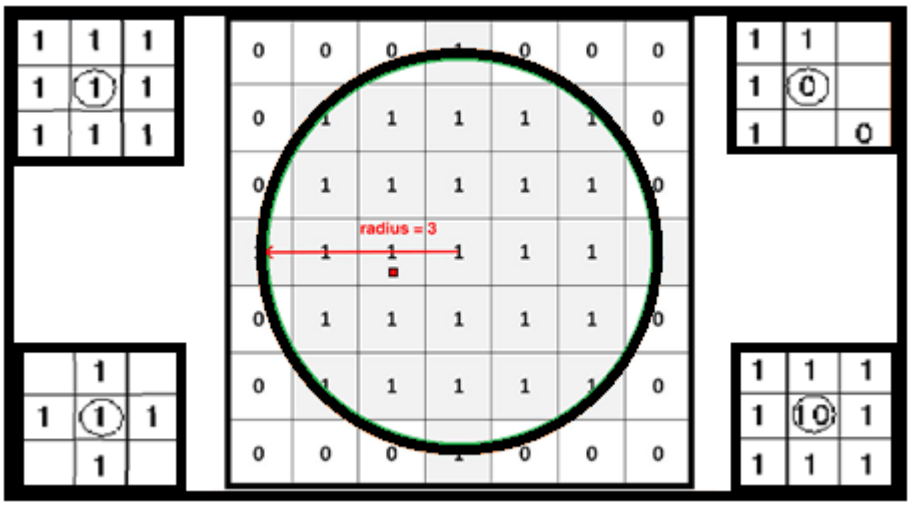

Figure 2.12 Some cases of the structuring elements

(Haggerty, Juliana & Wang et al. 2014)

Every point of the structuring element can have value. In the simplest structuring elements utilized with the binary images for operations like erosion, the elements have only one value, appropriately represented as a one. More complex components, including those used for morphological operations on a grayscale, can have other pixel values.

2.7.1 Dilation and Erosion

Dilation and erosion are among the simplest morphological processes. Dilation adds a pixel to the object boundaries in an image, while erosion removes a pixel at the boundaries of objects. The shape and the size of the structuring element used are determined by the number of the pixels which are removed or added to the objects in an image. In the morphological erosion and dilation operations, the status of any given pixel in the output image is calculated by applying a rule in the input image to the relevant pixel and its neighbors of the input image. The rule used to handle the pixels determines the process as dilation or erosion.as Figure(2.13) displays erosion and dilation rules (Mitra, 2014).

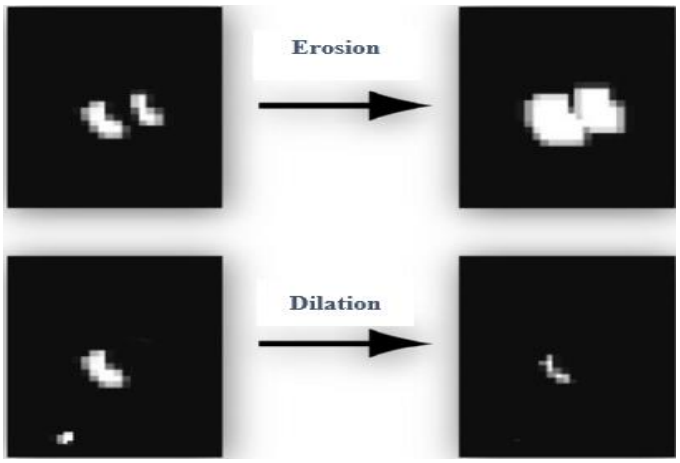

Figure 2.13 Erosion and Dilation

(Ikebe, Masayuki et al. 2005)

The following Figure (2.14) explains the binary image dilation. Note the structuring element defining to the neighborhood of the pixel of interest, which is circled. The dilation function performs a convenient rule on Neighborhood pixels and gives a value to the respective pixel in the output image. That the morphological dilation function assigns the output pixel value to 1 because one of the elements identified by the neighborhood structuring element is one.

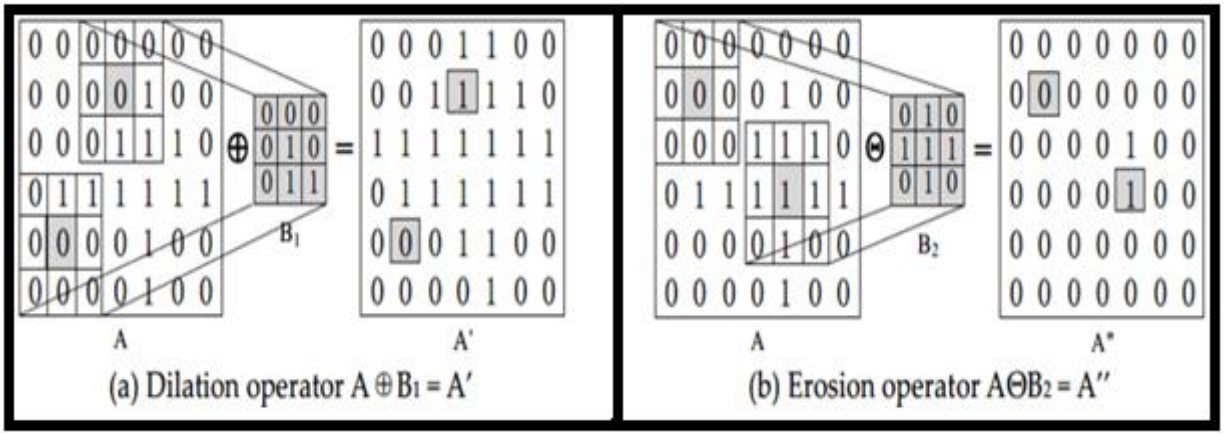

Figure 2.14 Morphological dilation for a binary image

(Zhang, Yunfei, et al. 2020)

2.7.2 Closing and Opening

The main operations of erosion and dilation are generally sequentially applied using a single structuring element. Those processes together are closing and openings.

The closing operation comprises a dilation followed by an erosion. Opening reverses, the order of operations (Davies, 2017), as the following equation (2.9 and 2.10):

$$\text{Closing: } A \bullet B = (A \oplus B) \ominus B) \qquad (2.9)$$

$$\text{Opening: } AoB = (A \ominus B) \oplus B) \qquad (2.10)$$

2.8 Image Segmentation Fundamentals

Image segmentation is one of the most important steps for feature extraction and analysis. The goal is to segment images into parts with homogeneous properties over space and time, such as color, texture, motion, and spatial-temporal structures. This can be formally defined as follows: if F is the set of all pixels in an image, and (M) is the measure of homogeneity of an area of connected pixels, then segmentation is a partition process which divides F into a subset of connected pixels n F1, F2,…, Fn such that:

$$M(Fi) = true \forall i \in \{1, \ldots . n\} \qquad (2.11)$$

$$M(Fi \cup Fj) = false \; if Fi \; is \; adjacent \; to \; Fj \qquad (2.12)$$

$$\bigcup_{i=1}^{n} Fi = F \; And \; Fi \cap Fj = \emptyset \; if \; i \neq j \qquad (2.13)$$

Image segmentation can be divided into at least two phases that have different definitions of homogeneity. The first phase is a partial segmentation, in which extracted regions with homogenous features do not correspond directly to semantic objects. The second phase is a complete segmentation, which results in semantic objects with their underlying regions. While partial segmentation can be achieved using some general algorithms, it usually requires specific domain knowledge to obtain a complete segmentation (Vyas, Yu and Paik, 2018). There are many types of image segmentation:

2.8.1 Segmentation Based on Edge Detection

Edge detection is an image processing technique for finding the boundaries of objects within images. It works by detecting discontinuities in brightness. Edge detection is used for image segmentation and data extraction in areas such as image processing, computer vision, and machine vision. And it's a Fundamental tool used in most image processing applications to obtain information from the frames as a precursor step to feature extraction and object segmentation. This process detects outlines of an object and boundaries between objects and the background in the image.

Physical edges provide important visual information since they correspond to discontinuities in the physical, photometrical and geometrical properties of scene objects. The principal physical edges correspond to Signiant variations in the reactance, illumination, orientation, and depth of scene surfaces. Since image intensity is often proportional to scene radiance, physical edges are represented in the image by changes in the intensity function. (Esmaeili, M, 2009). Edge detection is a technique of image processing used to identify points in a digital image with discontinuities, simply to say, sharp changes in the image brightness. These points where the image brightness varies sharply are called the edges (or boundaries) of the image.

Methods of Edge Detection

1- **Prewitt edge detection:** This method is a commonly used edge detector mostly to detect the horizontal and vertical edges in images.

2- **Sobel edge detection:** This uses a filter that gives more emphasis to the centre of the filter. It is one of the most commonly used edge detectors and helps reduce noise and provides differentiating, giving edge response simultaneously.

3- **Canny edge detection:** This is the most commonly used highly effective and complex compared to many other methods. It is a multi-stage algorithm used to detect/identify a wide range of edges.

4- **Laplacian edge detection:** The Laplacian edge detectors vary from the previously discussed edge detectors. This method uses only one filter (also called a kernel). In a single pass, Laplacian detection performs second-order derivatives and hence are sensitive to noise. To avoid this sensitivity to noise, before applying this method, Gaussian smoothing is performed on the image. As show in Figure (2.15).

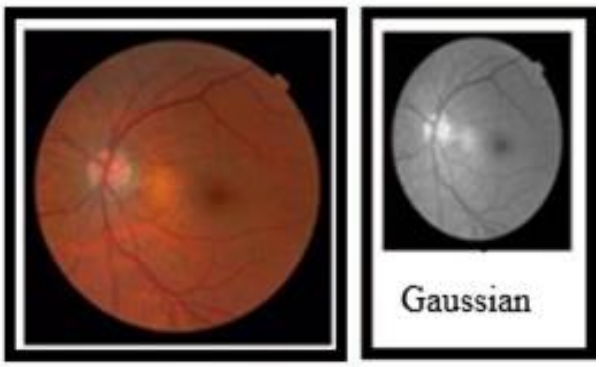

Figure 2.15 Gaussian smoothing for fundus image

2.8.2 Segmentation by Threshold

Threshold is one of the most effective methods for segmentation of images. Suppose that the histogram of intensity corresponds to an image, $f(x, y)$ consisting of light objects in dark background, As shown in Figure (2.16). (Liao, Chen and Chung, 2001).

Defining of Binary by Threshold (*T*) for image g(x, y) is shown in the equation (2.14) below:

$$g(x,y) = \begin{cases} 1 & if \quad f(x,y) > T \\ 0 & if \quad f(x,y) \le T \end{cases} \tag{2.14}$$

Where T is the threshold, g(x, y) = 1 for image elements (pixels) of objects (or any other convenient intensity) and g(x, y) = 0 for image elements of the background**.**

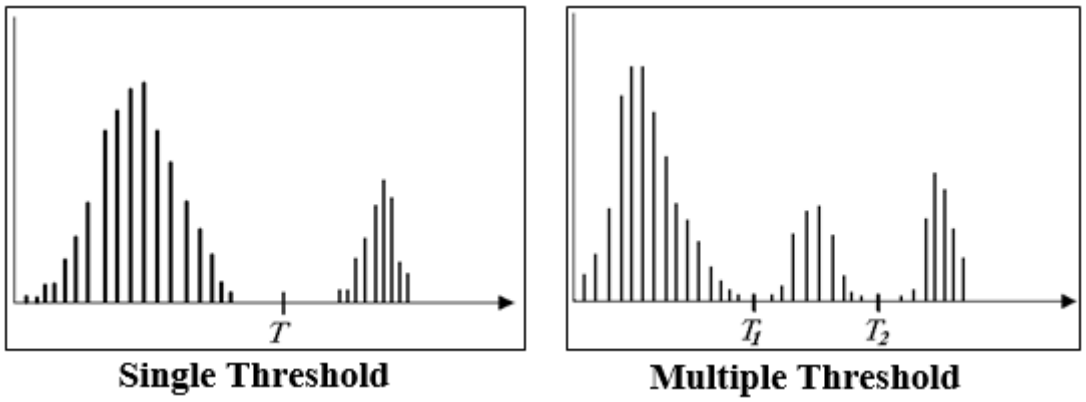

Figure 2.16 Threshold Types

(Ehsani Rad, Abdolvahab et al. 2013)

2.9 Features Extraction

Is the method to describe a set of features, or characteristics of the image, what will represent the information most effectively or meaningfully important for analysis and classification.

The aim of extracting features is to improve the efficiency and effectiveness of analysis and classification. This can be done via (Tian, 2013).

1- Removing redundancies in image data.

2- Remove variability in image data which is of little to no interest in classification and discard whole images if possible.

3- Rebuilding the data (in feature space) to improve the classifierperformance.

4- Extraction of spatial information (shape, size, texture, -----) which is keyto identifying the target.

Feature extraction has applied to the images in order to extract some features and represented them as a feature vector.

The definition of the feature is that it is a function of one or more measurements, each of which specifies a measurable quality of an item, and that computed so that it quantifies certain significant qualities of the object.

2.9.1 Texture Feature

The texture is a very useful property for a large range of images. Human visual systems are commonly believed to use texture for identification and interpretation. Generally, the color is typically a property of the pixel while the texture can be determined only from a set of pixels. A significant number of techniques for extraction texture features have been proposed. Dependent on the domain from which the texture features are taken, they can be mainly categorized into methods of spatial texture extraction methods of spectral texture extraction. For the first method, extraction of the texture features is done by computing the pixel statistics or finding the structures of a typical pixel in the original image domain, whereas, the extracting "spectral texture" is performed by transforming an image into the frequency domain and computed features from the transformed image (Tian, 2013).

An analysis of statistical texture, texture features are calculated from

the statistical distribution of observed groups of intensities at particular locations relative to each other in the image. Statistics can be classified into first-order, second-order and higher-order statistics according to the number of pixels in each group (M. Abdalla, Dress and Zaki, 2011).

2.9.2 First-Order Statistics

In the first-order, measures calculated from an individual pixel and do not consider pixel neighbor relationships.it includes the mean, standard deviation skewness and kurtosis (Nyein Hlaing,2015).as in equation (2.15) standard deviation(SD)is a measure of how dispersed the data is concerning the mean.

$$SDg = \sqrt{\sum_{g=0}^{l-1} ((g - \bar{g}))^2} \qquad 2.15$$

In fact the “g” is the pixel value that is ranged between 0 to 255,”L”is the color level that is ranged also between 0 to 255,”$\bar{g}$” is the mean of g,”p(g)” is the probability of g .

2.9.3 Second-Order Statistics

Measures consider the relationship between neighbor relationships (Nyein Nyein Hlaing, 2015). The "Gray Level Co-occurrence Matrix (GLCM)" technique is a method for extracting second-order statistical texture features.GLCM presented by Haralick. It provides information about the locations ofpixels that have identical values of gray level (M. Abdalla, Dress and Zaki, 2011).

"GLCM" is a matrix in which the number of image rows and columns is equal to gray levels number, G. The matrix pixel P (i, j | d, θ) is the two-

pixel relative frequency, split by distance "*d*", in a particular direction by the specified angle *(θ)*, one for intensity *"I"* and the other for intensity *"j"*.Figure (2.17) shows Example of directional Analysis P0, P45, P90, and P135 (Kekre and Thepade, 2008).As show in Figure(2.17).

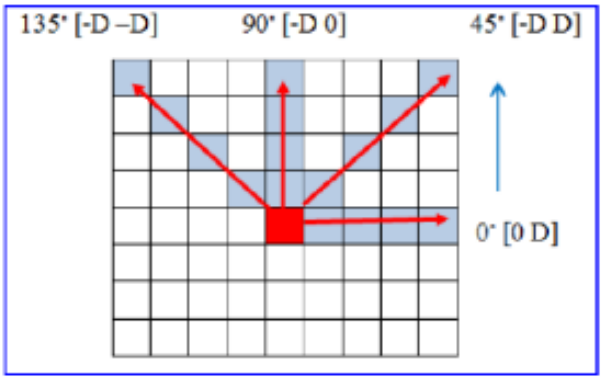

Figure 2.17 Geometry for measurement of gray level co-occurrence matrix for 4 distances d and four angles

(Mahmood et al. 2019)

Figure(2.18) depicts an example about construction of co-occurrencematrix with 8 gray levels calculated utilizing "one" for pixel distance and "Zero" degrees for direction. In this case, the element (1, 1) of matrix "g" isequal to 1 since it was only discovered once on the original image. In the same Fig for the element ("6, 2" is another example; Where three occurrences occur, since a pixel value of "6" has a pixel value of "2" immediately to the it's right. The other elements in "C" are calculated by the same method (Albregts.in 2008). As show in Figure (2.18).

Figure 2.18 Example about a generation of a Co-occurrence

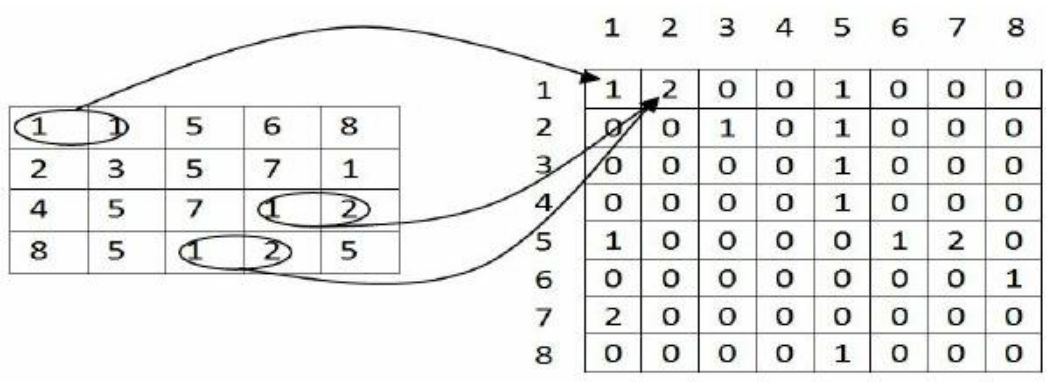

2.9.4 Eight Gray Levels Matrix

Four characteristics can be extracted from the co-occurrence matrix (g_d, Θ) that are as follows, where **i** reflects the row, **j** reflects the column and g (i, j) reflects the probability for every pair (i, j) in all the following equations.(Mohanaiah, Guru Kumar, 2013).

1- Energy**:** The measure provides information on how the spread of gray levels inthe image. The maximum value of energy is 1. When the energy is high mean that the number of the gray level in the image is few.

$$\text{Energy} = \Sigma_i \Sigma_j \, g(i,j)^2 \qquad (2.16)$$

2- Correlation**:** It is a measure of gray level linear dependence between the pixels at the specified positions relative to each other.

$$Correlation = \Sigma_{i,j} \frac{(i-\mu i)(j-\mu j)p(i,j)}{\sigma i \sigma j} \qquad (2.17)$$

3- Contrast**:** This measure is used to evaluate the intensity of the contrast betweenthe pixel and its neighbor on the whole image.

$$Contrast = \Sigma_i \Sigma_j \, (i,j)^2 \, g(i,j) \qquad (2.18)$$

4- Homogeneity**:** This feature measures the uniformity of the non-zero entries in the GLCM. If the GLCM concentrates along the diagonal GLCM

homogeneity of any texture is high, which means that there are manypixels with a similar of grey level values. When there is a large changein the value of the gray level, leads to low in GLCM homogeneity making higher in the GLCM contrast.

$$Homogeneity = \Sigma_i \Sigma_j \frac{1}{1+|i-j|} g(i,j \qquad (2.19)$$

2.9.5 Features Normalization

Normalization is a scaling technique in which values are shifted and rescaled so that they end up ranging between 0 and 1. It is also known as Min-Max scaling.

$$Norm\ Feature\ Vector = \frac{\text{Feature Vector} - \min}{\max - \min} \qquad (2.20)$$

Here, max and min are the maximum and the minimum values of the feature respectively.

When the value of X is the minimum value in the column, the numerator will be 0, and hence X’ is 0.On the other hand, when the value of X is the maximum value in the column, the numerator is equal to the denominator and thus the value of X' is 1.If the value of X is between the minimum and the maximum value, then the value of X’ is between 0 and 1. (Aniruddha, 2020).

2.10 Image Classification (Machine Learning)

The human classification of features in an image uses the visual interpretation elements to determine homogeneous groups of pixels reflecting different characteristics. Classification of digital image utilizing the spectral information represented by digital numbers in one spectral band

or more and tries to classify every single pixel based on this spectral information. This type of classification is termed spectral pattern recognition.

In each case, the goal is to allocate all pixels in the image to specified classes or themes. The resulting classification image consists of a mosaic of pixels, every one of which belongs to them and is a thematic "map" for the original image**.**

2.10.1 Artificial Neural Network Classification

A neural system is displayed in the Figure (2.19), the number of neurons interconnected together forms the artificial neural network. The neural network consists of a number of simple processing elements called nodes. The neurons are connected with other neurons in accordance with the weights allocated to the correspondence, the weights involve data that a net uses it to deal with the problem. The neuron sends out activation signals to other neurons. The neural network is composed of one or more layers (Taylor, 2017), (Chakraverty, Sahoo and Mahato, 2019).

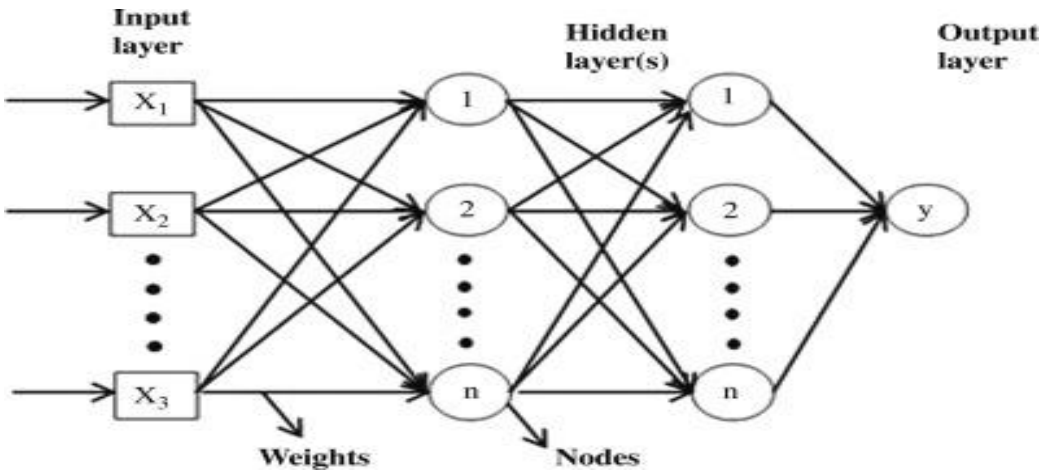

Figure 2.19 Artificial Neural Network Architecture

(Holmgren, G., Andersson et al. 2019)

The single layer weighted interconnection is present in a one-layer network, while in a multilayer ANN have input, hidden and output layers of neurons. The next movement of the neuron input layer represents the raw data that is sent to the system. In the hidden layer a neuron's movement is determined by the movement of input neurons and association weights at each input and also at the hidden layer of the units. The neuron movement in the output layer depends on the neuron movement in the hidden layer and the corresponding weights belong to the hidden and output layers. For a specific purpose, a trained neural network can be accomplished by changing the values that are connecting between the components. The neural networks are normally trained or modified to achieve greater accuracy when comparing target and output (Abiodun *et al.*, 2018), (Chakraverty, Sahoo and Mahato, 2019).

2.10.2 Support Vector Machine Classification

Support Vector Machine produces accurate classification results from complex and noisy data. Utilizing a decision surface that increases the margin between classes, it divides classes. The closest data points to the surface are frequently referred to as support vectors, and the surface is known as the ideal hyperplane. The support vectors are significant components of the training set. Nonlinear kernels are employed An SVM classifier may not be linear. In its most basic form, SVM can be a binary classifier. However, by merging several binary SVM classifiers, it can also function as a multiclass classifier (Build binary classifier for each possible class pair). For multiclass classification, SVM makes use of the paired classification method. The judgment values for each class of pixels used to estimate the success of SVM classification estimate the probability. The probability values saved as rule pictures are "true" in the sense that each

pixel's probability falls between 0 and 1, and the sum of those values is 1.

By selecting the scenario with the highest probability, SVM performs categorization. Pixels with all probability values below the specified threshold may be reported as unclassified pixels. SVM has a penalty parameter that permits some misclassification, which is important for non-separable training sets in particular. The trade-off between allowing for training errors and enforcing strict margins is controlled by the penalty parameter. It produces a soft margin that facilitates some misclassifications, such as allowing some training points to be located on the incorrect side of the hyperplane. Increases in the penalty parameter value result in higher costs for misclassification points and call for the development of more precise models, which may not be very broad. (Kowalczyk, 2017).

SVM classifier provides four types of kernels: radial basis function (RBF), linear, polynomial, and sigmoid.

The mathematical representation of each kernel is listed below:

$$RBF:\ K(x_i, xj) = \exp(-\gamma \left|\left|x_i\ Tx_j\right|\right|^{2}),\gamma > 0 \qquad (2.21)$$

$$Polynomial:\ K(x_i, xj) = (\gamma x_i\ Tx_j + r)\ d,\gamma > 0 \qquad (2.22)$$

$$Lienr:\ K(x_i, xj) = x_i\ Tx_j \qquad (2.23)$$

$$Sigmoid:\ K(x_i, xj) = tanh(\gamma x_i\ Tx_j + r) \qquad (2.24)$$

Where "**γ**" Is the gamma for all kernel forms accept linear in kernel function

"d" is the polynomial-degree concept for the polynomial kernel function.

"r" is the bias in the kernel function for the sigmoid and polynomial kernels.

"**γ**", "d" and "r" are parameters controlled by the user, when their correct

definition is high, the accuracy of the SVM solution increases.

Algorithm (2.1) SVM Classifier

Input: Feature vector of the training dataset, Feature extracted 'FE1 FE2…Fen'.

Output: Class label of input feature vector (test retina fundus image).

1: Start.

2: For the extracted for feature 'FE'.

3: Train 'FE' with re-sample randomly and replacement. Calculate the hypothesis 'Hi' of 'FEi'.

4: Perform majority voting of 'Hi'.

5: End.

6: Choose the kernel type for SVM.

7: Classify the test image according to the vector of the test image and train features vectors.

8: Return class label for the test image.

An SVM characterizes the information by seeking the perfect hyperplane that isolates all information purposes from the alternative category for one class. The SVM hyperplane comprises the one with the largest edge between the two classes. Margin means the maximal bit width parallel to the hyperplane, which does not have internal details (Zohra and Mohamed, 2009) (Kalra, 2016). The SVM classifier is shown in Figure (2.20 and 2.21), as algorithm (2.1) show steps of SVM classifier. (murty ,2016)

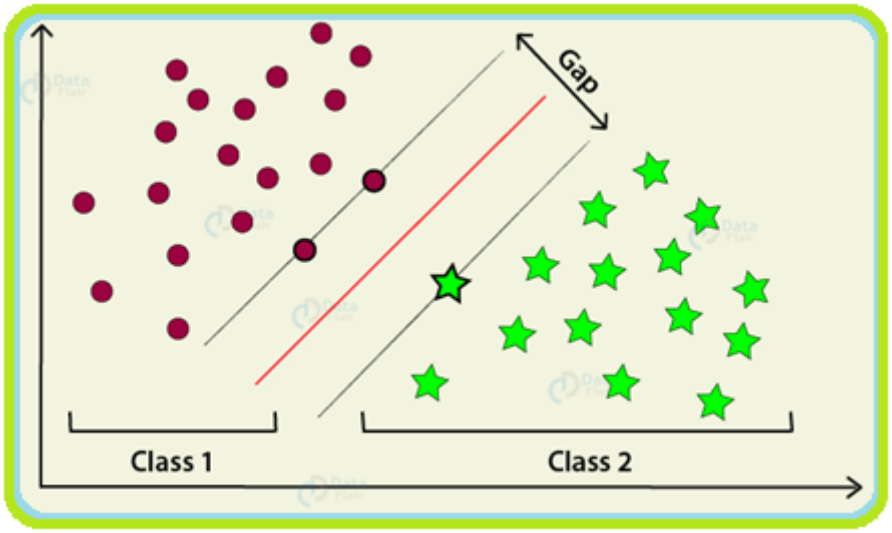

Figure 2.20 SVM

(Mustafa Sidhpuri ,2021)

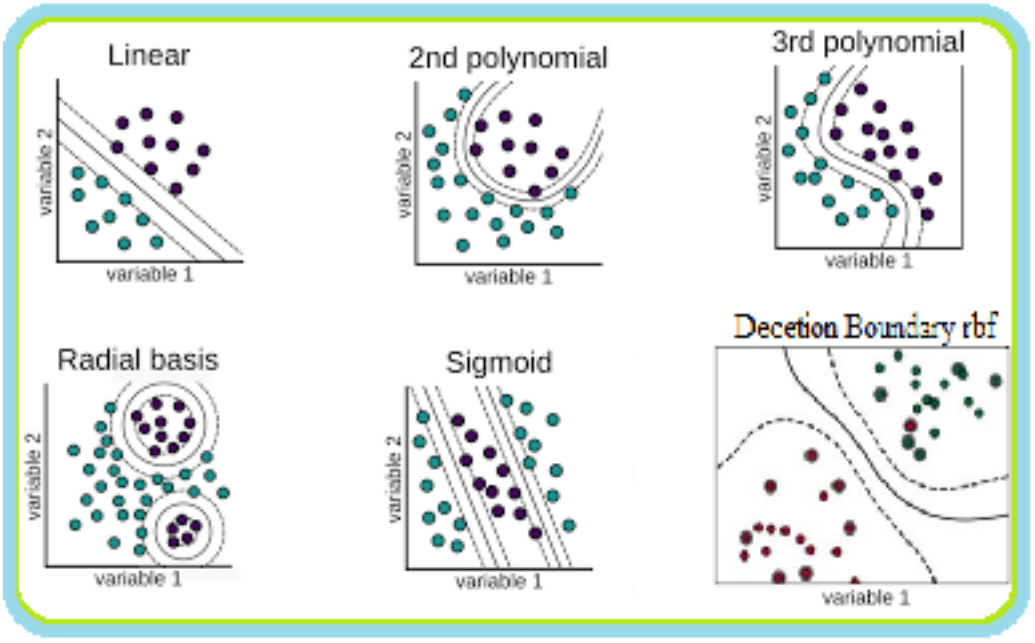

Figure 2.21 Types of Support vector machine kernel

2.11 Decision Tree Classifier

One of the reasons why can used decision tree is because it is an algorithm that usually simulates human thinking ability during decision making. And the goal of decision tree algorithm is to create a model that classifies a feature value, in which a decision tree uses a tree representation to solve the problem in which dependent values based on final values correspond to a class label.

2.12 Levels of Glaucoma Progression

It is very important to properly arrange the disease if you want to receive compensation for any actions you take. The decision tree algorithm identifies three levels of glaucoma (early, moderete , and Severe). Our clinical judgments must be guided by information and definitions from leading clinical trials in order to achieve the best results.(Zeyen TG, Caprioli J, 2014).

The normal cup to disc ratio (the diameter of the cup divided by the diameter of the whole nerve head or disc) is 0.3 (Marjanovic, I., 2011).

As for the moderate case of the disease, the value of the cup to disk ratio is (0.4<CDR<0.5). And (CDR>0.5) for severe stage (Jyoti Patil and Sharmila Chaudhari, 2021).

2.13 Evaluation Measures

The accuracy of the system has been evaluated utilizing popular measures such as "Accuracy", "Specificity", "Sensitivity" and "Precision" which explained in the Table (2.2). The "Confusion-matrix" supplies more

intuition classes are foreseeing suitably not only the performance of a predictive model, and which incorrectly, and error type are being created.

Table 2.2 Confusion matrix

	Positive Prediction	Negative Prediction
Positive Class	True Positive (TP)	False Negative (FN)
Negative Class	False Positive (FP)	True Negative (TN)

$$Accuracy = \frac{\mathrm{TP} + \mathrm{TN}}{\mathrm{TP} + \mathrm{TN} + \mathrm{FP} + \mathrm{FN}} \quad (2.25)$$

$$Sensitivity = \frac{\mathrm{TP}}{\mathrm{TP} + \mathrm{FN}} \quad (2.26)$$

$$Specificity = \frac{\mathrm{TN}}{\mathrm{TN} + \mathrm{FP}} \quad (2.27)$$

$$Precision = \frac{\mathrm{TP}}{\mathrm{TP} + \mathrm{FP}} \quad (2.28)$$

$$Area\ Under\ Curve = 1/2\left(\frac{\mathrm{TP}}{\mathrm{TP} + \mathrm{FN}} + \frac{\mathrm{TN}}{\mathrm{TN} + \mathrm{FP}}\right) \quad (2.29)$$

When (TP) is the number of abnormal fundus images classified as abnormal, (TN) is the number normal images classified as normal ,(FP) is the number of normal images classified as abnormal,(FN) is the number of abnormal fundus images classified as normal.(Idrees et al.,2017).

Chapter Three: The Proposed System

3.1 Introduction

In this chapter, can have provided an accurate description of the work of the proposed retinal fundus image diagnostics system in full detail. The general structure and all the algorithms used to build the system and reach the full and comprehensive results to solve the problem were also clarified. Started from the preprocessing stage and ended with the classification algorithms stage adopted in training and testing the software work.

3.2 Proposed System

The are two main stages of the suggested system are features extraction and classification. Pre-processing, Optic Disc Segmentation, Optic Cup Segmentation, Blood Vessels Segmentation, and Feature Extraction are the processes that these phases go through. Preprocessing includes cropping the input image, detecting the optic disc, determining the region of interest (ROI), enlarging the (ROI), and then automatically segmenting the optic disc, cup, and blood vessels. Then, a set of texture features is extracted for each optic disc image.

The classification contains two phases training and testing. The training phase revolves on built classifier structure from training about 70% from fundus retina images dataset that contains healthy and glaucomatous images. Testing for the new unlabeled (unclassified) retina fundus image is performed using "ANN" and "SVM" classifiers that built before in the training phase. Then the retina fundus image will be classified as “0” or “1”. The dataset used is "ORIGA" which includes 650 images of 168 glaucomatous images and 482 no glaucoma images, also in the second stage, took the cases in which the result of the classification was “1” only and

applied it according to the decision tree algorithm to find out whether the disease was in its condition (early, moderate or severe). As show in Figure (3.1).The accuracy of the system has been evaluated by utilizing popular evaluation mensuration such as "Accuracy", "Precision", “Sensitivity ", and “Specificity".

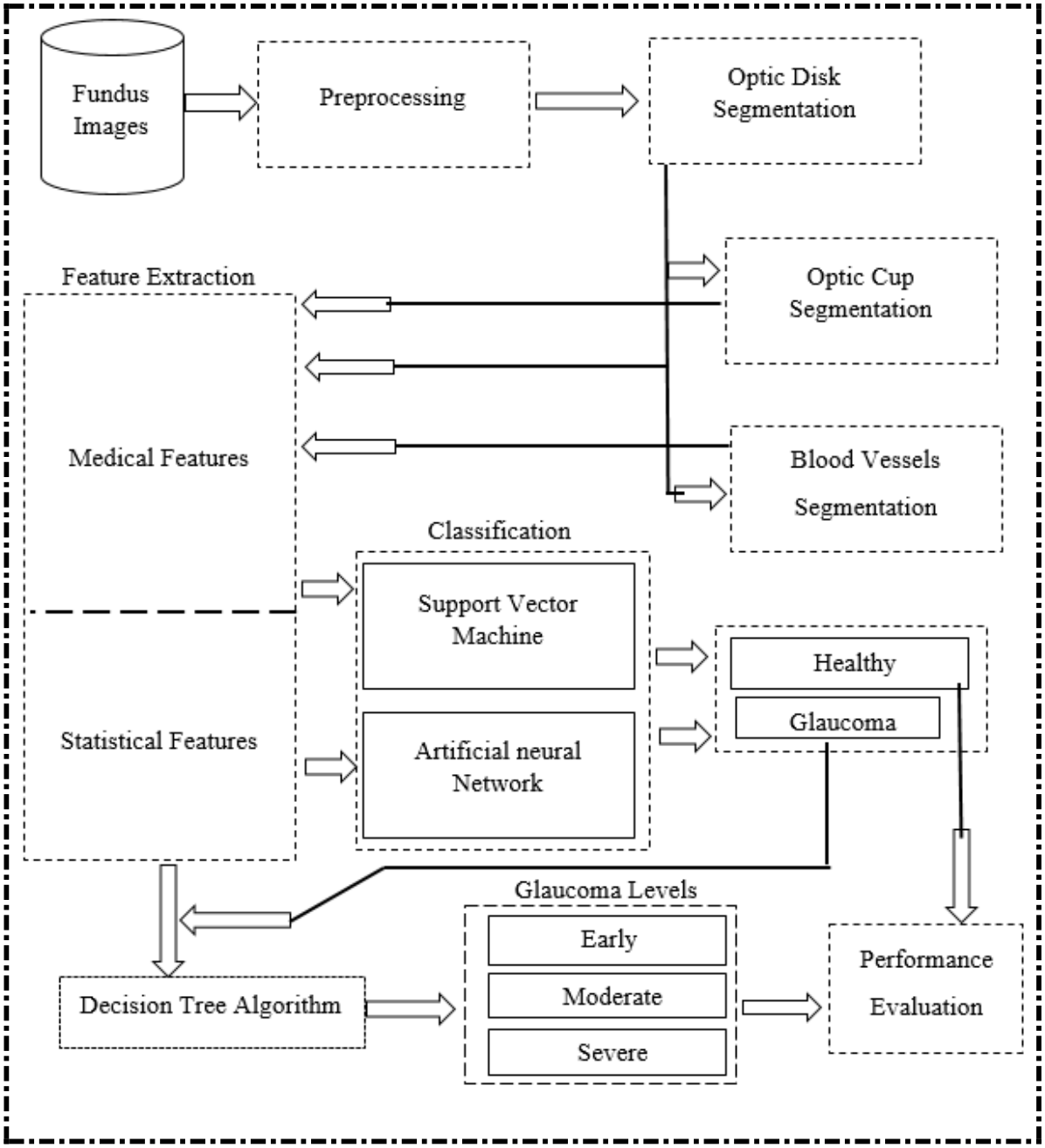

Figure 3.1 Block diagram of the proposed system

3.3 Preprocessing Phase

Preprocessing of retinal image is essential to address illumination fluctuations brought on by image acquisition under varied situations and to

make sure the dataset is consistent and only exposes features that are relevant. This procedure reduces the effort of the subsequent steps and can aid in the accurate localization and segmentation of the retinal structures.

All steps of the preprocessing phase are shown in Figure (3.2).

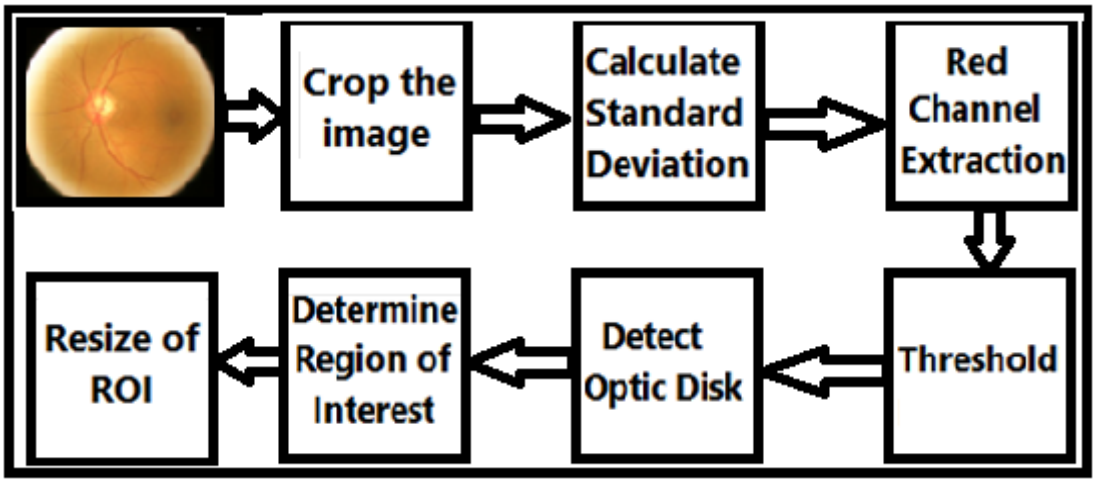

Figure 3.2 Steps of the preprocessing phase

3.3.1 Cropping Input Image

This phase begins with image cropping to removing the undesirable portions of the image such as noise blur, reflections and black parts on the borders of the retinal images in the used dataset.

To obtain the cropped image, the equation (2.5) is applied as where "*RGB*" is the cropped image, "[0.23**m*, 0.1**n*]" is the location of first pixels in the upper right corner, "[0.5**m*, 0.7**n*]" is the width and heightof the cropped image respectively.

3.3.2 Calculation of Standard Deviation (SD)

This step is very important in order to use later for comparison in the second phase, Standard Deviation (SD) for entire cropped image is

calculated according to following equation (2.15).Where “g” is the pixel value that is ranged between 0 and 255, “L” isthe color level that is ranged also between 0 and 255, “$\bar{g}$” is the mean of g, “P (g)” is the probability of g.

3.3.3 Extract the Red Channel

For OD identification and segmentation, the red channel carries more detailed information than the other channels: as a result, extract the red channel from the cropped image was applied in this step as shown in the following equation (3.1).

$$\mathrm{R}(m,n,c) = \mathrm{RGB}(\mathrm{m},n,\mathrm{RedChannel}) \qquad (3.1)$$

Where “***c***” is the color channels, “m, n” index’s.

3.3.4 Detection of the Optic Disk

When comparing the red channel image with a specific threshold and using the maximum intensity of the red channel as a threshold, the suggested work uses threshold intensity to establish the OD position. As shown in the following equation(3.2).

$$\mathrm{BlackWhite}\ (x,y) = \begin{cases} 1 & if\ \mathrm{Red\ Channel}\ >\ \mathrm{Max\ Intensity}\ -4 \\ 0 & otherwise \end{cases} \qquad (3.2)$$

The “*Max Intensity*” is often 255,“Black White ” is threshold operation, And the reason subtracted the value of "4" is because some parts of the optical disc have an intensity less than the maximum by a very small value, The resulted image is a binary image contains the OD with some of the undesirable objects which appear depending on the (SD) of the image of the red channel, when the value of (SD) is lower, then the presence of this object

is lower and vice versa.

To remove unwanted objects, the resulting binary image is labeled with an eight-connections and removed all connected components (objects) that have fewer than (1000) pixels from the binary image.

The final step in this section is the elimination of the objects which are smaller than OD and keeping the larger object which is often the OD There are some rare retinal imageswhere the largest object is not the OD, which is nearest to the (OD).

The OD has detected accurately but it contains some unwanted objects and appears as a single object. The OD was not detected and instead of an object with the same threshold and an area larger than the OD was detected, the second stage of the proposed work will handle such cases in the retinal images.

3.3.5 Determine the Region of Interest (ROI)

The ROI is chosen, which encompasses the region of the OD and the region surrounding it by some pixels to make a square or rectangular region, in order to prevent processing extraneous regions in the image and to reduce the likelihood of incorrect segmentation.

3.3.6 Resize the (ROI)

The image are downsized in this step to lower the computing cost and create a uniform scale for all images to 400 * 400 pixels.The equation (2.6) is implemented to perform the resize operation.

3.4 Segmentation Stage

Function is to localize and divide organisms that have important traits such as OD, OC, and BV. It is the second phase and the core of the proposed system because the following phase depends on the accuracy of the outputs of this phase.

It consists of four steps, each step processes a single object, the most important step is the first step of OD segmentation because its output will be as input to the rest steps.

It consists of four steps, each step processes a single object, the most important step is the first step of OD segmentation because its output will be as input to the rest steps.

3.4.1 OD Segmentation

Glaucoma can be clinically diagnosed by measuring the CDR, which is calculated as the ratio of the OC area to the OD area. Since the borders might be impacted by blood vessels that enter OD, it is frequently possible that the OD boundaries discovered during segmentation do not accurately reflect the OD's morphology. In order to appropriately shape the disc boundaries for estimation, circular fitting is used. The proposed OD segmentation is robust to segment OD even if interrupted by the visible blood vessels. The Figure (3.3) shows the steps of OD segmentation.

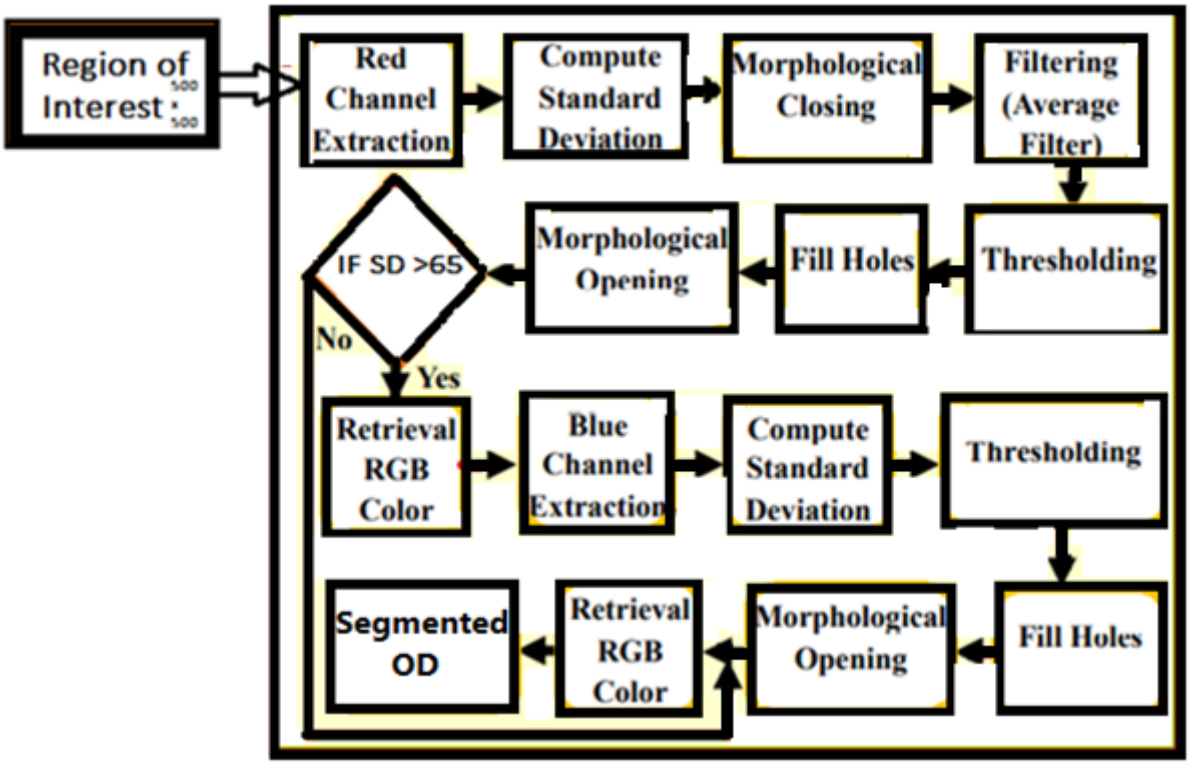

Figure 3.3 Steps of OD segmentation

3.4.1.1 Red Channel Extraction

The OD region can be seen very clearly in the red channel of the RGB bottom image. OD can be seen as the brightest part of the "red" channel compared to other channels.

3.4.1.2 Computation of Standard Deviation (SD)

This step is very important in order to be used to compare the image from which the optic disc can be extracted accurately without additional processing, starting with section (3.4.1.8) and ending (3.4.1.11).SD for the entire cropped image is computed according to the equation (2.15).

3.4.1.3 Morphological Closing of Red Channel

The closing procedure is typically used to close small gaps and fills

in background areas of a picture when a suitable structural element can be located that fits the regions that need to be kept.

It is possible to think that the blood vessels are retinal-background gaps. The optimal structuring element in this morphological operation to eliminate the blood vessels is a disk shape, which must be larger than the largest width of the vessel in the image. The size used of the structuring element (SE) is 10 with disk-shape.

To remove BV effect in the OD region, the closing operation was performed, since BV that may have a threshold similar to the threshold of some regions around the OD, and thus may cause the poor segmentation efficiency.

3.4.1.4 Filtering

The average filter was used to lessen the degree of intensity fluctuation between a pixel and its neighbors. This process will enhance the histogram of the image and blur any residual vessel edges.

3.4.1.5 Image Threshold

In the Threshold method, extraction of an object is done. OD is extracted from its background by assigning an intensity value "T" which is known as a threshold value. Intensity value "T" is assigned such that pixel is either classified as an OD point or background point.

The selection of an efficient threshold is a prime problem. Many of automatic Threshold methodologies may not do well especially when the images of a dataset are not having good contrast, the automatic value of threshold in the suggested system is given as follows:

$$\text{Threshold } (OD) = \begin{cases} 1 & if\ OD(RedCha.) > \text{Max Intensity} - \text{SD Red Cha.}/\ 2 \\ 0 & otherwise \end{cases} \quad (3.3)$$

Where "*Max Intensity*" is often 255, "$SD_{\ Red\ Channel}$" is the standard deviation for the red channel. And the main reason for "$SD_{\ Red\ Channel}$ "divide on value "2" is some image is a contrast ranged between the max intensity of an image to less than the amount of that intensity, as whose contrast is well distributed.

3.4.1.6 Holes Filling

Two issues will arise if there are gaps in the resulting image, particularly in the OD region: The first is the inaccuracy of colors retrieval to the OD, which is an important step for extracting the OC or extracting the blue channel for later use in segmentation the OD accurately, the second problem is a defect in the calculation of OD area, therefore, to avoid above problems this step is performed.

3.4.1.7 Morphological Opening

The opening process eliminates the small items from the foreground of an image, allowing for the reconstruction of object contours using the pi xels that were removed that were smaller than the structuring element. The appropriate structuring element radius is (5 to 15) with disc shape.

The OD boundaries are smoother, the small objectsin and are removed but it contains isolated or connected objects with OD, this case occurs when the contrast of an image is not well. The next steps will process such as cases.

3.4.1.8 Retrieval of RGB Colors

To get rid of any undesired objects in the image, the true colors (red,

green, and blue) of the retinal image are recovered to the OD binary image that was segmented in the previous phase. Which have standard deviation more than or equal 65.5 or to segment OC and BV if the standard deviation of the image was less than 65.5, the following algorithm (3.1) describes this operation.

Algorithm (3.1): Retrieval of RGB colors

Input: Binary image of Optic Disk.

Output: OD with true color (red, green, blue).

1: Load the binary image of OD, load ROI image

2: Convert binary image of OD and ROI from (unit8) to (double).

3: For each true color:

4: OD (*m,n)* = multiply the binary image of OD and ROI image, pixel by the corresponding pixel.

5: Return OD with RGB

6: End

The segmented OD with true color, and have a standard deviation of more than 65.6, therefore OD is not segmented accurately. According to the allimages have a standard deviation of more than 65.5, The “m,n” is the location of pixel for optic disk in ROI..

3.4.1.9 Extract Blue Channel

Among the three true color channels in the retina image, the blue

channel will be suitable for detecting every portion unrelated to the OD, the following equation (3.4) .and by using the main extract the blue channel from the OD because the blue channel contains few details of the data.

$$\mathrm{B}\ (m, n, c)\ = \mathrm{OD}\ (\mathrm{m}, n, \mathrm{Blue\ Channel}) \qquad (3.4)$$

Where "***c***" is the color channels and "m, n" is a pixel.

3.4.1.10 Image Threshold

Standard Deviation of the entire blue channel is calculated, then the equation (3.5) is applied to calculate the threshold value:

$$\mathrm{BlackWhite}\ (OD) = \begin{cases} 1 & if\ OD\ Blue\ Channel\ >\ SD\ Blue\ Channel * 2 \\ 0 & otherwise \end{cases} \qquad (3.5)$$

Where "OD $_{\text{Blue Channel}}$" is the OD image with a blue channel, "$SD_{\ Blue\ Channel}$" is the standard deviation of the blue channel. The main reason for doubling ($SD\ Blue\ Channel$ *2) the SD value is to neglect of the pixels with a low color value.

3.4.1.11 Morphological Operations

To improve OD segmentation, some morphological procedures will be used, the first is an opening operation with structuring element as disc shape and the size is (5 or 10).

Then, fill holes' step is applied.

In very rare cases, if there are some small unwanted objects in the image, it is possible removing by choosing the larger region, then applying morphological opening with structuring element as disc shape and small size as 5.

3.4.1.12 Retrieval of RGB Colors

By applying what was mentioned to retrievethe true colors to the resulted binary image of OD in order to extract the parts of the OD which are OC and BV.

3.4.1.13 Optic Disk Circular Fitting

Although the segmentation operation that was carried out in the previous steps was very accurate, preferred to do this process in order to compare the results and choose the best. The equation below is applied to obtain the circular shape for the OD.

$$\begin{pmatrix} xi(t) \\ yi(t) \end{pmatrix} = \begin{pmatrix} ri\cos t \\ ri\sin\ t \end{pmatrix} \qquad (3.6)$$

for i=1, 2, and $\forall \in t\ (0, 2\pi)$, where "r_i" represents the radius ofthe outer and inner discs.

3.4.2 Optic Cup Segmentation

OC segmentation is more difficult than segmentation of OD because of the high density of BV in the OC region and glaucoma changes the shape of the OC region. Figure (3.4) and algorithm (3.2) explain OC segmentation steps.

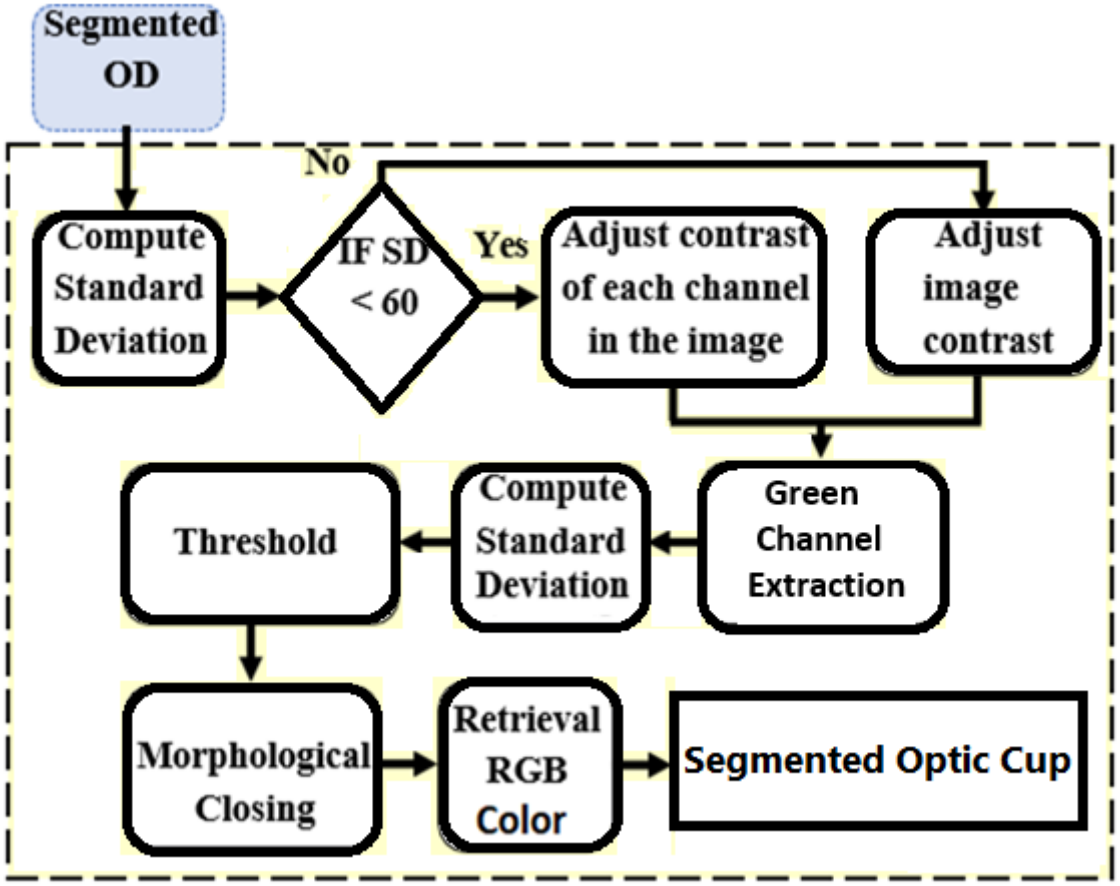

Figure 3.4 OC segmentation steps

Algorithm (3.2): OC Segmentation

Input: Optic Disk (RGB) segmented.

Output: Optic Cup (RGB) Segmented.

1: Load image of OD.

2: Calculate the Standard deviation of the OD image.

3: If Standard deviation of OD image >= 60

4: Adjust image contrast to 0.1 as the value of low input and 0.9 as value of high input.

5: Else Adjust each channel of the image to 0.2, 0.2, 0 as the value of low input for R, G, B color respectively, and to 0.6, 0.8, 0.5 as the Value of high input for R, G, B color respectively.

6: Extract a green channel.

7: Calculate standard deviation (SD) for the green channel.

8: Select threshold as value large than or equal MaxIntensty- $SD_{Green\ Channel} / 4$.

9: Closing operation with disk (SE) of 50.

10: Retrieval of RGB Colors to OC.

11: Fitting a circular shape for OC boundary.

12: Return Segmented OC.

13: Fitting a circular shape for OC boundary.

14: Return Segmented OC.

15: End

3.4.2.1 Adjustment of OD Contrast

The image needs to be well contrasted in order for an automatic threshold to segment OC properly, it is clear that the OC of the first image has bright more than the others, in order to improve the contrast, the adjustment will be applied on the images depending on the standard deviation of each image.

The adjustment is performed as shown in the following equation if the standard deviation of the image is less than 60, each channel of the image is assigned value as low and high input as shown in the following equation (2.7).

Otherwise, the adjustment is performed on the entire image by certain value for all channels without customizing anyone as shown in the following equation (2.8).

3.4.2.2 Extract Green Channel

The red channel covers the full area of OD in the segmented image of OD, and since the blue channel contains a little information, the green channel is the better channel for OC extraction. The OC region is brighter in the OD region with the presence of the blood vessels

3.4.2.3 Image Threshold

The standard deviation for the entire green channel is determined for the OC extraction threshold, then applied tocalculate the threshold value:

$$\text{BW (OD)} = \begin{cases} 1 \;\; if \;\; OD(GreenChannel) > \text{Max Intensity} - \text{SD Green Channel} / 3 \\ 0 \;\; otherwise \end{cases} \quad (3.7)$$

Where "*Max Intensity*" is often 255, "$SD_{Green\ Channel}$" is the standard deviation of the green channel. And the value 3 was used for the division. This came from the many experiments that were conducted on a set of dataset images, as this value is one of the best values that give better results.

3.4.2.4 Morphological Closing

Closing operation is used to identify the binary image of OC and eliminate gaps between its components. The structuring element must be larger than the largest gaps in the image. The optimum size used of the structuring element(SE) is 50 with a disc shape.

3.4.2.5 Retrieval of RGB Colors

By applying the method which was mentioned to retrieve the true colors to the resulted binary image of OC.

3.4.2.6 Circular Fitting of the OC Boundary

This technique involves OC circular fitting, which is carried out similarly to how OD circular fitting has been done**,** in order to compare between the previous OCsegmentation and the results of this operation and choose the best results.

3.4.3 Blood Vessels Segmentation in Optic Disc

The optic disc is the meeting point of the blood vessels, which have a role in the diagnosis of glaucoma, when the eye suffers from glaucoma, blood vessels will exist highly in temporal or nasal side. Figure(3.5) depicts OC segmentation steps and implemented to do this operation.

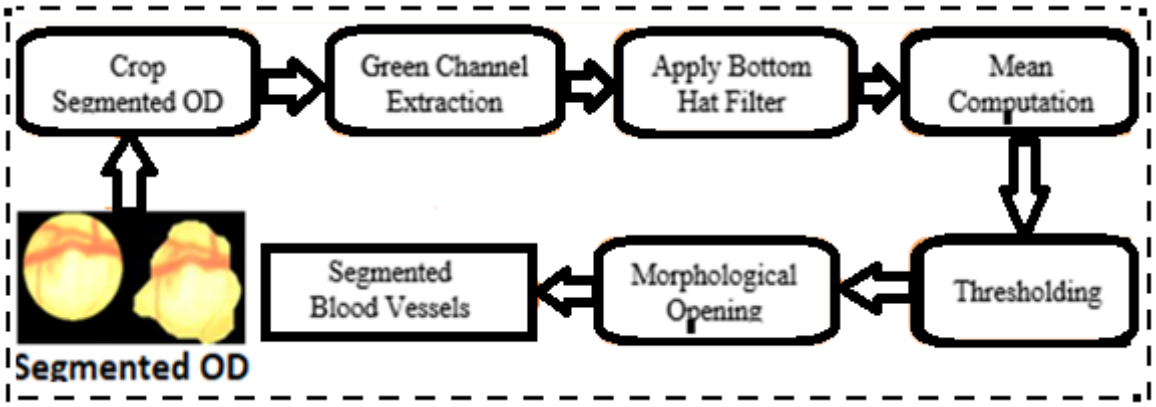

Figure 3.5 Steps of BV segmentation

3.4.3.1 Cropping of OD Image

In order to find the BV of OD accurately, the images of OD are cropped and unnecessary black regions on the image boundaries are eliminated so that the resulting image is the region of OD with a black region of 20 pixels only.

3.4.3.2 Green Channel Extraction

The red channel has visible vessels, while the blue channel has low contrast and little information, but there is too much noise in this channel when the blood vessels are extracted, therefore the green channel will be better than other channels.

3.4.3.3 Morphological Bottom-hat

Bottom-hat filtering is used to remove the fine features and little objects from an image, producing an image with "objects" or "elements" that are smaller than the structural element. The appropriate structuring element used is a disc shape of 6.

3.4.3.4 Image Threshold

The average (Mean) of all the pixels in the resulting image is determined, and the thresholder image which includes blood vessels with undesirable objects is created by applying the following equation.

$$\text{Threshold} = \text{Mean} + 6 \qquad (3.8)$$

The value added to the Mean for the threshold formulation must beequal or greater than the value of the structuring element to extract blood vessels with the lowest possible noise. The value (6) was added to the threshold because the value used in the previous process of bottom-hat filtering was (6).

3.4.3.5 Morphological Opening

To get rid of unwanted objects resulting from the thresholder images, the opening process was performed using a (SE) of 10 with a disc shape.

3.5 Features Extraction Phase

During this procedure, extracted features from the image using a variety of segmentation techniques and textures. As show in Figure (3.6).

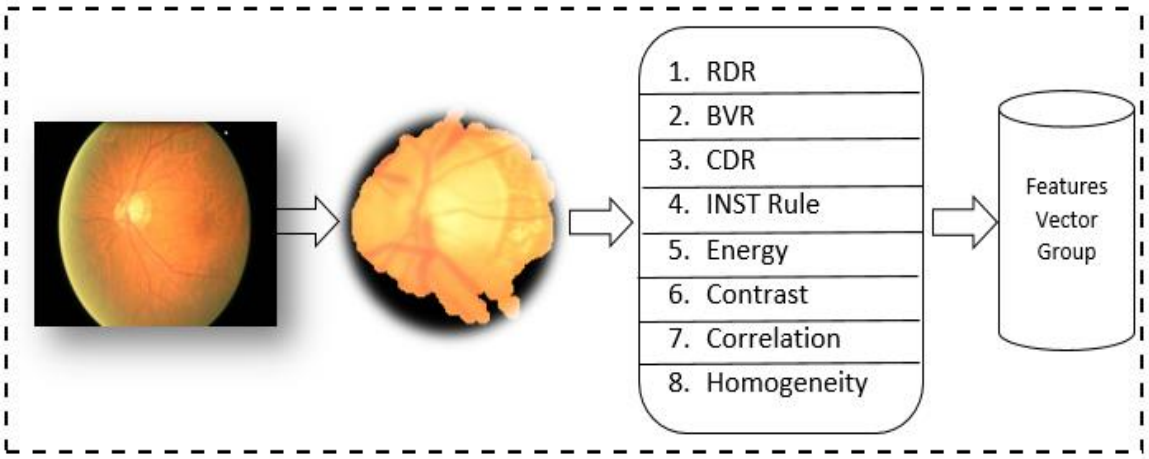

Figure 3.6 Block diagram of features extraction

The following Figure (3.7) explains in detail the steps of features extraction.

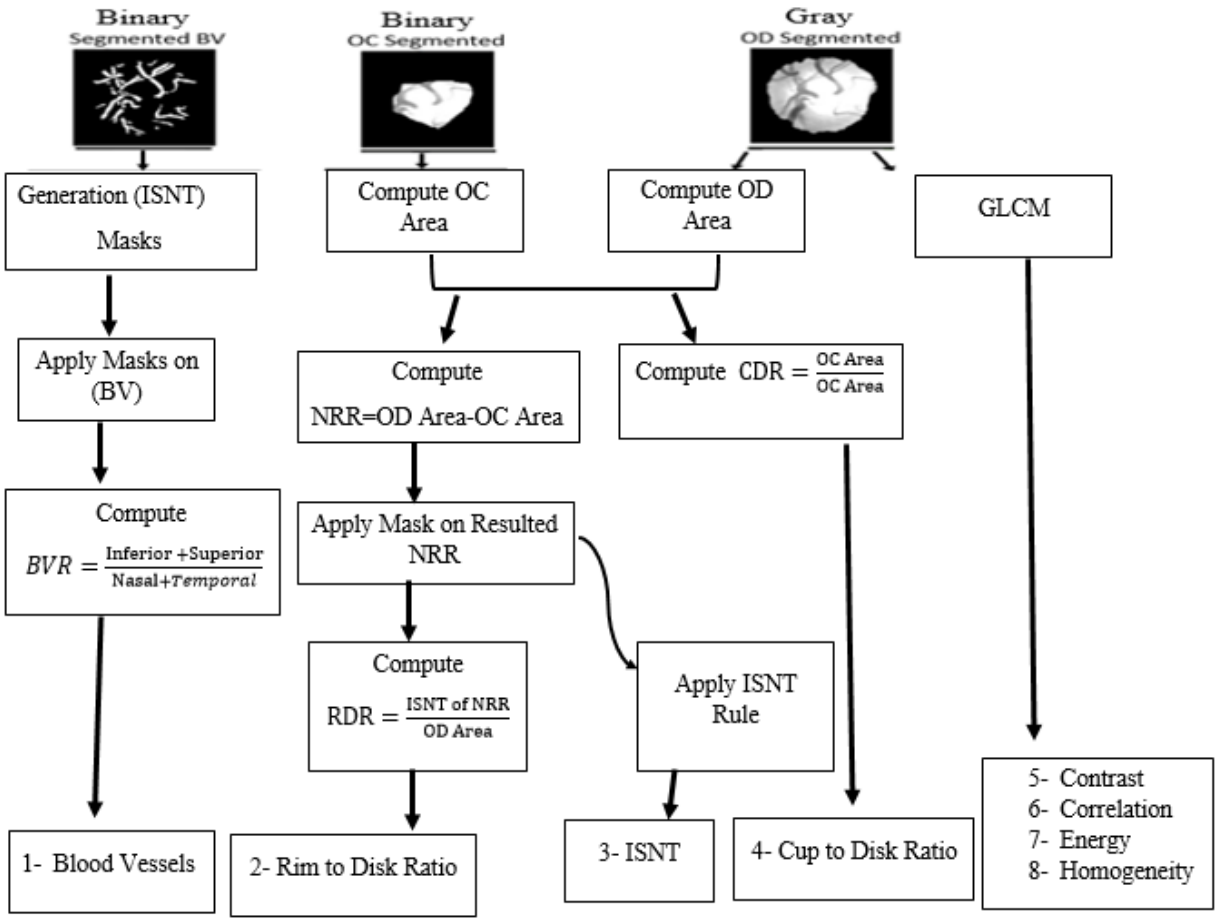

Figure 3.7 Steps of features extraction

3.5.1 Cup to Disc Ratio (CDR)

This feature is computed by dividing the OC area by the OD area. Clinically, if the "CDR" value is less than 0.3, the eye is suspected of healthy, otherwise, it is glaucoma.

3.5.1.1 Computation of the OD Area

In the binary image of the segmented OD, the OD area only represents the white region, it is equal to the summation of pixels which have the value 1.

3.5.1.2 Computation of the OC Area

Additionally, in the computation of the OD area, the segmented OC area is solely represented by the white portion in binary image.

3.5.2 Inferior Superior Nasal Temporal (ISNT) Rule

This symptom is the second glaucoma warning sign. This rule must first be discovered in order to be put into practice (NRR), then Creation the (Inferior, Superior, Nasal and Temporal) masks to apply iton the NRR.

3.5.2.1 Neuro Retinal Rim (NRR) Computation

The Neuro Retinal Rim is the area that is between the OD and OC boundaries. To precisely determine the (NRR), the binary image of OD is cropped and unnecessary black regions on the image boundaries are eliminated so that the resulting image is the OD with a black region of 20 pixels only, and then the following equation (3.9) is implemented:

$$\text{NRR} = \text{OD Cropped} - \text{OC Cropped} \quad (3.9)$$

3.5.2.2 Masks Images Creation

The mask pictures serve as an image filter, therefore they are designed to ensure that the desired quadrant has value 1, or a white zone, and that all other quadrants have value 0, or a black region.

The image of the mask for each quadrant is created through the exploitation of the centroid value and array characteristics.

The lowermost quadrant called the inferior quadrant. This quadrant's mask will be white region and other quadrants are all black regions, creates the inferior quadrant mask.

Algorithm(3.3): Inferior Quadrant Mask Creation

Input: The Number of Rows and Columns for NRR Image

Output: Inferior Quadrant Region.

1: [Rows, Columns] = size (NeuroRetinalRim);

2: CenterRows = Round (Rows / 2)

3: CenterColumns = Round (Columns / 2)

4: Inferior= Set zeros (Rows, Columns)

5: InitColumns=1;

6: For I = Rows **to** -1 **to** CenterRows

7: For J = Columns **to** -1 **to** InitColumns

8: Inferior (I, J) = 1;

9: End For

10: InitColumns = InitColumns +1;

11: Columns = Columns -1;

12: End For

13: Return Inferior Quadrant Mask

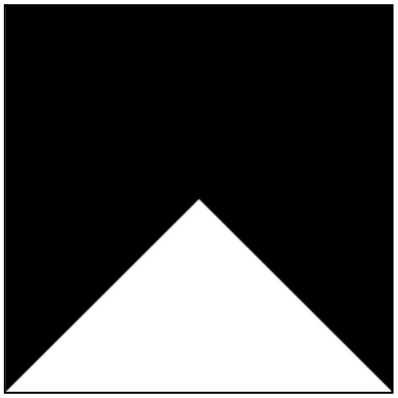

Figure 3.8 Inferior mask

Figure (3.9) states the resulted images of inferior regions of NRR.

Figure 3.9 Inferior regions of NRR

Superior quadrant is the quadrant at the top and the mask of this quadrant must be white region and all the other quadrants are black regions.

The algorithm (3.4) creates the Superior quadrant mask as shown in the Figure(3.10).

Algorithm (3.4): superior Quadrant Mask Creation

Input: The Number of Rows and Columns for NRR Image

Output: Superior Quadrant Region.

1: [Rows, Columns] = size(NeuroRetinalRim);

2: CenterRows = Round (Rows / 2)

3: CenterColumns = Round (Columns / 2)

4: Superior = Set zeros (Rows, Columns)

5: InitColumns=1;

6: For I = 1 **to** CenterRows

7: For J = InitColumns **to** Columns

8: Superior (I, J) = 1;

9: EndFor

10: InitColumns = InitColumns +1;

11: Columns = Columns -1;

12: EndFor

13: Return Superior Quadrant Mask

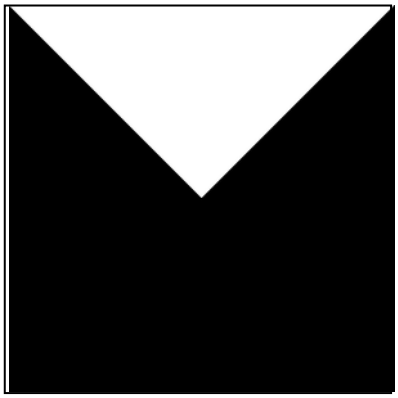

Figure 3.10 Superior mask

Figure(3.11) shows the resulted images of superior regions of NRR.

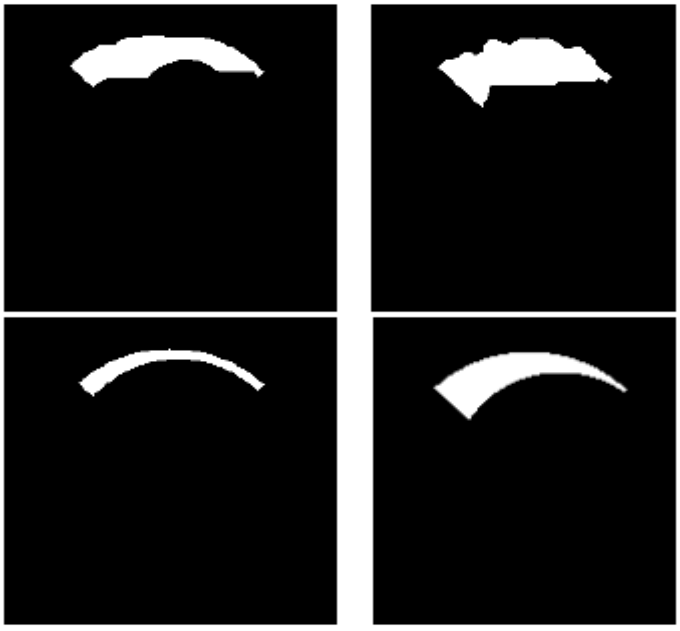

Figure 3.1**1 Superior regions of NRR**

Temporal quadrant is at the left for the right eye and nasal of the left eye and vice versa as shown in the following Figure(3.12).

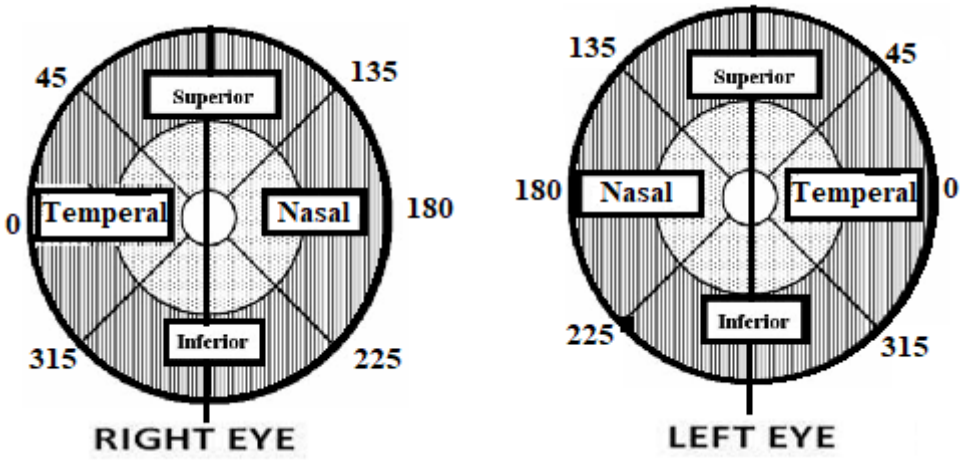

Figure 3.12 Nasal and Temporal regions in the right and left eye

The left-quadrant mask has white region and the other quadrants must have black regions as shown in the following Figure(3.13) obtained from applying the algorithm (3.5).

Algorithm (3.5): Temporal Quadrant Mask Creation

Input: The Number of Rows and Columns for NRR Image

Output: Temporal Quadrant Region.

1: [Rows, Columns] = size (NeuroRetinalRim);

2: Center Rows = Round (Rows / 2)

3: Center Columns = Round (Columns / 2)

4: Initial Row=1;

5: For J= 1 **to** Column

6: For I= Initial Row **to** Row-1

7: Temporal (i,j)=1;

8: End For

9: Initial Row= Initial Row +1;

10: Row= Row-1;

11: If Row <=1 than Break;

12: End IF;

13: End For

14: Return Inferior Quadrant Mask

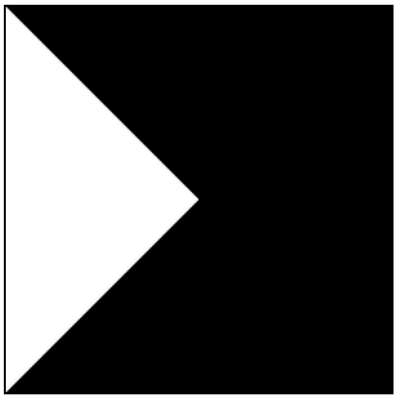

Figure 3.13 Temporal (left quadrant) mask

The following images are the temporal regions of NRR.

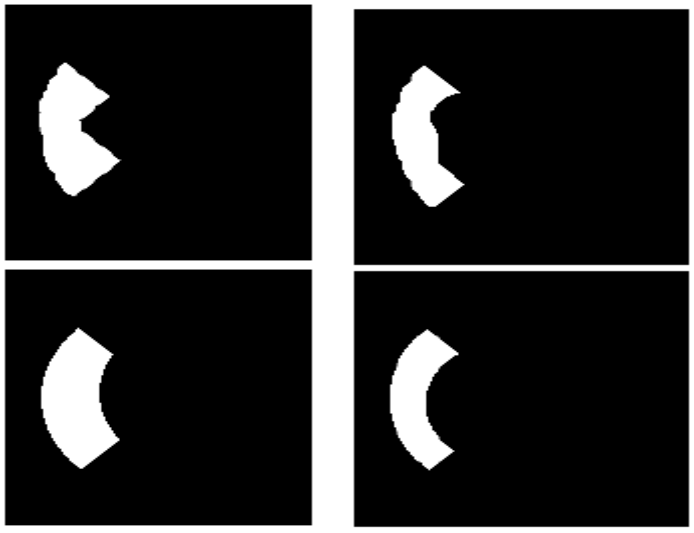

Figure 3.14 Temporal regions of NRR

The rightmost for the right eye is the nasal quadrant and temporal of the left eye. The mask for right quadrant is a white region in the right side, and other quadrants have black region as shown in Figure(3.15) which obtained from applying the algorithm (3.6).

Algorithm(3.6): Nasal Quadrant Mask Creation

Input: The Number of Rows and Columns for NRR Image

Output: Nasal Quadrant Region.

1: [Rows, Columns] = size (NeuroRetinalRim);

2: CenterRows = Round (Rows / 2)

3: CenterColumns = Round (Columns / 2)

4: Nasal = Set zeros (Rows, Columns)

5: InitRows=1;

6: For J = Columns: -1: Center Colum

7: For I = InitRows to Rows-1

8: Nasal (I, J) = 1;

9: EndFor

10: InitRows= InitRows+1;

11: Rows=Rows-1;

12: If Row<=1 then Break;

13: EndIf

12: EndFor

13: Return Nasal Quadrant Mask

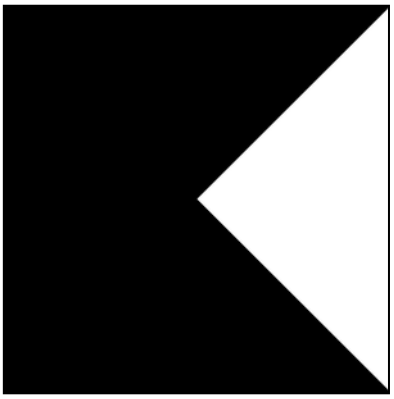

Figure 3.15 Nasal (right quadrant) mask

The following images are the nasal regions of NRR.

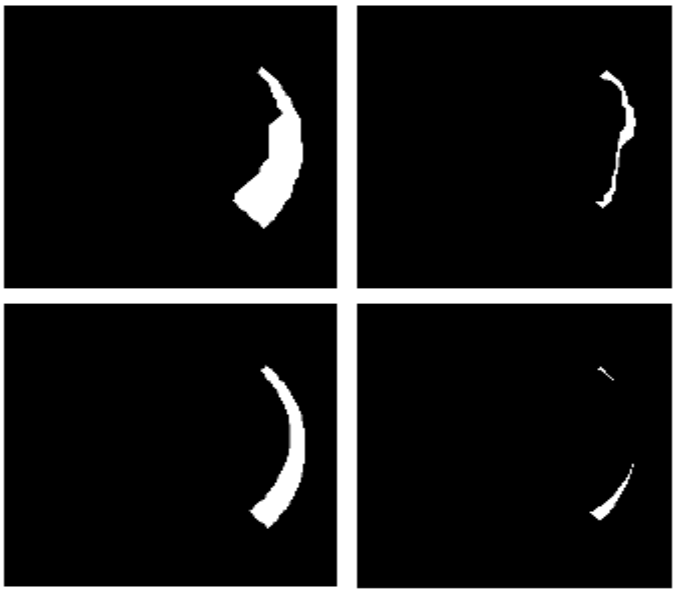

Figure 3.16 Nasal regions of NRR

3.5.3 Rim to Disc Ratio (RDR)

When used with the CDR indication, this indicator can be used to differentiate between mild and severe disease instances because it is more sensitive than the CDR.

The equation (2.3) is applied to RDR computation If RDR value is less than 0.5, the eye is normal, otherwise, the eye issuspected of glaucoma.

3.5.4 Blood Vessels Ratio (BVR)

Similar to how inferior, superior, temporal, and nasal masks were used in the NRR, these masks are used to obtain inferior, superior, tempora l, and nasal of BV when applied to the segmented BV. Then the following equation (2.4) computes the BVR.

The value of BVR in the glaucomatous eye is less than BVR value in the healthy eye because of the density of blood vessels in the Temporal and Nasal regions of the glaucoma eye.

3.5.4.1 Blood Vessels in Inferior Region

The algorithm (3.3) for the inferior region was applied to the segmented BV.

3.5.4.2 Blood Vessels in Superior Region

Depicts the resulted binary images were obtained bythe carry out algorithm (3.4) for the superior region of BV.

3.5.4.3 Blood Vessels in Temporal Region

The temporal regions of BV when implementation of the algorithm (3.5) on the segmented BV.

3.5.4.4 Blood Vessels in Nasal Region

By applying the algorithm (3.6) on the segmented BV.

3.5.5 Texture Features

This last stage of extracting the features of the statistical measurement which is highly dependent on the optic disc, which is the characteristic of contrast, correlation, energy and homogeneity.

3.5.5.1 Gray Level Co-occurrence Matrix

The applied mathematics method of analyzing textures that contain the spatial relationship between the pixels is called a gray-level co-occurrence matrix (GLCM). Features extracted from the retinal image from four directions (0, 45, and 90,135). Tacked four directions; a single horizontal offset may not be sensible to a vertically oriented texture. Therefore, multiple GLCMs for a single input image is created. To perform this operation, define an array of offsets, these offsets specify pixel relationshipsof varying directions and distances.

Initially create a matrix from a given image. In our work the image is a color image of OD.

Such as illustrated above which creates an offset that specifies four directions.

Offset = [0 1, -1 1, -1 0, -1 -1].and the equation of features computation were mentioned in section (2.9.4).

The applied computation steps and features for "GLCM" are described in the algorithm (3.7).

Algorithm (3.7): "GLCM" Matrix Features

Input: Optic Disc Image, θ, d=1.

Output: Co-occurrence matrices

1. Start.
2. For each direction (θ) do the following:
3. A: Compute the co-occurrence matrixes for each pair (j , d)
4. For each theta (θ) value // θ (0,45,90,135)
5. For all b=0 to Height – 1
6. For all a=0 to Width - 1
7. Set i= G(b,a)
8. Set j= G(b, a+d)
9. Cm-0(i, j)= Cm-0(i, j) +1
10. Set i= G(b,a)
11. Set j= G(b+d, a+d)
12. Cm-45(i, j)= Cm-45(i, j) +1
13. Set i = G(b,a)
14. Set j = G(b+d, a)
15. Cm-90(i, j) = Cm-90(i, j)+1
16. Set i= G(b,a)
17. Set j= G(b+d, a+d)
18. Cm-135(i, j)= Cm-135(i, j)+1 Set i= G(b,a) Set j= G(b+d, a+d)
19. End for
20. End for
21. B: Compute GLCM (energy, contrast, homogeneity and correlation)
22: Return Co-occurrence matrices

3.5.6 Features Normalization

After computing the four texture feature based on the co-occurrence matrices, using equations (2.16) to (2.19).And computing the four medical features using the equation (2.1) to (2.4).

Normalization, or feature scaling, is an essential system for information pre-processing. It is an important process that is used in order to enhance the classification rate. It works by scaling the values of the features so that they are within a specific range of determined size in [0…1]. There are many methods for data normalization.

The linear normalization of features vector (Feature Vector) is performed according to the formula in equation (2.20), and in section (2.9.5):

Where Norm _Features Vector is a normalized features vector in the range [0...1].Min is the minimum value in the features vector. Max is the maximum value in the features vector. The steps for computation of the normalization process are depicted in the algorithm (3.8) below:

Algorithm (3.8): Feature values Normalization

Input: Feature vector: any type of Feature vector

Output: Normalized feature vector.

1: Compute the (max, and min) values in the Feature vector.

2: *for 1=1 to length (Feature vector).*

3: *Compute feature normalization from the feature*

4: *By apply equation Norm Feature Vector=* $\frac{Feature\,Vector - min}{max - min}$

5: *End*

6: Return *(Norm Feature*

3.6 Classification Phase

The process of classification depends on the construction of the classification model (classifier) that builds based on a predefined set of data classes (training data set). The construction of the classifier is called the learning phase (or training phase) which is a series of stages beginning with preprocessing for input retina fundus images and ending with building the classifier.

In the testing phase, the classification model is used to classify the unknown retina fundus image as diseased or healthy (positive, negative). It is attempted to identify an object (input retina fundus image) by comparing its features with a given set of features (positive, negative) obtained from the

learning stage. The classification method that is used in this work is supervised learning because all the datasets are pairs consisting of the input pattern and the desired class. Tow classifiers (ANN and SVM) are used in this work. The Figure (3.19) below depicts the classification phase.

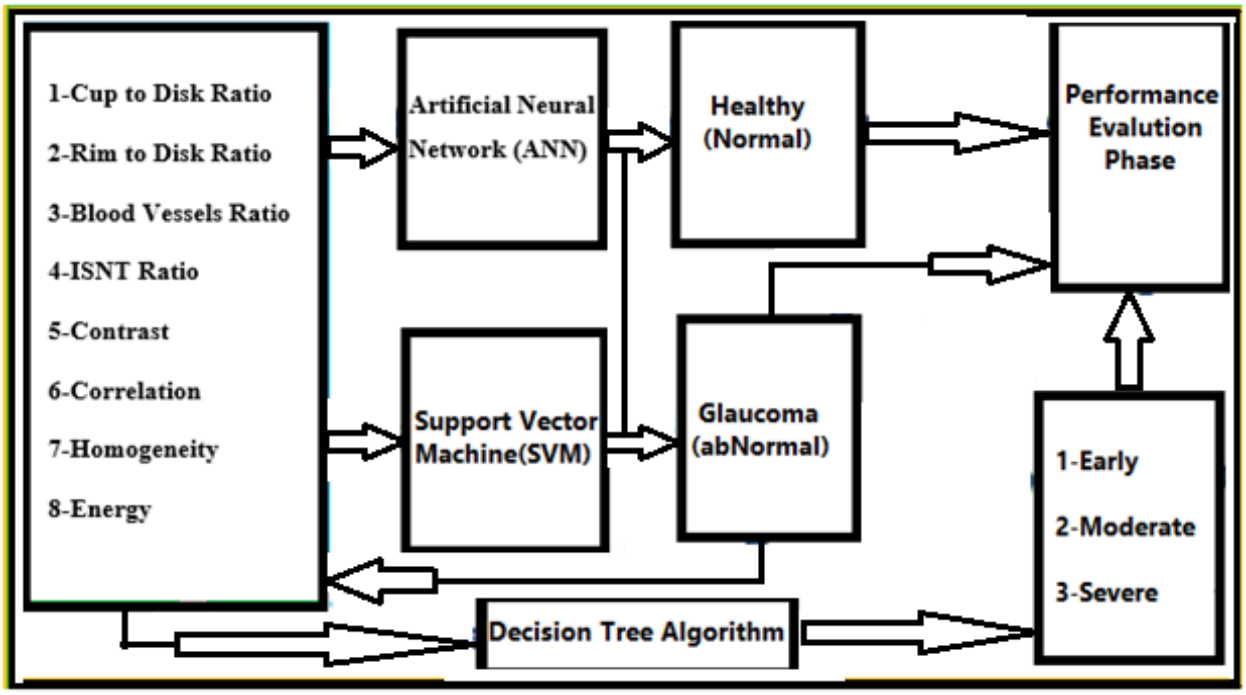

Figure 3.19 Steps of classification Phase

3.6.1 Artificial Neural Network (ANN)

In general, three network training function Bayesian regularization backpropagation, scaled conjugate gradient backpropagation, and Levenberg-Marquardt backpropagation update the weight and bias values. The first type is better for difficult problems, the second network is typically fastest, and the last type is distinguished by requiring less memory. The dataset was separated into two groups, much like SVM. "Test" and "Training", the classifier usedis the binary classifier with the function of Bayesian regularization backpropagation to handle nonlinear features. The

backpropagation error used is 0.001.

3.6.2 Support Vector Machine Classifier (SVM)

The binary classifier, which is the "SVM" classifier's native state, employs the "SVM" classifier. It was employed in this study to make a positive or negative glaucoma prediction. There are two phases in the image classification process. When the "SVM" is being trained, the dataset is divided into two groups of images positive and negative image, and generation feature vector for characteristics and class label for each group. In a testing phase comparing the features vector input with the features vector obtained from the training phase, and return the class label.

Higher-dimensional data with fewer difficulties could be got by used the "SVM" classification, "SVM" will utilize "RBF" as a kernel. Two groups of data will be set as a "Test" and "Training". To clarifying the efficiency of "SVM" classifier model the "Test" set is utilized. "Test" dataset has been utilized by validation to keep away from the possible bias of the efficiency, an assessment because of "Over-Fitting" of the model to training datasets.

3.7 Stages of Glaucoma Progression

In this section, a new, innovative and previously unfamiliar method has been relied upon, through which, I can know the stage or level of glaucoma disease, or what is known as glaucoma. The eight features extracted in the previous were largely relied upon. In addition, with the help of tree algorithm the decision tree determined the level of the disease, as well as limiting it to about three levels only, which are early, moderate and severe. Where and after reviewing and making sure of the medical aspect and other sources and taking into account the ratios determine as (0.3 to 0.3999 for the first stage, 0.4 to 0.4999 for the intermediate stage, and 0.5 or

greater than that for severe stage)and sort them each according to his stage.as show in Figure(3.20).

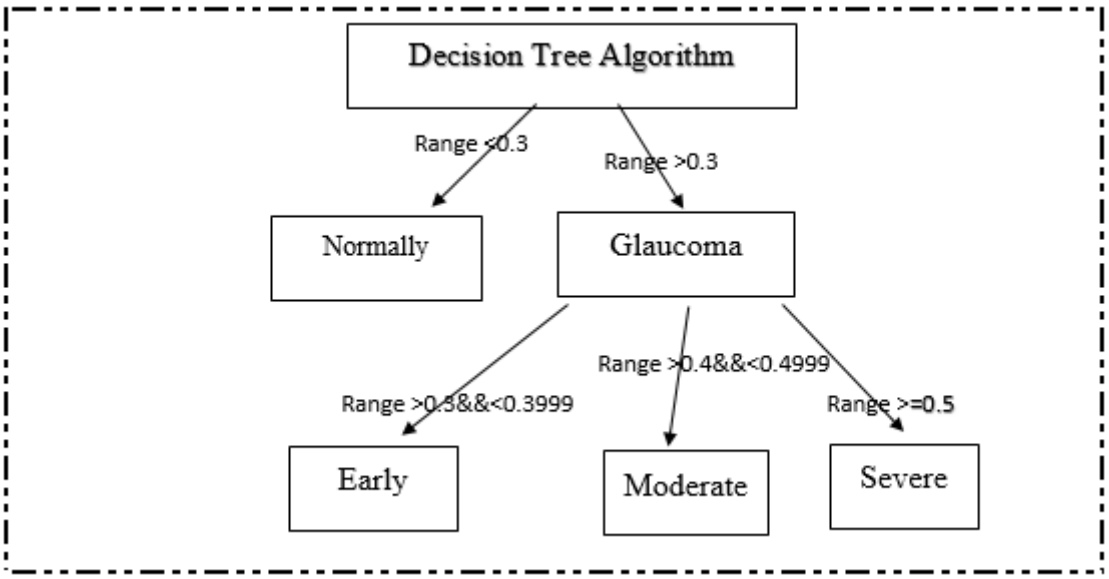

Figure 3.20 Glaucoma level determinants

3.8 Evaluation Measures

The purpose was to evaluate the accuracy of the system using widely used metrics such as accuracy, specificity, sensitivity and accuracy. For more information see section (2.13).

Chapter Four: Results and Discussion

4.1 Introduction

In the proposed system, mathematical equations inspired by the (WHO) and the ophthalmologist have been adopted to examine patients who also need the clinic.

Optical disc and cup segmentation algorithms are developed, and the vascular segmentation algorithm was improved for use in the automatic diagnosis of glaucoma by examining several features. One of the most important contributing factors to this is that the abnormal (affected) eye has a key point as a protocol, which is the increase in the area of the optic cup. In this system to obtain high efficiency.

All algorithms have been examining and evaluated by calculating performance using the "ORIGA" dataset that has RGB retinal fundus images takes from different separate tested sets. Figure (4.1) is a sample for the left and right retina fundus images.

Color fundus images for test set consist of normal and abnormal retinal images. The classification capabilities depending on the adopted extraction features. The suggested system was implemented with MATLAB (MATLAB 2021) system. Windows 10 service 64-bit operating system as programs run, for the ‘HP’ laptop computer with the processor: Intel® Core (TM) i7-4600U CPU@2.10GHz 2.70, RAM 8 generations.

4.2 ORIGA Dataset

ORIGA is the data set used, and it contains a proposed objective performance measurement method, focusing on optical disc, cup segmentation, and cup-to-disc ratio (CDR). Currently, ORIGA (-light) contains 650 retinal images as Table (4.1) annotated by trained professionals from the Singapore Eye Research Institute. Color fundus images for the training and testing sets consisted of normal and abnormal retinal images. A wide variety of image markers, crucial to the diagnosis of glaucoma, have been annotated. ORIGA (-light) is available for online access upon request. Figure (4.1) displays of the left and right retina fundus images.

Table 4.1 Total of images for ORIGA dataset

	Abnormal	Normal	Total	
Training	116	336	452	650
Testing	52	146	198	

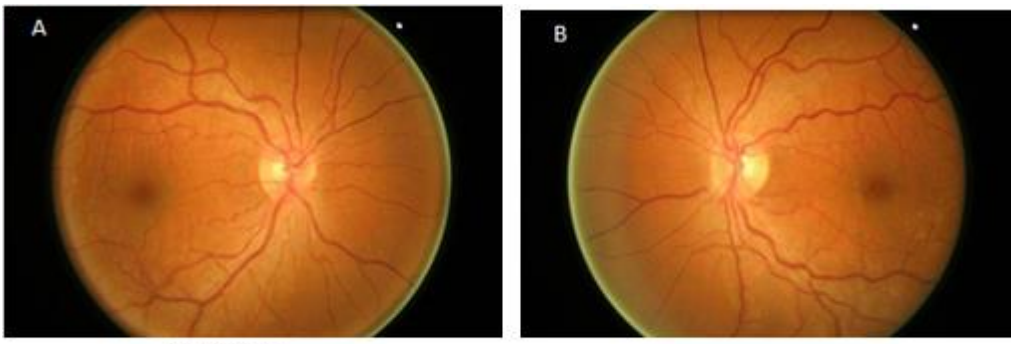

Figure 4.1 Samples of the dataset

4.3 Implementation of the Proposed System

In fact, the retinal image goes through several stages, the most important of which are the initial processing stage, the Segmentation stage, and the feature extraction stage from the retinal fundus images, as shown in Figure (3.1),and in sec(3.2).

4.3.1 Result of Optic Disc Segmentation

The proposed algorithm for optic disc segmentation has high finenessin different conditions of illumines.

The main and basic factor in the image of the retina is OD for glaucoma diagnosis because it contains the other structure anatomical parts which the optic cup, the region between the optic disc and the optic cup and the blood vessels, after detection of OD location in pre-processing phase, the retina image will be feeding the segmentation phase.

In fact, the main basis for identifying the optical disc by the red channel, the optic disc in the red channel is brighter than other channels, some retina images have not well contrast and that influences on segmentation of OD accurately, therefore the standard deviation is calculated which measured the intensity of the color distribution. All segmentation processes are based on "Morphological Techniques and Intensity Threshold". Figure (4.2) states some results of OD segmentation from retina images.

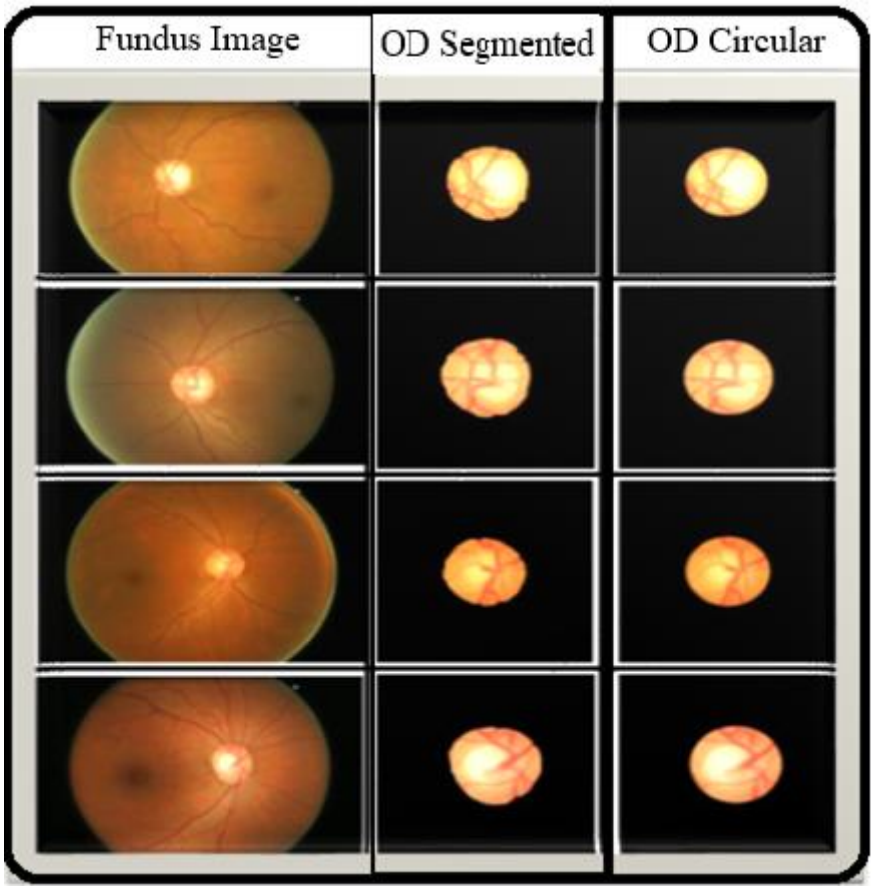

Figure 4.2 Results of OD segmentation in retinal images

Figure (4.3) shows various samples of segmented OD for images have a standard deviation of more than 65.

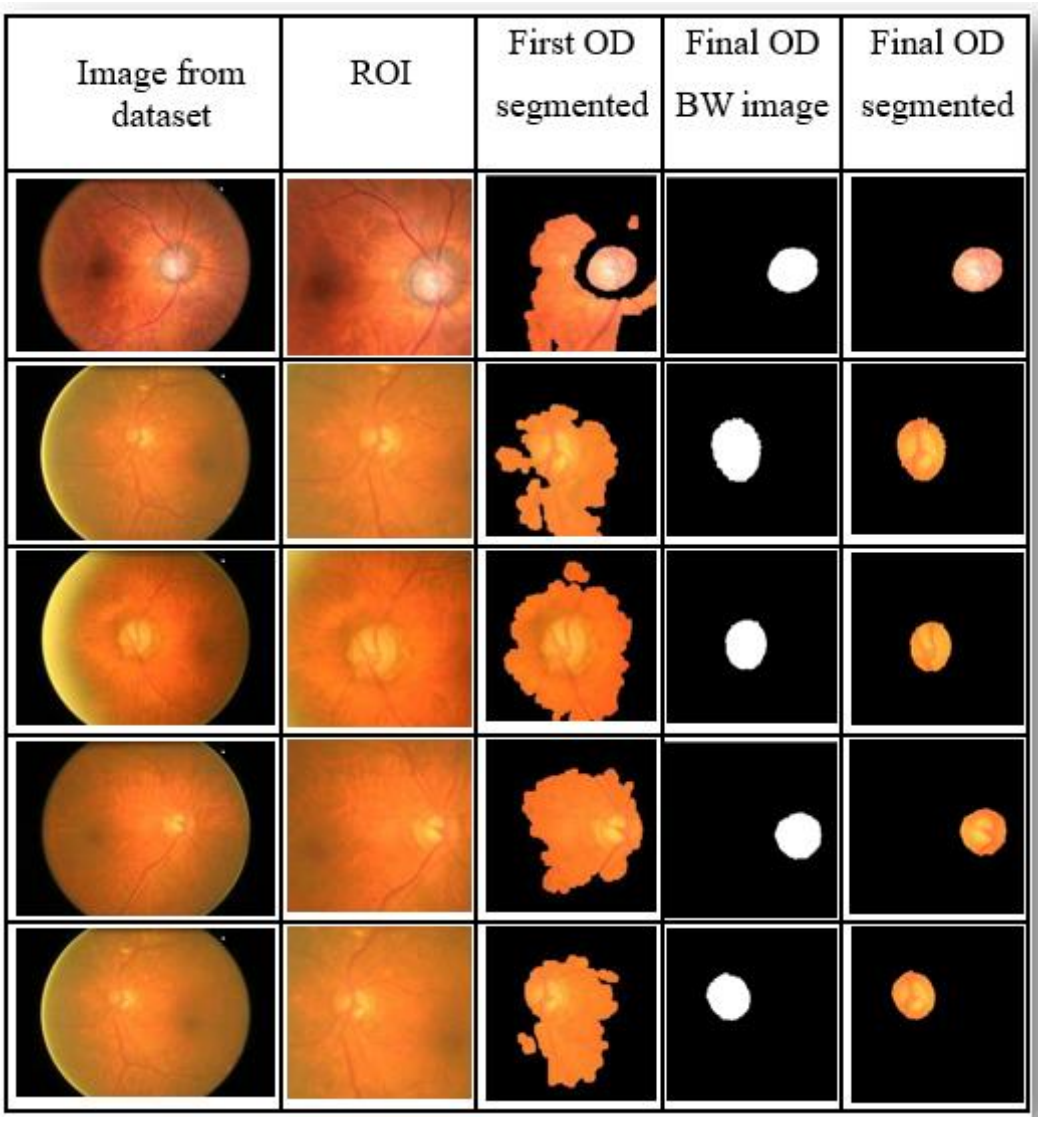

Figure 4.3 Various samples of segmented OD

Accuracy of the four basic positions was used to utilizing to recognize them "OD"segmentation fineness and the scale of performance for Optic Disk segmentation, Table (4.2) shows the confusion matrix of OD segmentation.

Table 4.2 Comparative OD Segmentation results

Research	Dataset	Accuracy
Al-Bander et al.in 2018	MESSIDOR	97%
Hafsa Ahmed * et al. April 22-24, 2014	DMED, FAU	97.5%
Kanchana and Naga Kiran, in 2019	DIARETDB1 With 60 image	94%
Rutuja Shinde.2021	RIM-ONE,DRIVE	98.6%
Sharma et al, In 2019	RIM, DRIONS	95.8%
Hayder et al, In 2020	Origa, Rim-One 3 and Drishti	97.1%
Juneja et al, In 2020	50 fundus images	95.8%
Proposed method	ORIGA MESSIDOR RIM DRISTHI	98.9% 96.5% 95.4% 93.2%

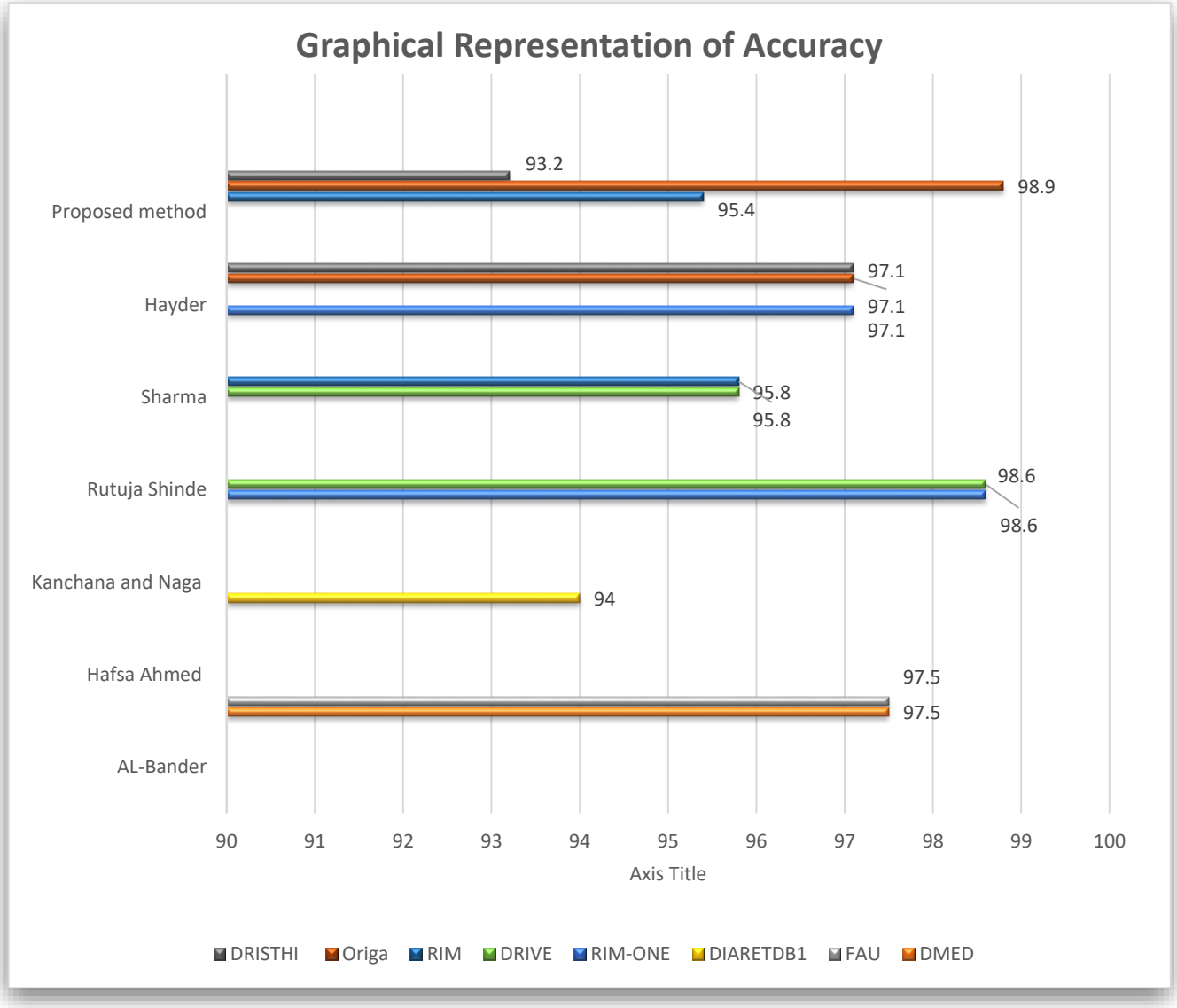

Figure 4.4 Accuracy of OD segmentation results

4.3.2 Result of Automatic Segmentation of Optic Cup

The second stage of segmentation is the optic cup and is of great significance in the diagnosis of glaucoma, since the area after "Optic Cup" segmentation must be calculated. Figure (4.5) shows some results of "Optic Cup" segmentation.

The four definition of the terms ("TP", "TN","FN" and "FP") used with the "Optic Disk" segmentation applied with the "Optic Cup", but the difference is that the region is the "Optic Cup" instead of "Optic Disk".

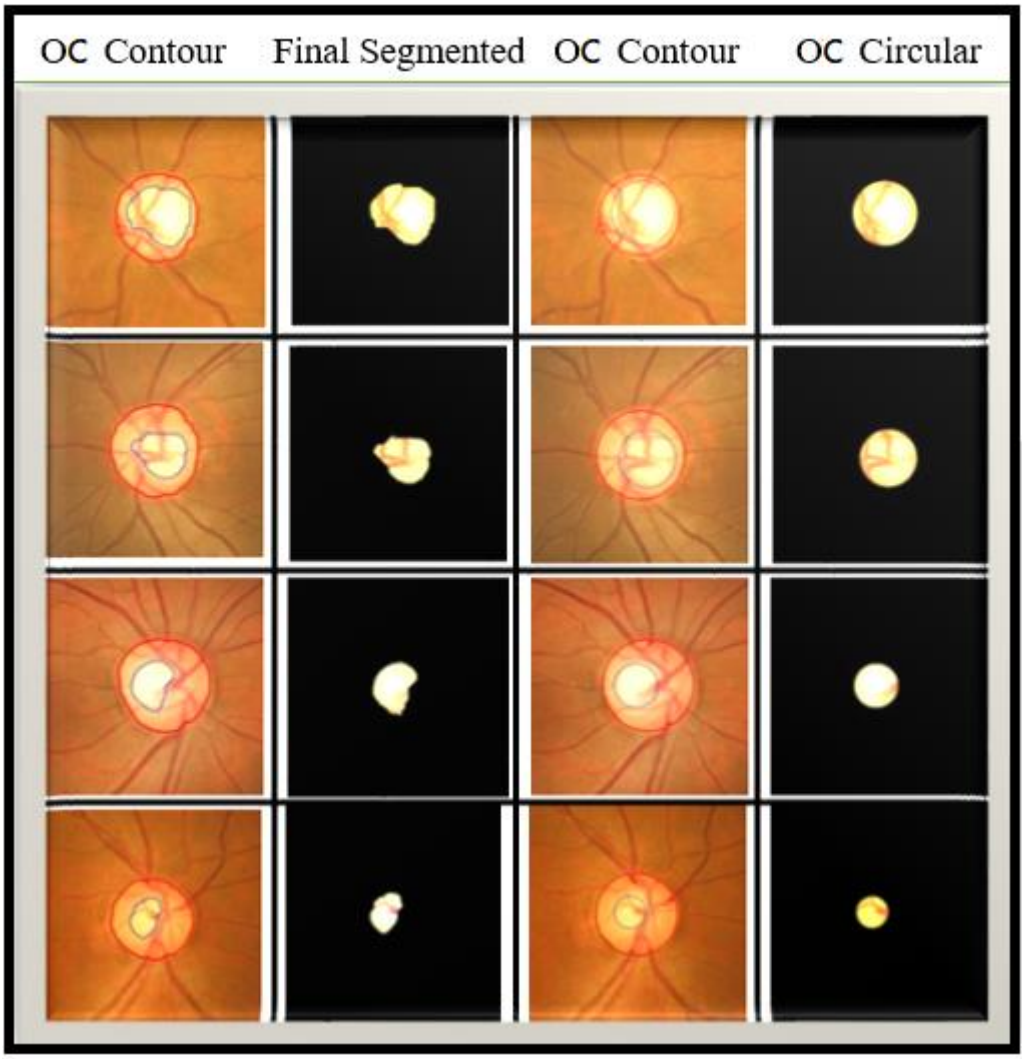

Figure 4.5 Results of OC segmentation in retinal images

Modified imperceptibly by color values to improve contrast with my suggested method of split optical disc made the optic cup area appear clearly, then by applying the proposed threshold and morphological operations, OC segmentation was done accurately so that all the optic cup images were extracted from the optic disc images without any loss for the optic cup.

4.3.3 Result of glaucoma diagnosis by Cup to Disc Ratio (CDR)

The third important stage in the diagnosis of glaucoma is the stage Cup to Disk Ratio, the confusion matrix for the diagnosis of glaucoma using the (CDR) index.

4.3.4 Result of ISNT Rule

Through the CDR, the ISNT index is important in the diagnosis of glaucoma, and the characteristics of this norm are explained in (2.3.2).

4.3.4.1 Results of Neuro Retinal Rim (NRR)

The boundary between Optic Disk and Optic Cup (the inner boundary) is NRR.As in Figure (4.6) depicts the NRR segmentation of OD images.

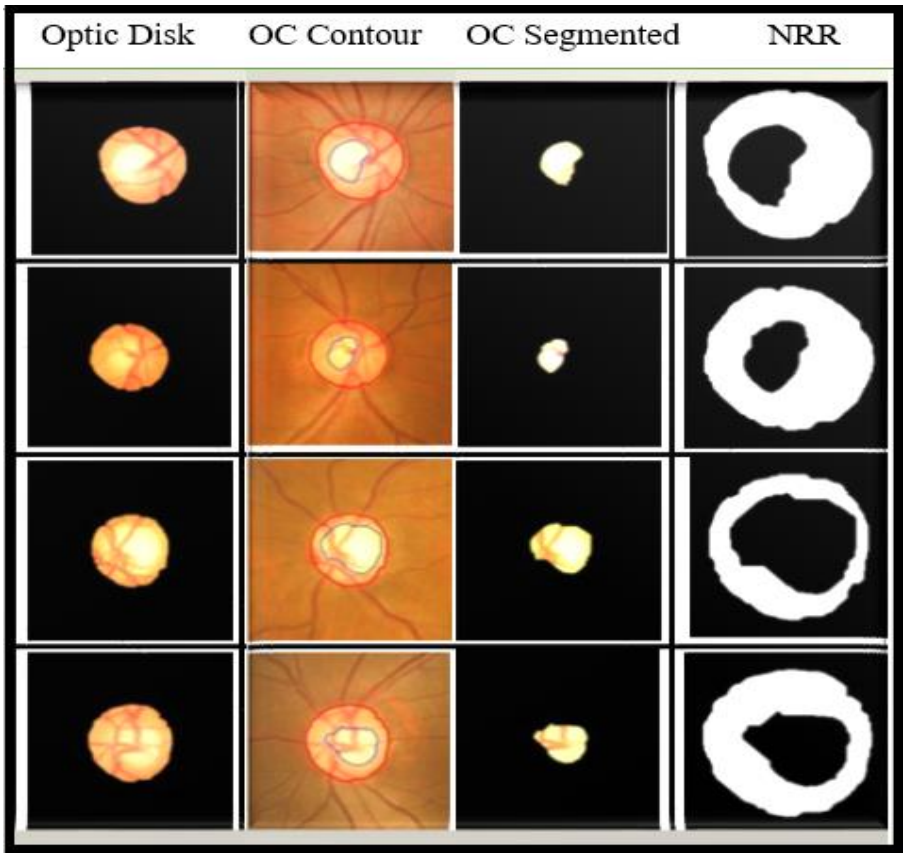

Figure 4.6 Results of NRR segmentation in OD images

4.3.4.2 Results of ISNT Regions

The (ISNT) generated masks for (Superior, Nasal, Inferior and Temporal) regions are applied on the resulted NRR as shown in Figure (4.7).

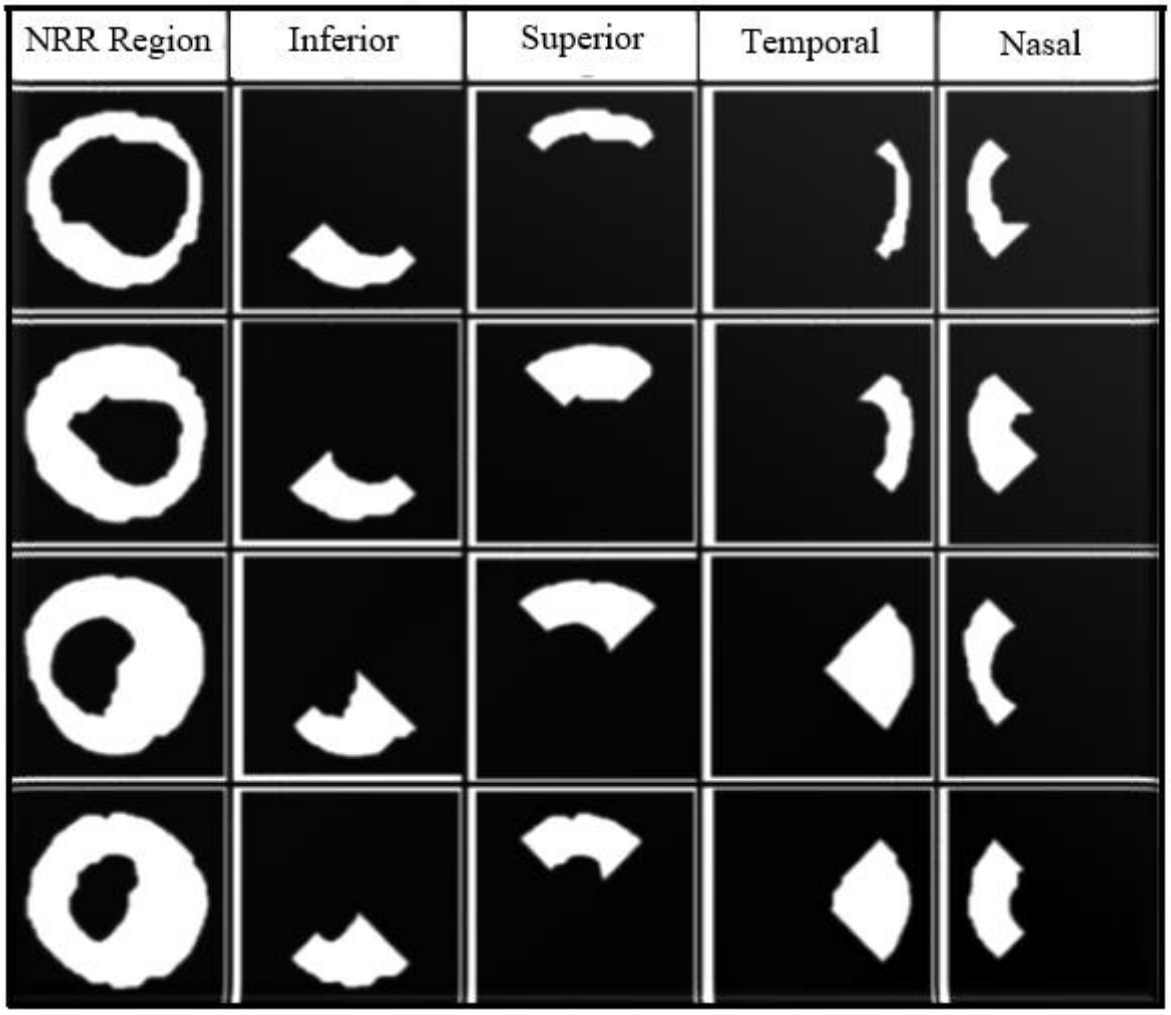

Figure 4.7 Results of ISNT regions

4.3.5 Result of Rim to Disc Ratio (RDR)

The results obtained from this operation are close to the results of the CDR operation due to the segmentation accuracy of both the optic disc and cup and the adoption of the value 0.5, which represents the average values for this measure.

4.3.6 Result of Blood Vessels Ratio (BVR)

In the glaucoma eye, the blood vessels in the optic disc will be high density in the left or right side compared to the healthy eye.

4.3.6.1 Result of Blood Vessels Segmentation

The proposed improved algorithm was able to extract blood vessels in all images of the optic disc accurately as stated in the Figure (4.8) below:

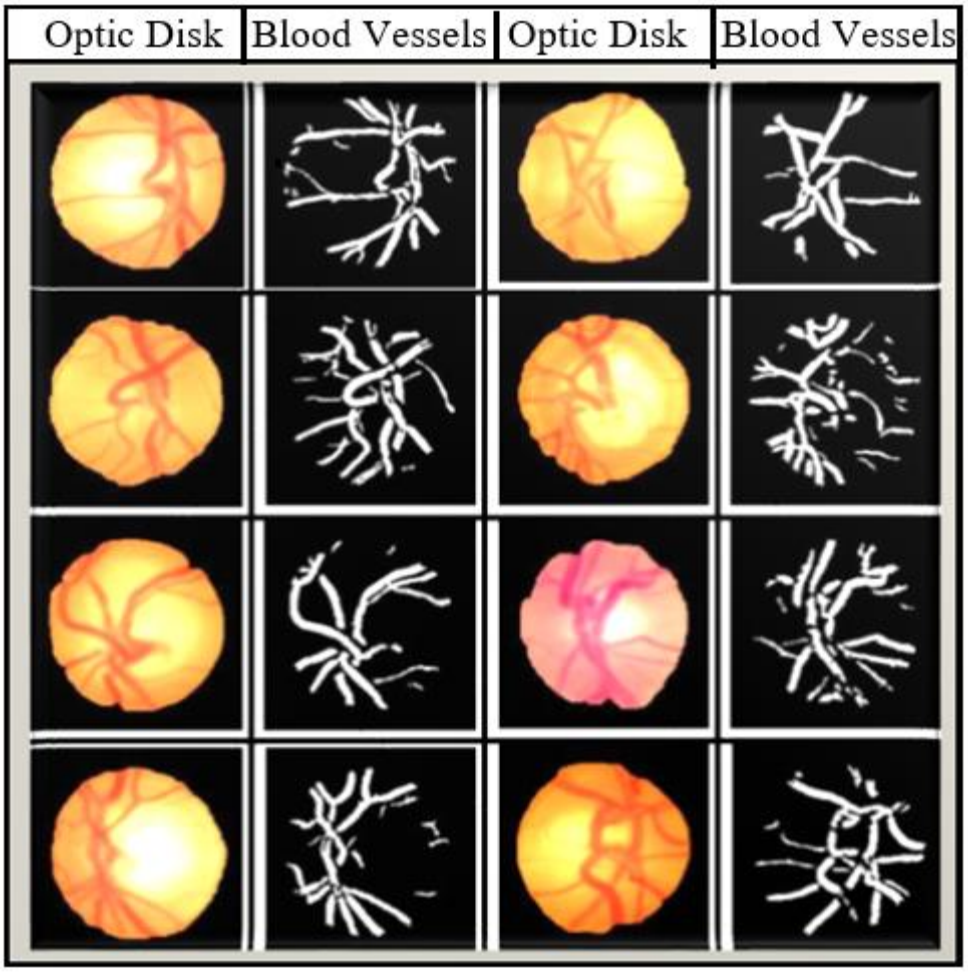

Figure 4.8 Results of blood vessels segmentation

4.3.6.2 Results of ISNT Regions for Blood Vessels

The ISNT masks were applied to the segmented blood vessels in order to compute the Blood Vessels Ratio (BVR). In the most of glaucoma eye, the resulted blood vessels in the Nasal and Temporal region was large than the resulted blood vessels in Inferior and Superior region, but in some images with glaucoma eye, the blood vessels were on the opposite, that is, the blood vessels resulted in the Inferior and Superior region large than the Nasal and Temporal region, the reason for these cases is that the disease in these eyes is in its early stages, the (BVR) satisfies the moderate and severe cases. As Figure (4.9) below states some of the results obtained for ISNT regionsof blood vessels

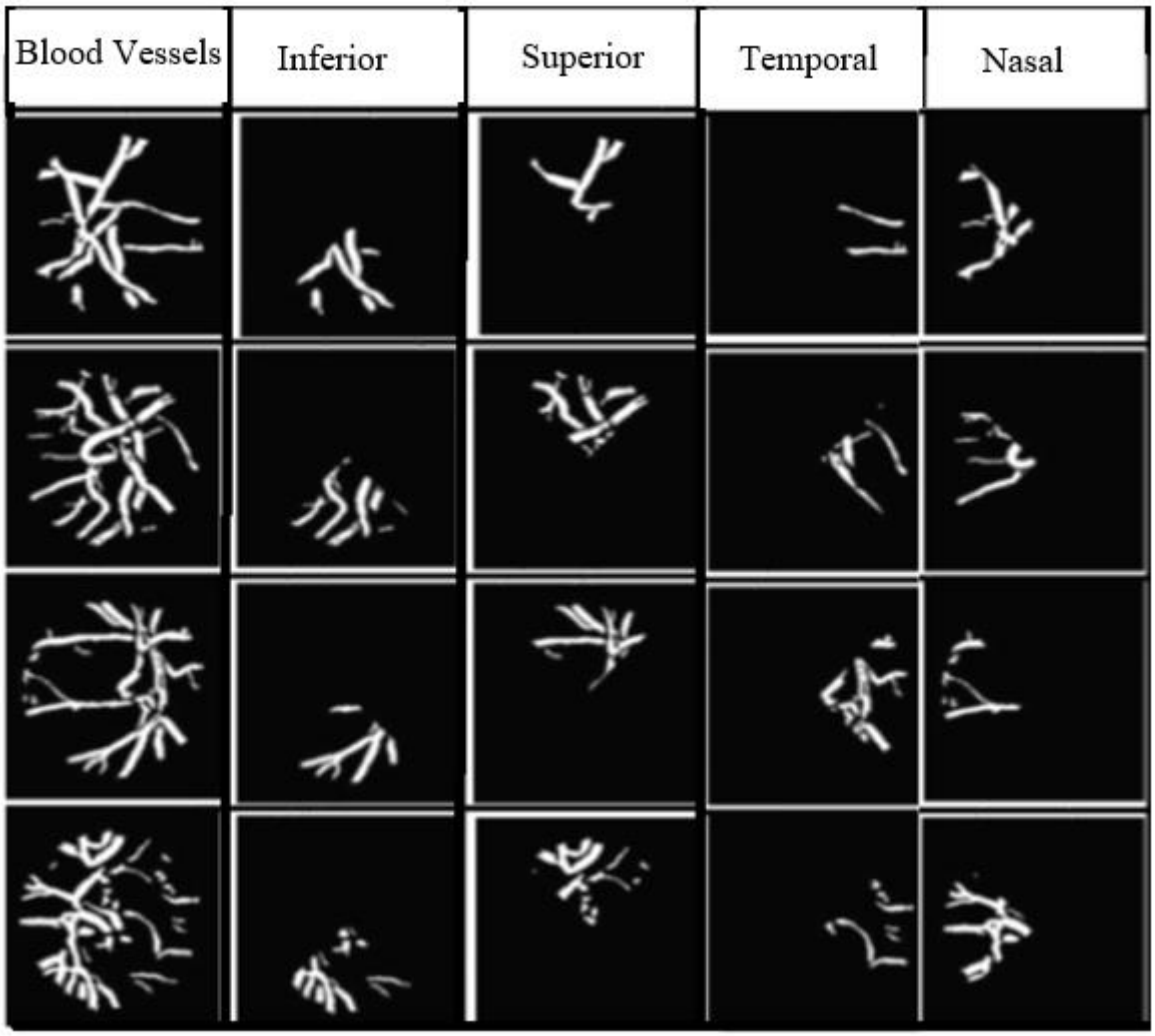

Figure 4.9 Results of ISNT regions of blood vessels

In fact, the Confusion matrix of glaucoma diagnosis by (BVR) is presented in table (4.3), Where (TP) refers to the number of glaucoma images that have blood vessels in Nasal or Temporal region larger than blood vessels in Inferior or Superior region, (TN) refers to the number of healthy images that have bloodvessels in Nasal or Temporal region less than blood vessels in Inferior or Superior region, (FP) indicates the number of healthy images that have bloodvessels in Nasal or Temporal region larger than blood vessels in Inferior or Superior region, (FN) indicates the number of glaucoma images that have blood vessels in Nasal or Temporal region less than blood vessels in Inferioror Superior region.

Table 4.3 Confusion matrix of glaucoma diagnosis using (BVR)

		Positive class	Negative class
Positive class	Glaucoma	N,T > I,S	N,T < I,S
		101	67
Negative class	Healthy	N,T > I,S	N,T < I,S
		28	454

4.3.7 Normalized Features

The main dependence in the correct diagnosis of the disease, as well as in determining the fate of other fragments to extract and extract their features, is directly dependent on the optic disk segmentation algorithm and is very important and for rate this algorithm should be utilizing "Sensitivity", "Specificity", "Precision", and "Accuracy" for all images used.

Shows features for some images after normalized used for classification method in table (4.4).

Table 4.4 Normalized features extracted from OD of fundus images

	CDR	ISNT	RDR	BVR	Energy	Contr.	Homo.	Corrl.	Target
1	0.267909	0.280721	0.731021	0.280721	0.067998	0.237061	0.461645	0.761275	0
2	0.331064	0.371129	0.667888	0.371129	0.085537	0.349116	0.361461	0.729509	0
3	0.355288	0.323649	0.643919	0.323649	0.09138	0.448313	0.334359	0.646406	1
4	0.20653	0.225136	0.793441	0.225136	0.117315	0.261322	0.486869	0.735102	0
5	0.36679	0.263084	0.628848	0.263084	0.06364	0.231712	0.337979	0.798408	0
6	0.240755	0.251137	0.758791	0.251137	0.083287	0.199234	0.42585	0.775981	1
7	0.250679	0.212156	0.748883	0.212156	0.154845	0.355178	0.457428	0.643579	0
8	0	0.189286	1	0.189286	0.204107	0.126028	0.898926	0.67308	1
9	0.227985	0.291027	0.771655	0.291027	0.140811	0.398457	0.795134	0.673444	0
10	0.212222	0.230137	0.787687	0.230137	0.123265	0.279327	0.526457	0.761865	0
11	0.295555	0.255774	0.703843	0.255774	0.128375	0.352424	0.626059	0.750507	0
12	0.330768	0.323898	0.668305	0.323898	0.067694	0.189936	0.576494	0.869521	0
13	0.357849	0.395788	0.616077	0.395788	0	0.155734	0.269077	0.862581	1
14	0.328128	0.264593	0.671031	0.264593	0.08025	0.15565	0.478061	0.890418	0
15	0.276698	0.238389	0.720902	0.238389	0.078859	0.169354	0.43188	0.821177	0
16	0.166059	0.421717	0.833274	0.421717	0.054826	0.357987	0.419973	0.573457	0
17	0.247738	0.28021	0.751984	0.28021	0.110738	0.347906	0.471227	0.702859	0
18	0.492021	0.336973	0.506066	0.336973	0.171008	0.696858	0.306287	0.500408	1
19	0.286719	0.267767	0.712591	0.267767	0.116194	0.296488	0.582666	0.702035	0
20	0.311897	0.233722	0.687262	0.233722	0.110377	0.420014	0.457409	0.687441	1
21	0.20543	0.302636	0.79313	0.302636	0.018529	0.28641	0.253165	0.698201	0
⋮	0.218058	0.224339	0.781806	0.224339	0.046111	0.257099	0.420153	0.718568	⋮
450	0.325947	0.282411	0.667576	0.282411	0.031085	0.219857	0.303839	0.828484	0

The number (1) refers to the glaucoma eye and (0) refers to the healthy eye.

4.3.8 Result of retinal image classification

The prediction system has been constructed from the data obtained from the ORIGA dataset, this dataset contains normal and abnormal images. Figure(4.10) clarifies class accuracy when training more data images. Images are divided into (450 for training and 195 for testing), training set has 335 normal and 115 abnormal images, and the testing set has 145 normal and 50 abnormal images.

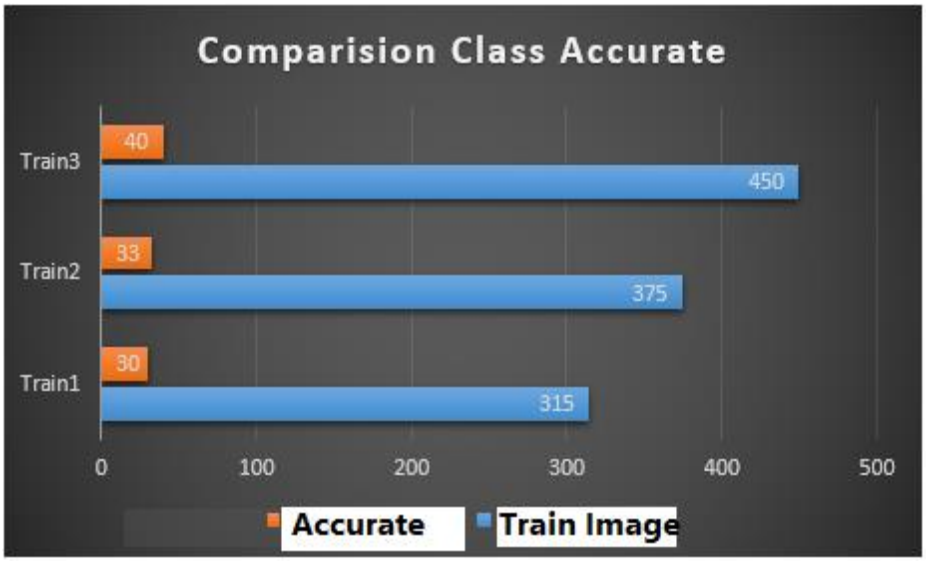

Figure 4.10 Comparison between classes accurate according to the number of train data

In this training phase, a training group was built with two sets of images called normal and abnormal. This group is input to the preprocessing module and generates images appropriate for later processing. These images are passed to a feature extraction module and generate corresponding train features vector. A train features vector is constructed as M x N matrix, where M is the images number and N is extracted features vector, Table (4.4) represents a sample of normalized features extracted which contains eight features value for each image. The purpose of these features is to assist in the process of classification of image as it positive or negative status.

At the testing phase, a set of normal and abnormal images is given as input to the testing phase. Each test image is passing to the preprocessing module, then the output image is passed to the feature extraction module.

The extracted features feed the classification phase in order to classify an image as a positive or negative status using the classifiers ("ANN") and ("SVM").

4.3.8.1 Result of retinal image classification using ANN

The (BR) was used as a function of bias, which indicates Bayesian organization because it has the potential to challenge problems to solve nonlinear data.

Eight input features have been worked on, one for each feature. The hidden layer is single with ten nodes, the output layer was one output neuron, and the backpropagation error was 0.001. The architecture of ANN is depicting in the following Figure (4.11).

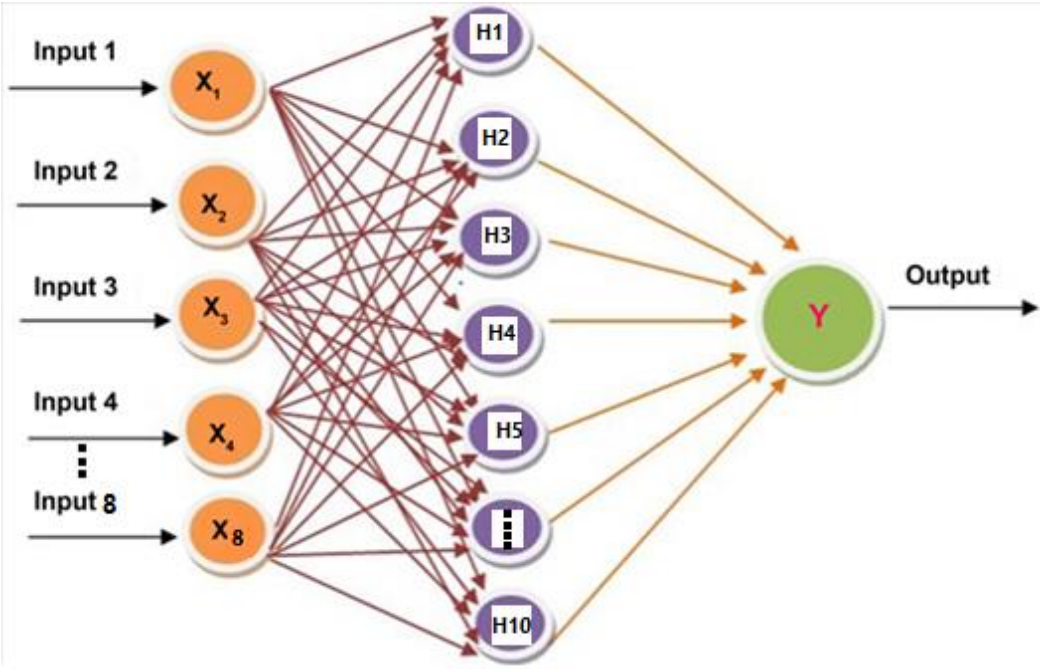

Figure 4.11 ANN architecture

Where (TP) is the glaucomatous images number classified as correct,(TN) is the healthy images number classified as correct,(FP) is the healthy images number classified as incorrect,(FN) is the glaucomatous images number classified as incorrect. Figure (4.12) shows the confusion matrix and performance measures of "8" features utilized ANN classifier.

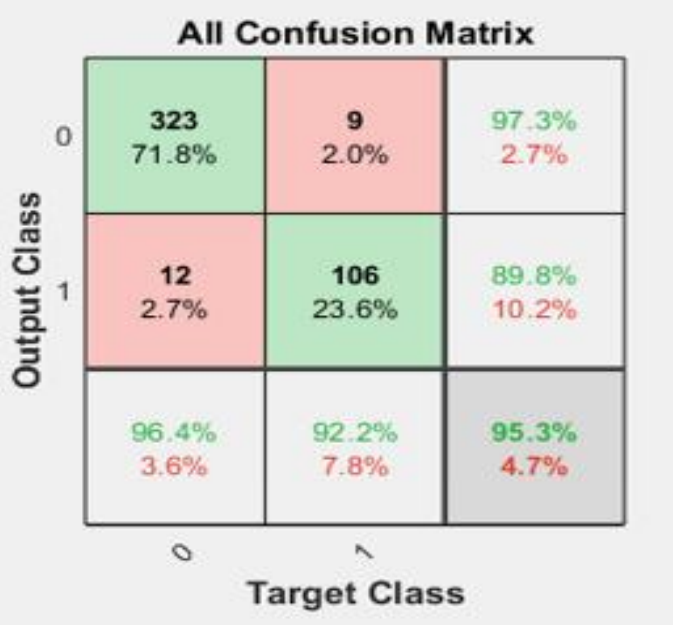

Figure 4.12 Confusion matrix of ANN

In fact by dependence on the table (4.4) which explained that 450 images of OD were extracted successfully from 650 image, five image (3 image with glaucoma, 2 images are healthy) were excluded because the OD segmentation was false, the confusion matrix as show in the following table (4.5).

Table 4.5 Performance measures of (ANN)

	Positive Prediction	Negative Prediction
Positive Class	113	3
Negative Class	2	332

Performance measures are as follows: Accuracy is 95.3%, Sensitivity is

97.3, Specificity is 89.8, Precision is 96.4, and Area under Curve is 92.2.

4.3.8.2 Result of retinal image classification using SVM

When dependence on section (2.10.2) the "RBF" kernel function is applied because it is better for more accurate with non-linear features, Figure(4.13)shows a comparison between different Kernel function used in the test set.

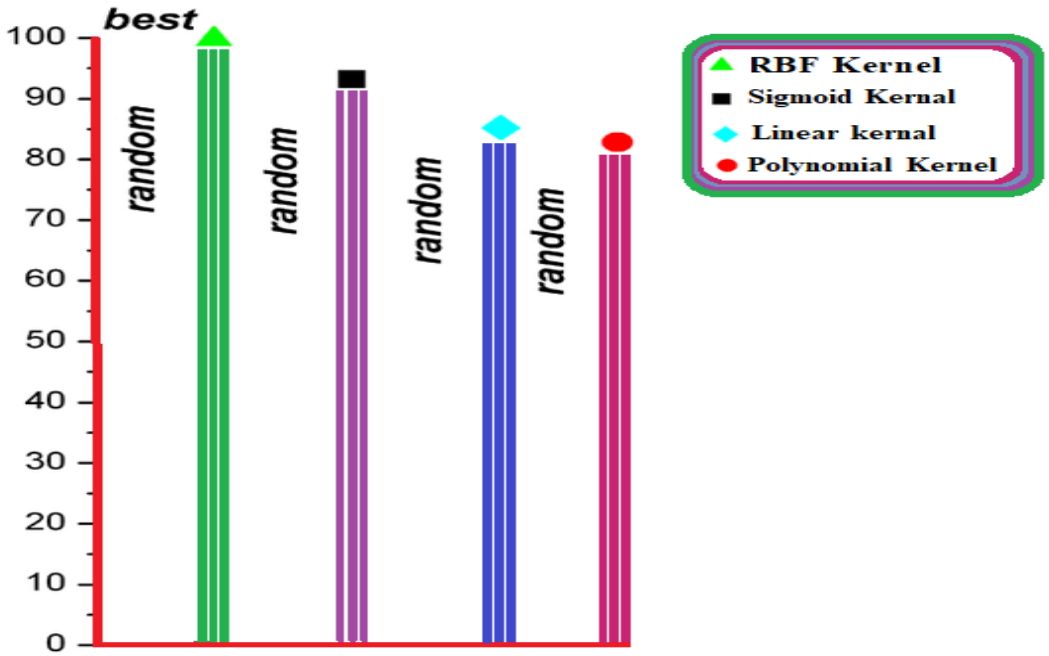

Figure 4.13 Result of accuracy value by different kernels

Table 4.6 Confusion matrix for using the "SVM" classifier

	Positive Prediction	Negative Prediction
Positive Class	114	3
Negative Class	2	331

Performance measures are as follows: Accuracy is 98.8%, Sensitivity is 97.4%, Specificity is 99.3%, Precision is 98.2%, and Area under Curve (AUC) is 98.4%.

Table 4.7 Comparison of the proposed method's efficiency with other algorithms

Research		Accuracy %	Sensitivity %	Specificity %	Area Under Curve%
Proposed Method	SVM	98.8	97.4	99.3	98.4
	ANN	95.3	97.3	89.8	92.2
(Fu *et al.*, 2018)			92	84	91
(Zhou *et al.*, 2018)					84.5
(Li *et al.*, 2018)					83.8
(R. Zhao *et al.*, 2019)					90.5
(Martins,et al.2020)		87	-	85	93

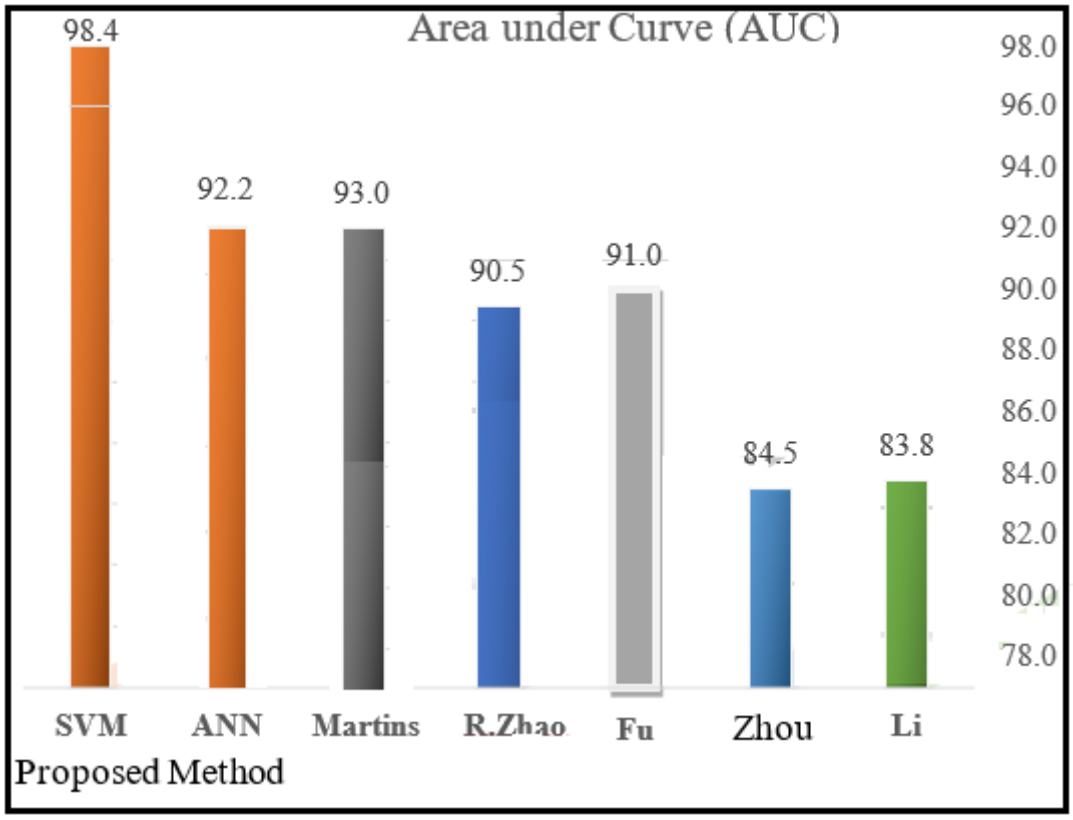

Figure 4.14 Graphical representation for Comparison of the proposed method's efficiency with other algorithms

4.3.9 Result of Glaucoma Progression

The results obtained from this process were based on the percentages that were classified, which represent the average values for this scale (from 0.3 to 0.3999 for early stage, from 0.4 to 0.4999 for moderate stage, and from 0.5 and top for severe stage. Table (4.8) shows the confusion matrix for the (glaucoma stage) index, where it represents the number of glaucoma images considered as (early, moderate, severe) (TP), to the number of non-(early, moderate, severe) images that are considered non-(early, moderate, severe) (TN), (FP) to indicate the number of (early, moderate, severe) images It is considered non-(early, moderate, severe), finally (FN) refers to the number of non-(early, moderate, severe) images and is considered (early, moderate, severe).

Work was carried out on images containing only glaucoma and that did not exceed only 168 images in all "ORIGA" dataset.

Where "TP" is the number of "early" fundus images classified as "early", "TN" is the number of "non-early" fundus images classified as "non-early", "FP" is the number of "early" fundus images classified as "non-early" ("False-Positives") and "FN" is the number of "non-early" fundus images classified as "early" ("False-Negatives").And this applies to all other levels as show in Table(4.8).

Table 4.8 Confusion matrix of Glaucoma Stage

	Positive prediction			Negative prediction		
	Early	moderate	Severe	Early	moderate	Severe
Positive class	29	115	21	0	0	0
Negative class	0	0	0	139	53	147

Performance measures are as follows: Accuracy is 99.4%, Sensitivity is 99.4%, Specificity is 99.4%, Precision is 99.4%, and Area under Curve (AUC) is 99.4%

In this paragraph, by dependent on 150 glaucoma retinal image I tested the accuracy of the decision tree algorithm classifications based on 4 features only, specifically the medical features (CDR,RDR,BVR,ISNT) and compared them with the accuracy of the eight (statistical and medical) advantages, as shown in the Table below (4.9). Where it was concluded that the greater the number of features used in the algorithm increased the accuracy of the diagnosis by dependent on 150 glaucoma.

Table 4.9 Comparison of Confusion Matrix for Medical vs. Medical and Statistical Features

Number of Feature	Early			Moderate			Severe			Accuracy
	E.	M.	S.	M.	E.	S.	S.	E.	M.	
4 Feature	45	15	0	54	21	0	6	0	9	70%
8 Feature	60	0	0	75	0	0	15	0	0	100%

4.3.10 Results of Execution Time

the proposed algorithm to classify any input of RGB retinal image requested an average time of fewer than (2.7) seconds to option result a positive or negative ,in fact the time include all features such as (OC,OD ,ROI,NRR,BV,FE),and test time. As show in Figure (4.16).

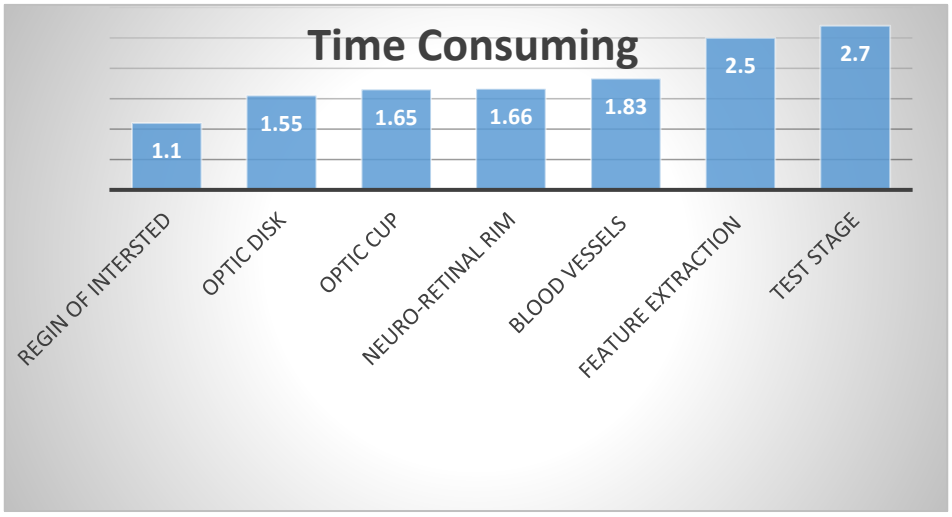

Figure 4.16 Execution Time average of a single fundus image

Chapter Five:

Conclusions and Suggestions for Future Work

5.1 Conclusion

The main conclusions of the results obtained from carrying out of the suggested system for glaucoma diagnosis in the retinal image are:

1. The evaluation of the proposed system is done utilizing "SVM" and "ANN" classifiers on the common dataset ("ORIGA") sensitivity, specificity and accuracy have been 95.3% with (ANN) and 98.9% with (SVM) respectively.
2. The accuracy of the work detect for the levels determine of glaucoma (early, moderate, severe) by dependence on the features is 99.4% with decision tree algorithm.
3. Automatic techniques aiming at segmenting optic disc and cup are innovated based on image processing approaches that strategically combine techniques based on morphology and intensity Threshold that seeks to eliminate false positives in order to achieve precise optic disc segmentation.
4. The planned method is a lot of dependable within the means of selecting features from the segmented optic disc (CDR, ISNT Rule, RDR, BVR contrast, Correlation, Energy and Homogeneity (for that it provides promising and correct results. Also, because it relies on all potential marks for the disease diagnosis.
5. The algorithm for recognizing Blood Vessels networks in the optic disc utilizes a Watershed segmentation or a bottom-hat transform and the mean of the image as a threshold focus on the vessels which leads to increasing the image contrast.
6. Increasing the number of features used in the last classification of the decision tree algorithm is a good case, which achieves higher accuracy than our reliance on a few advantages.

5.2 Suggestions for Future Works

In the future, it is possible to work on developing the study using some suggestions as following:

1) Working on a data set that contains two diseases at the same time, such as diabetes or any other disease that affects the parts of the eye, in addition to glaucoma, and working to detect glaucoma in the absence of another disease.
2) Increasing the number of features to obtain more accuracy in classification, such as extracting all blood vessels and not confining them within the optic disc, and adding Parapapillary atrophy (PPA) as a feature, which due to glaucoma changed the patient outside the OD according to severity stages.
3) Expanding the capacity of the proposed system by a large data set of fundus images up to thousands of images.
4) Developing a system that predicts the glaucoma disease it actually occurs and relying on some inputs such as genetics, African descent, or other diseases that cause eye pressure or damage to eye cells, which may cause glaucoma in the patient's near future.
5) Development of work that determines the level of progression of glaucoma and access to the five stages(normal visual field , early , moderate , severe , end-stage) instead of the three levels used in this research.

References:

Abdel-hamid, L., (2019) ,‘Glaucoma Detection from Retinal Images Using Statistical and Textural Wavelet Features’.

Abiodun, O. I. *et al.*, (2018), ‘State-of-the-art in artificial neural network applications: A survey’, *Heliyon*. Elsevier Ltd, 4(11), p. e00938. doi: 10.1016/j.heliyon.2018.e00938.

Ahmad, A. Yamin, A. Shakeel, S. O. Gillani and U. Ansari, "Detection of glaucoma using retinal fundus images, (*2014)* "*International Conference on Robotics and Emerging Allied Technologies in Engineering (iCREATE)*, pp. 321-324, doi: 10.1109/iCREATE.2014.68283888.

Akil, M. *et al.* ,(2018), ‘Computational efficiency of optic disk detection on fundus image: a survey’, p. 15. doi: 10.1117/12.2304941.

Al-Bander, B., Al-Nuaimy, W., Williams, Bryan M, *et al.* ,(2018), ‘Multiscale sequential convolutional neural networks for simultaneous detection of fovea and optic disc’, *Biomedical Signal Processing and Control*. Elsevier Ltd, 40, pp. 91–101. doi: 10.1016/j.bspc.2017.09.008.

Al-Bander, B., Al-Nuaimy, W., Williams, Bryan M., *et al.*, (2018), ‘Multiscale sequential convolutional neural networks for simultaneous detection of fovea and optic disc’, *Biomedical Signal Processing and Control*. Elsevier Ltd, 40, pp. 91–101. doi: 10.1016/j.bspc.2017.09.008.

Al-Bander, W. Al-Nuaimy, B. Williams and Y. Zheng, (2018), "Multiscale sequential convolutional neural networks for simultaneous detection of fovea and

optic disc", Biomedical Signal Processing and Control, vol. 40, pp. 91-101,. Available: 10.1016/j.bspc.2017.09. 008.

Albregtsen, F. ,(2008) ,'Statistical Texture Measures Computed from Gray Level Coocurrence Matrices', *... Laboratory, Department of Informatics, University of ...*, pp. 1–14. doi: 10.2307/302397.

An, G. *et al.* ,(2019), 'Glaucoma Diagnosis with Machine Learning Based on Optical Coherence Tomography and Color Fundus Images',*Journal of Healthcare Engineering*, 2019. doi: 10.1155/2019/4061313.

Anil, S. and Issac, P. E., (2018), 'Survey on Various Methods of Detecting Glaucoma', *International Journal of Trend in Scientific Research and Development*,Volume-2(Issue-2),pp.1664–1671. doi: 10.31142/ijtsrd10704. Availableat:http://www.ijetsr.com/images/short_pdf/1500867615_487-493-ietep748_ijetsr.pdf.

Balasubramanian & Sagar, Anantha & Saradhi, G. & Chandrasekaran, Venkatachalam. ,(2008),. Automatic Localization and Segmentation of Blood Vessels, Optic Disc, and Macula in Digital Fundus Images. 10.1007/978-0-387-74938-9_37.

Bourne, R. ,(2010),. Contrast Adjustment. In: Fundamentals of Digital Imaging in Medicine. Springer, London. https://doi.org/10.1007/978-1-84882-087-6_6.

C S, F. and E N, S. ,(2019), 'Glaucoma Detection Using Fundus Images and OCT Images', *SSRN Electronic Journal*. doi: 10.2139/ssrn.3445912.

Carrillo, J. *et al.* ,(2019), 'Glaucoma Detection Using Fundus Images of the Eye', *Symposium on Image, Signal Processing and Artificial Vision, STSIVA 2019 - Conference Proceedings*. IEEE, pp. 1–4. doi: 10.1109/STSIVA.2019.8730250.

Chakraverty, S., Sahoo, D. M. and Mahato, N. R. ,(2019), *Concepts of Soft Computing, Concepts of Soft Computing*. doi: 10.1007/978-981- 13-7430-2.

Cheran, L. E. *et al.*, (2004), 'Protein microarray scanning in label-free format by Kelvin nanoprobe', *Analyst*, 129(2), pp. 161–168. doi: 10.1039/b314058j.

Chethan Kumar N.S, D. S. K.,(2017), 'Image Processing Techniques for Automatic Detection of Glaucoma - A Study', *international journal of Latest Technology in Engineering, MAnagement & Applied Science (IJLTEMAS)*, VI(Vii), pp. 112–119.

Damasevicius, Robertas.,(2010),"Optimization of SVM parameters for recognition of regulatory DNA sequences". TOP. 18. 339-353. 10.1007/s11750-010-0152-x.

Das, P., Nirmala, S.R. & Medhi, J.P ,(2016)," Diagnosis of glaucoma using CDR and NRR area in retina images. *Netw Model Anal Health Inform Bioinforma* "5**,** 3. https://doi.org/10.1007/s13721-015-0110-5.

Davies, E. R.,(2017), "*Computer Vision: Principles, Algorithms, Applications, Learning: Fifth Edition*." 5th edn, *Computer Vision: Principles, Algorithms, Applications, Learning: Fifth Edition*. 5th edn. Academic Press.

De Stefano, A., White, P. R. and Collis, W. B.,(2004), 'Training methods for image noise level estimation on wavelet components', *Eurasip Journal on Applied Signal Processing*, 2004(16), pp. 2400– 2407. doi: 10.1155/S1110865704401218.

Dutta, K. *et al.*, (2018), 'Automatic evaluation and predictive analysis of optic nerve head for the detection of glaucoma', *2018 2nd International Conference on*

Electronics, Materials Engineering and Nano-Technology, IEMENTech2018.IEEE,pp.1–7. doi: 10.1109/IEMENTECH.2018.8465169.

Ehsani Rad, Abdolvahab & Rahim, Mohd & Rehman, Amjad & Altameem, Ayman & Saba, Tanzila., (2013),. Evaluation of Current Dental Radiographs Segmentation Approaches in Computer-aided Applications. IETE Technical Review. 30. 210-222. 10.4103/0256-4602.113498.

Esmaeili, M., Rabbani, H., Mehri, A., Dehghani, A., (2009), "Extraction of retinal blood vessels by curvelet transform", 16th IEEE International Conference on Image Processing (ICIP), pp.3353-3356, DOI: 10.1109/ICIP.2009.5413909.

Fan, Z. *et al.*, (2018), 'Optic Disk Detection in Fundus Image Based on Structured Learning', *IEEE Journal of Biomedical and Health Informatics*, 22(1), pp. 224–234. doi: 10.1109/JBHI.2017.2723678.

Farrah, Tariq & Dhillon, Baljean & Keane, Pearse & Webb, David & Dhaun, Neeraj. ,(2020),"The eye, the kidney & cardiovascular disease: old concepts, better tools & new horizons. Kidney International". 98. 10.1016/j.kint.2020.01.039.

Fernandez-Granero, M. A. *et al.*, (2017) ,'Automatic CDR Estimation for Early Glaucoma Diagnosis', *Journal of Healthcare Engineering*, 2017. doi: 10.1155/2017/5953621.

Fu, H. *et al.*, (2018) ,'Disc-Aware Ensemble Network for Glaucoma Screening from Fundus Image', *IEEE Transactions on Medical Imaging*, 37(11), pp. 2493–2501. doi: 10.1109/TMI.2018.2837012.

Gao, Y., Yu, X., Wu, C., Zhou, W. *et al.*, (2019), 'Accurate optic disc and cup segmentation from retinal images using a multi- feature based approach for glaucoma assessment', *Symmetry*, 11(10). doi: 10.3390/sym11101267.

Gao, Y., Yu, X., Wu, C., Zhou, W., Lei, X., *et al.* ,(2019), 'Automatic Optic Disc Segmentation Based on Modified Local Image Fitting Model with Shape Prior Information', *Journal of Healthcare Engineering*, 2019. doi: 10.1155/2019/2745183.

Gao, Yuan & Yu, Xiaosheng & Wu, Chengdong & Zhou, Wei & Wang, Xiaonan & Chu, Hao. ,(2019),. Accurate and Efficient Segmentation of Optic Disc and Optic Cup in Retinal Images Integrating Multi-View Information. IEEE Access. PP. 1-1. 10.1109/ACCESS.2019.2946374.

Garnavi, R. ,(2020), *AI Holds Promise for Glaucoma, a Leading Global Cause of Blindness*.Availableat: https:///research/2019/05/ai-glaucoma/.

Gómez-Valverde, J. J. *et al.*, (2019), 'Automatic glaucoma classification using color fundus images based on convolutional neural networks and transfer learning', *Biomedical Optics Express*, 10(2), p. 892. doi: 10.1364/boe.10.000892.onzalez, R. C. and Woods, R. E. (2018) *Digital Image Processing (4th Ed)*.

Guo, Y. Mai, X. Zhao, X. Duan, Z. Fan, B. Zou, B. Xie ,(2018),"A mobile app using the measurement of clinical parameters for glaucoma screening" IEEE Access, pp. 77414-77428.

Gyimah and D. K. Dake, ,(2019),"Using Decision Tree Classification Algorithm to Predict Learner Typologies for Project-Based Learning," *2019 International*

Conference on Computing, Computational Modelling and Applications (ICCMA), , pp. 130-1304, doi: 10.1109/ICCMA.2019.00029.

Haggerty, J.M., Wang, X.N., Dickinson, A. *et al.* Segmentation of epidermal tissue with histopathological damage in images of haematoxylin and eosin stained human skin. *BMC Med Imaging* **14,** 7,(2014),. https://doi.org/10.1186/1471-2342-14-7.

Haggerty, Juliana & Wang, Xiao-nong & Dickinson, Anne & O'Malley, Christopher & Martin, Elaine.,(2014),. Segmentation of epidermal tissue with histopathological damage in images of haematoxylin and eosin stained human skin. BMC medical imaging. 14. 7. 10.1186/1471-2342-14-7.

Hagiwara, Y. *et al.* ,(2018), 'Computer-aided diagnosis of glaucoma using fundus images: A review', *Computer Methods and Programs in Biomedicine*, pp. 1–12. doi: 10.1016/j.cmpb.2018.07.012.

Haruta, M., Kodama, R. and Yamakawa, R.,(2017), 'Optical coherence tomography detection of characteristic retinal nerve fiber layer thinning in nasal hypoplasia of the optic disc', *Eye (Basingstoke)*. Nature Publishing Group, 31(12), pp. 1685–1688. doi: 10.1038/eye.2017.134.

Hassan, M. *et al.* ,(2017), 'Robust Hidden Markov Model based intelligent blood vessel detection of fundus images', *Computer Methods and Programs in Biomedicine*. Elsevier Ireland Ltd, 151, pp. 193–201. doi: 10.1016/j.cmpb.2017.08.023.

Holmgren, G., Andersson, P., Jakobsson, A. *et al.* Artificial neural networks improve and simplify intensive care mortality prognostication: a national cohort

study of 217,289 first-time intensive care unit admissions. *j intensive care* **7,** 44 ,(2019),. https://doi.org/10.1186/s40560-019-0393-1.

Ibraheem, Noor & Hasan, Mokhtar & Khan, Rafiqul Zaman & Mishra, Pramod. ,(2012),. Understanding Color Models: A Review. ARPN Journal of Science and Technology. 2.

Ikebe, Masayuki & Asai, Tetsuya. ,(2005),. A Digital Vision Chip for Early Feature Extraction with Rotated Template-Matching CA. Journal of Robotics and Mechatronics. 17. 10.20965/jrm.2005.p0372.

Joshua, A. O., Nelwamondo, F. V. and Mabuza-Hocquet, G.,(2019), 'Segmentation of Optic Cup and Disc for Diagnosis of Glaucoma on Retinal Fundus Images', *Proceedings - 2019 Southern African Universities Power Engineering Conference/Robotics and Mechatronics/Pattern Recognition Association of South Africa, SAUPEC/RobMech/PRASA 2019*, pp. 183–187. doi: 10.1109/RoboMech.2019.8704727.

Juan J. Gómez-Valverde, Alfonso Antón, Gianluca Fatti, Bart Liefers, Alejandra Herranz, Andrés Santos, Clara I. Sánchez, and María J. Ledesma-Carbayo, ,(2019),."Automatic glaucoma classification using color fundus images based on convolutional neural networks and transfer learning," Biomed. Opt. Express 10, 892-913.

Juneja, M., Singh, S., Agarwal, N. *et al.*,(2020),. Automated detection of Glaucoma using deep learning convolution network (G-net). *Multimed Tools Appl* **79,** 15531–15553 https://doi.org/10.1007/s11042-019-7460-4.

Jyoti Patil and Sharmila Chaudhari. ,(2021), "Determination of Glaucoma Grade with Cup to Disc Ratio". *Acta Scientific Ophthalmology* 4.3 44-53.

Kalra, R. ,(2016), ‘A survey on Machine Learning Techniques in Health Care Industry’, 3(2), pp. 128–132.

Kanchana, V. and Naga Kiran, D. ,(2019), ‘Recognistion of glaucoma using otsu segmentation method’, International Journal of Research in Pharmaceutical Sciences,10(3), pp. 1988–1996.doi: 10.26452.

Kanchana, V. and Naga Kiran, D. ,(2019), ‘Recognistion of glaucoma using otsu segmentation method’, *International Journal of Research in Pharmaceutical Sciences*, 10(3), pp. 1988–1996. doi: 10.26452/ijrps.v10i3.1407.

Kannan, R. and Radhika, T. ,(2012), ‘Diabetes mellitus and oral health’, *Journal of Orofacial Sciences*, 4(1), p. 7. doi: 10.4103/0975- 8844.99874.

Kanse, S. S. and Yadav, D. M. ,(2019), ‘Retinal Fundus Image for Glaucoma Detection: A Review and Study’, *Journal of Intelligent Systems*, pp. 43–56. doi: 10.1515/jisys-2016-0258.

Kavya, N. and Padmaja, K. V. ,(2018), ‘Glaucoma detection using texture features extraction’, in *Conference Record of 51st Asilomar Conference on Signals, Systems and Computers, ACSSC 2017*, pp. 1471–1475. doi: 10.1109/ACSSC.2017.8335600.

Kekre, H. B. and Thepade, S. D. ,(2008), ‘Boosting Block Truncation Coding with Kekre ’ s LUV Color Space for Image Retrieval’, *Engineering*, pp. 172–180.

Kinser, J. M. ,(2019), *Image Operators - Image Processing in Python*. 37.Kowalczyk, A. (2017) ‘Support Vector Machines Succinctly’, *Journal of Chemical Information and Modeling*, 53(9), pp. 1689–1699. doi: 10.1017/CBO9781107415324.004.

Kumar, J. R. H. *et al.* ,(2019), ‘Rim-to-Disc Ratio Outperforms Cup- to-Disc Ratio for Glaucoma Prescreening’, *Scientific Reports*. Springer US, 9(1), pp. 1–9. doi: 10.1038/s41598-019-43385-2.

Kumar, J.R.H., Seelamantula, C.S., Kamath, Y.S. *et al.* Rim-to-Disc Ratio Outperforms Cup-to-Disc Ratio for Glaucoma Prescreening. *Sci Rep* **9,** 7099 ,(2019),. https://doi.org/10.1038/s41598-019-43385-2.

Kumar, J.R.H., Seelamantula, C.S., Kamath, Y.S. *et al.* Rim-to-Disc Ratio Outperforms Cup-to-Disc Ratio for Glaucoma Prescreening. *Sci Rep* **9,** 7099 ,(2019),. https://doi.org/10.1038/s41598-019-43385-2.

Kumar, Jayant & Kohli, Piyush & Kannan, Naresh & Krishnakumar, Krishin & Arthur, Dhipak & Ramasamy, Kim. ,(2021),. Comparison of two ultra-widefield imaging for detecting peripheral retinal breaks requiring treatment. Albrecht von Graæes Archiv für Ophthalmologie. 259. 10.1007/s00417-020-04938-8.

Latif, A. Rasheed, U. Sajid, J. Ahmed, N. Ali, N. I. Ratyal, et al.,(2019), Content-based image retrieval and feature extraction: a comprehensive review, Math. Probl. Eng.,.

Li, A. *et al.*,(2018), ‘Combining Multiple Deep Features for Glaucoma Classification’, *ICASSP, IEEE International Conference on Acoustics, Speech and Signal Processing - Proceedings*. IEEE, 2018- April, pp. 985–989. doi: 10.1109/ICASSP.2018.8462089.

Liao, P. S., Chen, T. S. and Chung, P. C. ,(2001), ‘A fast algorithm for multilevel Threshold’, *Journal of Information Science and Engineering*, 17(5), pp. 713–727. doi: 10.6688/JISE.2001.17.5.1.

M. Abdalla, A. M., Dress, S. and Zaki, N. ,(2011), ‘Detection of Masses in Digital Mammogram Using Second Order Statistics and Artificial Neural Network’, *International Journal of Computer Science and Information Technology*, 3(3), pp. 176–186. doi: 10.5121/ijcsit.2011.3312.

MacCormick, I. J. C. *et al.*, (2019), ‘Correction: Accurate, fast, data efficient and interpretable glaucoma diagnosis with automated spatial analysis of the whole cup to disc profile (PLoS ONE 14:1 (e0209409) DOI: 10.1371/journal.pone.0209409)’, *PLoS ONE*, 14(4),pp. 1–20. doi: 10.1371/journal.pone.0215056.

Mahmood, Faleh & Resen, Ali & Badr, Ahmed. ,(2019),. Wind characteristic analysis based on Weibull distribution of Al-Salman site, Iraq. Energy Reports. 6. 10.1016/j.egyr.2019.10.021.

Manikandan, T. *et al.* ,(2019),. ‘Glaucoma Detection in Retinal Images using Automatic Threshold and Marker - Controlled Watershed Transformation’, *International Journal of Innovative Technology and Exploring Engineering*, 9(1S), pp. 210–213. doi: 10.35940/ijitee.a1043.1191s19.

Marjanovic, I., ,(2011),. 'The Optic Nerve in Glaucoma', in T. Kubena (ed.), the Mystery of Glaucoma, IntechOpen, London. 10.5772/19811.

Martins, J., Cardoso, J. S. and Soares, F. ,(2020),. ‘Offline computer- aided diagnosis for Glaucoma detection using fundus images targeted at mobile devices’, *Computer Methods and Programs in Biomedicine*, 192. doi: 10.1016/j.cmpb.2020.105341.

Mitra, P. P ,(2014), ‘The circuit architecture of whole brains at the mesoscopic scale’, *Neuron*. Elsevier Inc., pp. 1273–1283. doi: 10.1016/j.neuron.2014.08.055.

Mohanaiah, P., Sathyanarayana, P. and Gurukumar, L. (2013) ‘Approach’, 3(5), pp. 1–5.

Muthmainah, M. V. *et al*,(2019), ‘Analysis of Retinal Fundus Images for Classification of Glaucoma’, *Proceedings - 2018 1st International Conference on Bioinformatics, Biotechnology, and Biomedical Engineering, BioMIC 2018*. doi: 10.1109/BIOMIC.2018.8610605.

Mvoulana, A., Kachouri, R. and Akil, M. ,(2019), ‘Fully automated method for glaucoma screening using robust optic nerve head detection and unsupervised segmentation based cup-to-disc ratio computation in retinal fundus images’, *Computerized Medical Imaging and Graphics*. Elsevier Ltd, 77. doi: 10.1016/j.compmedimag.2019.101643.

Noury, Erfan & Mannil, Suria & Chang, Robert & Ran, Anran & Cheung, Carol & Thapa, Suman & Rao, Harsha & Dasari, Srilakshmi & Riyazuddin, Mohammed & Nagaraj, Sriharsha & Zadeh, Reza. ,(2019), Detecting Glaucoma Using 3D Convolutional Neural Network of Raw SD-OCT Optic Nerve Scans.

Nugroho, H. Adi & Listyalina, Latifah & Wibirama, Sunu & KZ, Widhia. ,(2018),Automated determination of macula centre point based on geometrical and pixel value approaches to support detection of foveal avascular zone. International Journal of Innovative Computing, Information and Control. 14. 1453-1463. 10.24507/ijicic.14.04.1453.

Nugroho, Hanung Adi & Listyalina, Latifah & Wibirama, Sunu & KZ, Widhia. ,(2018), Automated determination of macula centre point based on geometrical and pixel value approaches to support detection of foveal avascular zone. International Journal of Innovative Computing, Information and Control. 14. 1453-1463. 10.24507/ijicic.14.04.1453.

Nyein Nyein Hlaing, K. ,(2018), 'First Order Statistics and Glcm Based Feature Extraction for Recognition of Myanmar Paper Currency', *The IIER International Conference,* (2011), pp. 1–6.

Oztas, Z., Akkin, C., Nalcaci, S. *et al.* ,(2017), Branch retinal vein occlusion: the importance of the topographical distribution of retinal vessels among risk factors. *Eye* 31**,** 726–731. https://doi.org/10.1038/eye.2016.318.

Pathan, S., Kumar, P. and Pai, R. M. ,(2018), 'The Role of Color and Texture Features in Glaucoma Detection', *2018 International Conference on Advances in Computing, Communications and Informatics, ICACCI 2018*, pp. 526–530. doi: 10.1109/ICACCI.2018.8554854.

Poon LY, Solá-Del Valle D, Turalba AV, et al. ,(2017), The ISNT Rule: How Often Does It Apply to Disc Photographs and Retinal Nerve Fiber Layer Measurements in the Normal Population? American Journal of Ophthalmology. Dec; 184:19-27. DOI: 10.1016/j.ajo.2017.09.018. PMID: 28947074; PMCID: PMC5705386.

Qidwai, U. and Chen, C. H. ,(2009), *Digital Image Processing An Algorithmic Approach with MATLAB, SpringerReference*. doi: 10.1007/SpringerReference_61945. Rahmati, M. (2015) 'Introduction ': 2(1), pp. 51–58.

Rot, P. *et al.* ,(2020), *Handbook of Vascular Biometrics*. Springer International Publishing. doi: 10.1007/978-3-030-27731-4.

Rutuja Shinde,(2021), "Glaucoma detection in retinal fundus images using U-Net and supervised machine learning algorithms, Intelligence-Based Medicine", Volume 5, 2021, 100038, ISSN 2666 5212,doi.org/10.1016/j.ibmed.2021.100038.

Sahu, S. *et al.* ,(2019) ,'Image Processing Based Automated Glaucoma Detection Techniques and Role of De-Noising: A Technical Survey', *Handbook of Multimedia Information Security: Techniques and Applications*, pp. 359–375. doi: 10.1007/978-3-030-15887-3_16.

Salam, A. A. *et al.*, (2016), 'Automated detection of glaucoma using structural and nonstructural features', *SpringerPlus*. Springer International Publishing, 5(1). doi: 10.1186/s40064-016-3175-4.

Samawi, H. J., Al-Sultan, A. Y. and Al-Saadi, E. H. ,(2020), 'Optic Disc Segmentation in Retinal Fundus Images Using Morphological Techniques and Intensity Threshold', in *2020 International Conference on Computer Science and Software Engineering (CSASE)*. IEEE, pp. 302–307.

Samawi, Hayder & Yousif, Ali & Al-Saadi, Enas. ,(2020),. Optic Disc Segmentation in Retinal Fundus Images Using Morphological Techniques and Intensity Thresholding.302-307. 10.1109/CSASE48920.2020.9142061.

Sambandam, B. T., Josephine, M. S. and Jeyabalaraja, V., (2017), 'Segmentation of optic disc and optic cup using krill herd algorithm for the assessment of glaucoma', *International Journal of Applied Engineering Research*, 12(21), pp. 10938–10944.

Sarkar, A., Sarkar, S. K. and Nag ,(2018), 'Automated Glaucoma Detection from Fundus Images using clustering and Ellipse-Fitting', 6(4), pp. 2–6.

Sedai, S. *et al.*, (2017), 'Segmentation of Optic Disc and Optic Cup in Retinal Fundus Images Using Coupled Shape Regression', (June 2018), pp. 1–8. doi: 10.17077/omia.1040.

Shahistha, Vaidehi, K. and Srilatha, J., (2020), ‘A Review on Automatic Glaucoma Detection in Retinal Fundus Images’, *Advances in Intelligent Systems and Computing*, 1079, pp. 485–498. doi: 10.1007/978-981-15-1097-7_41.

Sharma, A. *et al.*, (2019), ‘Optic Disc Segmentation in Fundus Images Using Anatomical Atlases with Nonrigid Registration’, *Communications in Computer and Information Science*, 1019 CCIS(January), pp. 14–27. doi: 10.1007/978-981-15-1387-9_2.

Shyam, L. and Kumar, G. S., (2017) ,‘Blood vessel segmentation in fundus images and detection of Glaucoma’, *2016 International Conference on Communication Systems and Networks, ComNet 2016*, (July), pp. 34–38. doi: 10.1109/CSN.2016.7823982.

Siddiqui, S. T., Alam, S. and Khan, Z. A. ,(2019), *Smart Innovations in Communication and Computational Sciences*. Springer Singapore. doi: 10.1007/978-981-13-2414-7.

Singh, L. K., Garg, H. and Pooja ,(2020), ‘Automated Glaucoma Type Identification Using Machine Learning or Deep Learning Techniques’, pp. 241–263. doi: 10.1007/978-981-15-1100-4_12.

Sundararajan, D. ,(2017), *Digital image processing: A signal processing and algorithmic approach, Digital Image Processing: A Signal Processing and Algorithmic Approach*. doi: 10.1007/978-981- 10-6113-4.

Talaat, M. A. *et al.*, (2019), ‘Glaucoma detection from retinal images using generic features: Analysis & Results’, *ACM International Conference Proceeding Series*, pp. 10–15. doi: 10.1145/3369973.3369976.

Taylor, M. ,(2017), ‘Neural Networks: A Visual Introduction for Beginners’, *European University Institute*, (2), pp. 2–5.

Thakkar, K. *et al.*, (2017), ‘Detection of Glaucoma from Retinal Fundus Images by analysing ISNT Measurement and features of Optic Cup and Blood Vessels’, *International Journal of Engineering Technology Science and Research IJETSR www.ijetsr.com ISSN*, 4(7), pp. 2394–3386.

Thakur, N. and Juneja, M. ,(2018), ‘Survey on segmentation and classification approaches of optic cup and optic disc for diagnosis of glaucoma’, *Biomedical Signal Processing and Control*, pp. 162–189. doi: 10.1016/j.bspc.2018.01.014.

Tian, D. P., (2013), ‘A review on image feature extraction and representation techniques’, *International Journal of Multimedia and Ubiquitous Engineering*, 8(4), pp. 385–395.

Turgut, B., (2017), ‘Pearls for Correct Assessment of Optic Disc at Glaucoma Diagnosis’, *US Ophthalmic Review*, 10(02), p. 104. doi: 10.17925/usor.2017.10.02.104.

Tyagi, V. ,(2018), *Understanding Digital Image Processing*, *Understanding Digital Image Processing*. New York: CRC Press Taylor & Francis Group. doi: 10.1201/9781315123905.

Venkatesan,R., Saranya,E.andScience,C.,(2018), ‘Retinal Image Processing Using Neural Networks For Disease Prediction, 3(2), pp. 202–209.

Veras, Rodrigo & Medeiros, F.N.s & Silva, Romuere & Ushizima, Daniela. ,(2013),. Assessing the accuracy of macula detection methods in retinal images. 2013 18th International Conference on Digital Signal Processing, DSP 2013. 1-6. 10.1109/ICDSP.2013.6622734.

Vyas, A., Yu, S. and Paik, J. ,(2018), 'Fundamentals of digital image processing', *Signals and Communication Technology*, (Ccd), pp. 3– 11. doi: 10.1007/978-981-10-7272-7_1.

Wang, Y. *et al.* ,(2019), 'Automatic Segmentation of Optic Disc and Cup in Retinal Fundus Images Using Improved Two-Layer Level Set Method', *Mathematical Problems in Engineering*, 2019. doi: 10.1155/2019/4836296.

Zeyen TG, Caprioli J. Progression of disc and field damage in early glaucoma. Arch Ophthalmol. ,(1993), Jan;111(1):62-5. doi: 10.1001/archopht.1993.01090010066028. PMID: 8424726 .

Zhao, R. *et al.,* (2019), 'Direct Cup-to-Disc Ratio Estimation for Glaucoma Screening via Semi-supervised Learning', *IEEE Journal of Biomedical and Health Informatics*, 2194(c), pp. 1–1. Doi:10.1109/jbhi.2019.2934477.

Zhao, X. *et al.*, (2019), 'Automatic segmentation of optic disc and cup for CDR calculation', *Optoelectronics Letters*, 15(5), pp. 381–385. doi: 10.1007/s11801-019-8200-8.

Zhou, K. *et al.,* (2018), *Computational Pathology and Ophthalmic Medical Image Analysis*. Springer International Publishing. doi: 10.1007/978-3-030-00949-6.

Zohra, B. F. and Mohamed, B. ,(2009), 'Automated diagnosis of retinal images using the Support Vector Machine (SVM).' *Proceeding STIC. Universite de M'sila, Aljazair.*, pp. 3–8.

Zou, B. *et al.,* (2019), 'A novel glaucomatous representation method based on Radon and wavelet transform', *BMC Bioinformatics*. BMC Bioinformatics, 20(Suppl 25), pp. 1–10. doi: 10.1186/s12859-019- 3267-6.

Published Papers

Published Papers

W. A. K. Al-Muswi and E. H. Al-Saadi, "Extraction of The Neural Edge and its Properties for The Retina Infected with Glaucoma," 2021 International Conference on Advance of Sustainable Engineering and its Application (ICASEA), 2021, pp. 89-93, doi: 10.1109/ICASEA53739.2021.9733062.

Abstract: Glaucoma is a prevalent disease of the retina. The primary objective of the current study is to improve the expectation system to ensure that a person might get a Glaucoma and using the effective algorithms to skillfully identify the parts which will be influenced. To recognize and isolate the optic disc, optic cup and neuro-retinal rim, the method is invented in the current study which in return helps in the recognition of the change in the cup size and comparing it with the disc cup. The algorithm employed two steps to individualize the optic disc from the anatomical structure of the retina image and the major step depends on the severity threshold. It is the function of the schematic technique to notice the previous disorders, their size and locations depending on following steps which are: subtracting the region of the optic cup from that of the optic disc, dividing the resulted regions into four quadrants, comparing them according to ISNT and calculating the rim to disc ration where the four modern catcher algorithms are Figured. Consequently, the researcher aims for the early discovering of the neural edge of the retina and its characteristics. This mechanism is used in more than 650 images of the retinal fundus of the ORIGA dataset is an important method for documenting retinal health. It has been worked on MATLAB 2021B where it accuracy reached to 98%.

URL: https://ieeexplore.ieee.org/stamp/stamp.jsp?tp=&arnumber=9733062&isnumber=9733007.

الخلاصة

الجلوكوما هو أحد الأمراض التي تصيب العين وتحديداً شبكية العين ، مما يؤدي في كثير من الأحيان إلى تلف أنسجة العصب البصري. يحدث هذا المرض بسبب زيادة ضغط العين. يعد فحص الصور السريرية لشبكية العين باستخدام طرق الفحص الحاسوبي أمرًا بالغ الأهمية ودقيقًا من الناحية المنطقية والسريرية ، كما أنه ينتج نتائج جيدة ودقيقة بعد دمج المدخلات الرئيسية بناءً على العمل وفق السياق المطبق لمؤشرات منشأ الصحة العالمية لهذا المرض وتنظيمها رياضيا وبرمجيا.

الدراسة الحالية لها هدفان رئيسيان: الأول هو تطوير نظام لتوقع أو اكتشاف ما إذا كان الشخص مصابًا بمرض الجلوكوما أم لا. والثاني هو تقييم ما إذا كان هذا المرض في المراحل المبكرة أو المتوسطة أو الشديدة من التقدم. تم الانتهاء منها جميعًا بمساعدة خوارزميات فعالة.

أبرز علامات الجلوكوما هو زيادة حجم الكأس البصري والقرص البصري ، وكذلك التضخم الذي يحدث في الأوعية الدموية ، وتضيق منطقة حافة الشبكية العصبية التي تقع بين البصري. الكأس والقرص البصري ، طريقة فعالة تعتمد على ألوان البكسل تم اقتراحها لقيم لون الجزء المراد استخراجه مع بقية الأجزاء الموجودة بداخله ، ويمكن مقارنتها بباقي أحجام الأجزاء الصحية من عيون خالية من أي مرض آخر. على الرغم من وجود وتداخل الأوعية الدموية مع القرص البصري ، فإن الخوارزمية المستخدمة لتحديد واستخراج القرص البصري يمكن أن تعمل بدقة لفصل القرص البصري عن التركيب التشريحي لصورة قاع الشبكية ، تستخدم الخوارزمية خطوتين: الأول يعتمد على عتبة الكثافة ، والثاني يعتمد على المنهجية المورفولوجية للكشف عن جميع وحدات عنصر الصورة ، مع استبعاد أي نوع من التزييف (الضوضاء).

تم استخدام طريقتين للذكاء الاصطناعي في هذه الدراسة: الشبكة العصبية الاصطناعية وآلة ناقل الدعم للكشف المبكر عن الجلوكوما بناءً على ثماني ميزات تم استرجاعها وتصنيفها إلى فئات إيجابية وسلبية نتيجة لذلك. كانت نتائج متفوقة على نتائج الشبكة العصبية الاصطناعية . عند تصنيف الصور ، فإن مزيج الميزات التي يستخدمها آلة ناقل الدعم يجعل من الصعب التمييز بين صور قاع العين العادية والمرضية ، لذلك تحتاج إلى استخدام نواة غير خطية للاقتراب من أفضل نتيجة. أخيرًا تم العمل على تطبيق فكرة وخوارزمية شجرة القرار لتحديد درجة المرض بناءً على السمات الثمانية المسترجعة من شبكية العين و لتحديد المستويات الثلاثة التي تم الكشف عنها (مبكر ، متوسط ، شديد) بدقة (99.4٪) ، دقة نتائج التصنيف لـ (الشبكة العصبية الاصطناعية) و (آلة ناقل الدعم) هي (95.3) و (98.8) على التوالي ، وبالتالي تكون النتائج جيدة جدا و واعدة.

جمهورية العراق
وزارة التعليم العالي والبحث العلمي
جامعة بابل
كلية تكنولوجيا المعلومات
قسم البرمجيات

كشف مرحلة الجلوكوما على أساس سمات الشبكية

رسالة

مقدمة الى مجلس كلية تكنولوجيا المعلومات للدراسات العليا بجامعة بابل والتي هي جزء من متطلبات نيل درجة الماجستير في فلسفة تكنولوجيا المعلومات – برمجيات

من قبل

وسام عدنان كريم عمران

بأشراف

أ.م.د إيناس حمود محيسن عبدالله

1444هـ 2022م